Clinical Applications and Advancements in the Understanding of Visual Image Quality Metrics

by

Gareth D. Hastings

A dissertation submitted to the

College of Optometry

in partial satisfaction of the requirements for the degree of

DOCTOR OF PHILOSOPHY

In

Physiological Optics

Committee:

Raymond A. Applegate, O.D., Ph.D. (Co-chair)

Jason D. Marsack, Ph.D. (Co-chair)

Daniel R. Coates, Ph.D.

Larry N. Thibos, Ph.D.

University of Houston

December 2019

DEDICATION

"It is true that as intellectuals we ought to stand on our own feet – but one cannot learn to do this until he has first recognized to what extent he requires the support of others."

Thomas Merton, Raids on the Unspeakable

ACKNOWLEDGEMENTS

I am deeply grateful to a great number of individuals that supported and contributed to the work presented in this dissertation and that also influenced, in a broader sense, my graduate school experience.

I am especially thankful to the co-chairs of my dissertation committee, Dr Raymond Applegate and Dr Jason Marsack, for encouraging me to write from the beginning, advising me to develop as much proficiency in coding (such as Matlab) as possible, and trusting me to work in the manner and setting that I most preferred – it went a long way to creating a productive work environment.

I came half way around the world to work with Dr Applegate and I was not disappointed; I feel that I have only just scratched the surface of the depth of knowledge that he possesses on these topics. I must thank him for supporting so much of my travel and for encouraging me to find external travel support during the last few years. I am particularly grateful for the warmth and generosity with which he and Rachel (and the rest of their family) welcomed me into their home to share numerous holidays and celebrations – they were all a surrogate family to me.

Soon after joining the VOI lab, Dr Marsack and I began having phenomenal brain-storming sessions that produced pages worth of ideas – these were some of my fondest academic times. I must thank him for his indefatigable support of the interferometry project: From the first time that we discussed the idea as well as throughout all of the assembly (whenever a replacement or more appropriate part was needed) and data-collection (where he protected and

prioritized my time on the system), he was unwavering in backing and defending me. I appreciated the frequent check-ins and his help and support in dealing with the many challenging and testing moments over the years.

Dr Daniel Coates gave generously of his time and was always willing to discuss and assist in developing the interferometry project – many of the impromptu hallway conversations that we shared added tremendous value to the design and analyses. I am grateful to him for offering me a place to stay when I needed it during ARVO.

I really appreciated Dr Larry Thibos being the external member of my committee. His input on the projects and publications with which he was involved was invaluable. I have many fond memories of my visit to Bloomington, during which time he and Elspeth were very kind and welcoming to me.

I owe a great thanks to Chi Nguyen. From the moment I joined the lab, she made an effort to make me feel welcome; including me in both academic and social events – I also enjoyed spending some holidays with her and her family. I will miss the regular lunches, walks, and talks that were shared. My whole experience in the U.S. would be quite different without her influence.

Dr Alexander Schill was remarkably patient with me and very generous with his time and knowledge from the early stages of learning Zemax and throughout the interferometry project. The interferometry system would not have been functional by this stage without his help. I could

not have counted the number of times I arrived at his door with a problem and left with not only a solution but an understanding.

I had a wonderful graduate school experience at the University of Houston and I credit much of that experience to the influence of Dr Laura Frishman on the Vision Science program. I benefitted greatly from professional advice that she offered me as well as from the supportive environment that she generously constructs for all the students.

I was fortunate to begin the graduate program with a good "batch" of classmates, which helped generate and sustain momentum over the years:

Dr Laura Pardon and I became "study-buddies" before the first Core class at the beginning of our first year. This evolved into a productivity- and accountability-monitoring role over the years. I am also grateful, in a broader sense, for the many things that we read, learned, and experienced together, which grew me as a person.

Drs Ashutosh Jnawali, Suman Adhikari, Suraj Upadhyaya, and Mythri Pullela have all become very dear to me after the experiences that we shared as a class.

I am grateful to Dr Jason Porter for introducing me to the Professional Development Program (PDP; run through the Institute of Scientist and Engineer Educators at the University of California, Santa Cruz). Both my experiences as a participant and as a team leader were inspiring and formative of my academic and professional identity.

In addition to people already mentioned above, the following individuals were co-authors on journal articles: Elizabeth Bell, Han Cheng, Roxana Hemmati, Chuan Hu, Matthew Kauffman, Sujata Rijal, Sarah Wilting, and Juliana Zanayed.

The following individuals were acknowledged in publications: John Bauer, Julia Benoit, Chris Kuether, Jason Porter, Sze Quan, Hope Queener, Kim Thompson, Diana Tran, Maria Walker, and the clinicians of the University Eye Institute Cornea and Contact Lens Services

The following individuals were co-authors on conference submissions and abstracts: David Berntsen, Augustin Nti, David Rio, Eric Ritchey, and Jos Rozema.

I am grateful for the following financial support, from which I have benefitted: NIH / NEI: R01EY019105 (JDM and RAA), R01EY008520 (RAA), P30EY07551 (UHCO Core Grant), The Borish Endowment (RAA), American Academy of Optometry Foundation Ezell Fellowships (GDH), Minnie Turner Fund (GDH).

TABLE OF CONTENTS

LIST OF FIGURES

LIST OF TABLES

GENERAL ABSTRACT

PURPOSE

To use the visual image quality metric VSX (the visual Strehl ratio) to optimize objective refraction and to evaluate ophthalmic corrections across modalities (spectacles, conventional and wavefront-guided scleral lenses). In doing so, to identify aspects of VSX that could be evolved towards improving its application to real world conditions as well as to individual eyes.

METHODS

Five experiments are described. (1) The sphere, cylinder, and axis spectacle corrections that objectively optimized VSX for 40 eyes (20 subjects) were compared with subjective refraction. Visual acuity and short-term preference with the two corrections were also compared. (2) Sphere, cylinder, and axis best-corrected normative values of VSX were determined using the same objective optimization method for 146 eyes (146 subjects) ranging from 20 to 80 years at fixed 7, 6, 5, 4, and 3 mm pupil sizes. (3) VSX as well as higher order root mean square (HORMS) wavefront error, visual acuity, and letter contrast sensitivity, were used to evaluate eyes with corneal ectasia corrected by conventional and wavefront-guided scleral lenses. In the final two experiments, the neural weighting component of VSX was (4) evolved to a model that respects the effects of retinal illuminance and age and (5) personalized using measured neural contrast sensitivity functions (measured using a custom orientation-specific Maxwellian-view laser interferometer) of individual eyes (both typical and those with keratoconus).

RESULTS

(1) For 36 myopic eyes, the VSX correction provided (statistically and clinically) equivalent visual acuity to subjective refraction and was preferred by 72% of eyes over subjective refraction. In four habitually undercorrected hyperopic eyes, the VSX correction was substantially more positive in power than subjective refraction and was not preferred. (2) Normative best-corrected values of VSX as a function of age and fixed pupil size were published. (3) While aberrations (HORMS), visual acuity, and letter contrast sensitivity reached typical levels for most eyes with ectasia when wearing wavefront-guided scleral lenses, these eyes did not reach the normative values of VSX. While the magnitude of higher-order aberrations was within typical levels, the distribution of residual aberration terms was markedly different. Secondary astigmatism was frequently elevated in these corrected ectatic eyes and is particularly devastating to visual image quality. (4) Best-corrected VSX calculated using the model of neural contrast sensitivity that accounted for both retinal illuminance and age, tracked changes in best-corrected visual acuity as a function of age (from literature) better than using a model that only accounted for retinal illuminance and better than using no neural weighting factor. (5) Measured neural contrast sensitivity functions of typical eyes did not substantially differ from that defined by the model. Eyes with keratoconus showed rotationally-asymmetric sensitivities that were comparable at some orientations to typical eyes in milder stages of disease but decreased (especially at higher spatial frequencies and at particular orientations) as disease severity worsened. Personalizing the neural weighting component of VSX did not make a clinical difference to the optimal sphere, cylinder, and axis correction. Measured neural contrast

sensitivity functions of eyes with keratoconus apodize (remove the tails / feet of) the PSF more substantially than the photopic function of typical eyes, which over-estimates the detrimental effects of highly-aberrated optics.

CONCLUSIONS

The visual image quality metric VSX objectively identified spectacle corrections that were clinically equivalent to subjective refraction for myopic eyes and served as a method of evaluating corrections across modalities that is more robust than residual diopters (over-refraction) and RMS wavefront error. Because measurement of orientation-specific neural contrast sensitivity is time-consuming and the gains over the model (that defines neural contrast sensitivity as a function of retinal illuminance and age) were not clinically significant, it is recommended that the model be incorporated into calculation of the metric.

Chapter 1: Introduction.

1.1 Purpose and context: Fundamental components of the visual system

Objective measures of visual quality are useful tools that can help clinicians and researchers by serving as surrogates for visual performance and avoid the impact of subjective variability and adaptation (although adaptation should still be considered when prescribing). Examples of potential applications include identifying optimal conventional ophthalmic corrections, informing and evaluating the design of more optically complex corrections (such as wavefront-guided or extended depth of focus lenses), and predicting performance (and change in performance) of ophthalmic corrections across modalities.

If one omits eye movements, the visual system can fundamentally be divided into an optical component and a neural component. In developing objective measures of visual quality for clinical and research purposes, it is desirable that both the optical and neural components be considered and respected. Moreover, it is desirable that (1) metrics have the same multiplicity as the phenomena that they describe, for example, if we seek to predict or evaluate visual acuity (the typical outcome of subjective refraction), which is described by a single value, then an appropriate metric would combine the optical and neural components and be expressed as a single simple number, and (2) good metrics are linear (proportional) – or at least monotonic – with the phenomenon that they characterize. Given, that ophthalmic corrections (and medicine in general) are becoming more individualized, the pursuit of personalized metrics to evaluate the appropriateness of corrections for a specific individual eye is also encouraged.

1.2 Definition and quantification of the optical component

In this dissertation, the optical component of the visual system is considered to be everything responsible for forming an image on the retina. This component includes any ophthalmic correction, for example spectacles or contact lenses, as well as all the surfaces and media of the eye. The accommodative system is part of the optical component and here accommodation is generally taken as being constant, that is, either relaxed for distance viewing or stable at another task-specific object plane.

Many methods exist to quantify the optical component; historically, the most common clinical unit has been the diopter (D), which provides a coarse measure of the refractive error of an eye (or combination of eye and ophthalmic correction). However, diopters are not a visual metric and generally fail to track perceived visual quality. A common illustration of this shortcoming is shown in Figure 1.1 where the visual effect of a constant amount of spherical defocus (0.5 D) varies dramatically at different pupil sizes.

1.2.1 Wavefront sensing, Zernike polynomials, root mean square (RMS) wavefront error

The most comprehensive description of the optical component of an eye is obtained with wavefront sensing, where the behavior of light passing through the eye is examined at, typically, hundreds of points within the pupil. Across the various methods of wavefront sensing (including Shack-Hartmann systems, Hartmann screens, and ray-tracing) the position of a point of light that has passed through the optics of an eye is compared to the expected position of that point

referenced to a known fiducial that is specific to the instrument as well as the condition (for example, distance emmetropia).

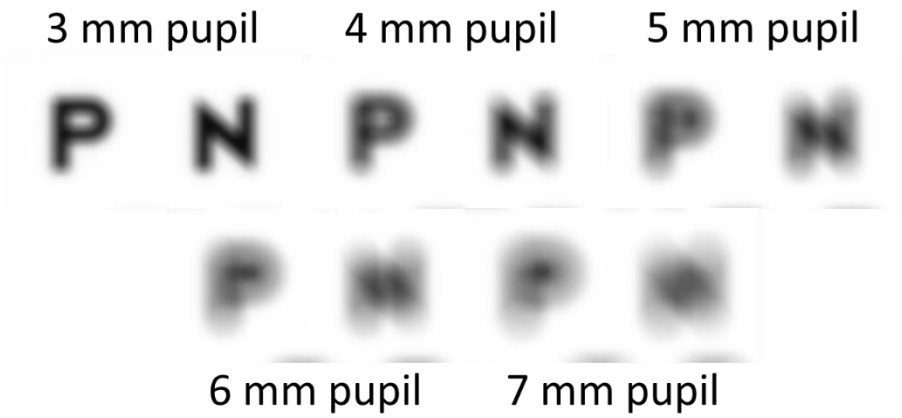

Figure 1. 1 The visual effect of diopters varies with pupil size making them an ambiguous metric of image quality. All five simulated retinal images have (only and exactly) the same amount of dioptric defocus (0.50 D).

The offsets of the measured point from the reference are used to calculate the slope of the wavefront of light over a small local area. These local slopes are collectively fit using a set of basis functions that define the wavefront over the pupil. The ANSI standard[1] recommends the Zernike polynomials as the functions to describe ocular wavefront error. The polynomials are weighted by a set of coefficients that quantify the relative contribution of each polynomial to the total wavefront error. These coefficients are normalized and specific to a particular pupil size and are algebraically scaled[2] when required to refer to a different pupil size. It is good practice to avoid scaling aberrations to a larger pupil size than what was measured,[3] therefore, aberration coefficients across individuals and conditions are generally compared at the largest common pupil size.

Unfortunately, it can be clinically cumbersome to work with Zernike polynomials, which can comprise 66 coefficients if a 10^{th} radial order fit is used. Moreover, Zernike descriptions of aberrations in the pupil plane do not unambiguously describe the quality of the image forming in the image plane. Consequently, a single-value metric was desired that could capture the quality of (how good or bad is) a wavefront error. One of the most widespread metrics is root mean square (RMS) wavefront error, which describes the magnitude of the difference of the wavefront error from the reference, in a standard deviation sense, over the pupil. Studies of higher order (HO; aberrations in and above the third Zernike radial order) RMS show that over a given pupil size the amount of higher order aberration in an eye increases consistently with age.[4,5]

In the presence of only one aberration (such as the spherical defocus in Figure 1.1), RMS is able to track the perceived visual quality of a wavefront error, however, when multiple aberrations are present, RMS frequently fails to do so. This limitation arises because RMS considers all aberrations as affecting vision equally (while different aberrations of the same magnitude generally affect vision uniquely[6,7]) and RMS fails to consider the visual interaction of aberrations (which can improve or degrade the perceived visual quality).[8]

1.2.2 Point spread functions (PSFs)

Metrics were sought that are more robust to the unique visual effects of different aberrations as well as the visual interaction of aberrations; many appropriate metrics can be derived from attributes of the point spread function (PSF) of an eye (or eye and ophthalmic correction). The PSF is the image (three-dimensional illumination distribution) formed by an optical system (such as an eye) of a point source object – which is the simplest and most

generalizable object – and is analogous to the impulse response of the optical component. The PSF of an eye can be calculated from a wavefront error measured via the squared modulus of the Fourier transform of the generalized pupil function. The best PSF is referred to as a diffraction-limited Airy disc – when the only imperfection of the optics is the Fraunhofer diffraction pattern for round apertures – and is specific to pupil size. (Many comparable metrics have been defined and developed based on the modulation transfer function (MTF) and optical transfer function (OTF); because the majority of this dissertation uses a metric based on the PSF, this introduction is similarly focused. As an additional aside, PSFs also describe the local effects of aberrations (such as multiple foci or *hotspots* better than MTFs, which describe the effects more globally.)

A common PSF metric is the Strehl ratio (ranging from 0 to 1 with 1 being best), which compares the peak of the PSF of an eye (or eye and ophthalmic correction) with the abovementioned diffraction-limited PSF at the same pupil size. Although PSF metrics such as the Strehl ratio consider the unique visual effects and interactions of all aberrations, they only consider the optical component of the visual system.

1.3 Definition and quantification of the neural component

The neural component of the visual system is considered as everything responsible for the detection and processing of the retinal image, which ultimately results in the visual percept experienced. While this component includes all structures and pathways from the retinal photoreceptors to the visual cortex and significantly delineated models for specific visual functions have been developed, in this dissertation, the neural component will be represented by

a single collective functional measure, and no attempt will be made to parse neural processing into its many sub-processes or responsible structures.

1.3.1 Neural contrast sensitivity weighting functions

One summative functional measure of the neural processing of the visual system is known as the neural contrast sensitivity function (nCSF). Analogous to conventional (total) contrast sensitivity, which quantifies the contrast resolution limits of the visual system as a function as spatial frequency (cycles per degree), the nCSF describes the contrast resolution limits of the retina, neural pathways, and visual cortex (as a function of spatial frequency) when the optical component of an eye is bypassed and theoretically does not degrade the retinal image. Neural contrast sensitivity has been reported to change with retinal illuminance[9–11] (Trolands) and age.[12–14]

1.3.2 Maxwellian-view laser interferometry

The method of measuring the nCSF that is most relevant to this dissertation is Maxwellian-view laser interferometry, in which, light is imaged into (made optically conjugate with) the entrance pupil plane of the eye. (In this technique, there is an assumption that the difference between the entrance pupil plane and anterior principal plane of an eye is negligible.) If two beams of monochromatic coherent light are imaged into the entrance pupil plane, the beams diverge within the eye and interfere on the retina forming a grating pattern. If the contrast of such a grating is manipulated to a resolution threshold, and the spatial frequency of the grating can be varied (by adjusting the relative separation of the two beams in the pupil), then the nCSF can be determined.

1.4 Visual image quality metrics

Visual image quality metrics[15] are the evolution of purely optical metrics, such as the Strehl ratio, to consider the sensitivity of the neural component of the visual system. This is most commonly achieved by combining a comprehensive measure of the optical component (wavefront error) with the nCSF, into single value. Historically, a photopic nCSF from Campbell and Green,[16] has served this purpose.

1.4.1. The visual Strehl ratio (VSX)

While many parts of this dissertation are applicable to any visual image quality metric, the visual Strehl ratio (VSX) calculated in the spatial domain (using the PSF) is the metric that will lead the clinical applications here and be used to illustrate developments made to the metrics. VSX is computed as follows:

$$\boldsymbol{VSX} = \frac{\iint \boldsymbol{PSF}_{(Eye)}(x,y) \cdot \boldsymbol{N}_{(Campbell\ and\ Green\ 1965)}(x,y)\boldsymbol{dxdy}}{\iint \boldsymbol{PSF}_{DL}(x,y) \cdot \boldsymbol{N}_{(Campbell\ and\ Green\ 1965)}(x,y)\boldsymbol{dxdy}}$$

where the metric is the ratio of the volume of the PSF of the eye to the volume of the diffraction-limited PSF at the same pupil size, where both PSFs are first weighted by the two-dimensional inverse Fourier transform of a nCSF from Campbell and Green.[16] Being a ratio, VSX also ranges from 0 to 1, with 1 being best. This computation of VSX is applicable to Chapters 2, 3, and 4, and is modified in Chapters 5 and 6. More recently, the use of a constant (3 mm) diffraction-

limited denominator has been advocated,[17,18] and this modification is also employed in Chapters 5 and 6.

Prior to the work of this dissertation, VSX had been shown predictive of subjective best focus,[15,19–21] and change in the base 10 logarithm of VSX (logVSX) was well correlated with visual performance[22] especially with logMAR visual acuity[23] independent of pupil size or underlying wavefront error.[24] Concurrent with the work of this dissertation, VSX has been shown useful in optimizing the objective refraction of specific demographics, such as individuals with Down syndrome[25] and keratoconus.(Bell, Hastings, Nguyen, Applegate, Marsack; submitted)

1.5 Optical and neural components of highly aberrated eyes

The optical component of visual image quality metrics is dependent on obtaining a good fidelity wavefront error measurement on that eye. In eyes with elevated levels of higher-order aberrations, such as those with keratoconus, significant loss of spots, substantial blurring of the spots, and poor fitting by the Zernike polynomials may result in questionable measurements. Despite these challenges, because of the density with which the behavior of light is sampled over the pupil, wavefront error provides the most appropriate characterization of the optical component of highly aberrated eyes. When a valid wavefront error measurement is recorded (which can be gauged, for instance, from Zernike fit error), the optical component of visual image quality metrics can be personalized to an individual eye.

The neural component of the metrics has been a representative nCSF measured at photopic levels on a young typical eye. Literature is divided on how the nCSF of highly aberrated eyes might differ from normal: Using adaptive optics and laser interferometry respectively, Sabesan[26] and Kayawara et al.[27] found nCSFs of eyes with keratoconus to be poorer than normal, while Michael et al.[28] found neural processing to be heightened, however all literature has found it to be different to that of normal eyes. The appropriateness of using the photopic nCSF of a typical eye in visual image quality metric calculations of highly aberrated eyes is unknown.

1.6 Overview of the experimental chapters

The first half of this dissertation describes the application of existing visual image quality metrics for the clinical purposes of optimizing objective refraction and evaluating ophthalmic corrections across modalities (such as spectacles and conventional and wavefront-guided scleral lenses). During these applications, certain aspects of the metrics were identified that could be evolved and personalized to individuals and real world conditions, and the second half of the dissertation describes the subsequent development and implementation of some of these improvements. Evolving visual image quality metrics in these ways is shown to improve their ability to track physiological visual performance with age and to be more personalized to an individual.

1.6.1 Chapter 2

Because the visual image quality metric VSX had previously been shown predictive of subjective best focus, and change in logVSX was well correlated with change in logMAR visual acuity, VSX was used to objectively identify sphere, cylinder, and axis prescriptions from wavefront error measurements (in a simulated through-focus sense) for normal eyes. The performance of these objectively optimized prescriptions was compared to subjective refractions on a sample of eyes and was found to provide clinically equivalent (and not statistically different) visual acuity in the majority of myopic eyes, and was subjectively preferred in acute comparison with subjective refraction.[29]

1.6.2 Chapter 3

The aforementioned utility of VSX to identify prescriptions that provided equivalent levels of visual performance to the gold standard (subjective refraction), as well as previous literature that demonstrated the robustness of VSX to track visual quality better than residual diopters or RMS wavefront error, suggested that VSX could be used to evaluate the visual quality of ophthalmic corrections across modalities. A necessary aspect of such a metric is normative benchmark levels of the metric value for conventionally well-corrected typical eyes. To provide these benchmarks to the community / literature, the sphere, cylinder, and axis prescription that optimized VSX was objectively found from the WFE measurements of 146 normal eyes ranging in age from 20 to 80 years and for pupil sizes from 3 to 7 mm.

In agreement with the prevailing qualitative understanding of visual quality, best VSX was quantitatively found in young eyes at small pupil sizes and worsened as pupil size increased

and as age increased, with increase in pupil size having a more substantial effect. Normative values of SCA best-corrected VSX as a function of age and pupil size were peer-reviewed and published for reference.[30]

1.6.3 Chapter 4

The normative values of best-corrected VSX were used to evaluate best-conventional and individualized wavefront-guided scleral lenses on eyes with corneal ectasia. For the majority of these eyes, wavefront-guided scleral lenses reduced the amount (RMS) of higher order aberrations to within normal levels and corrected visual acuity and contrast sensitivity to within normal levels, however, only two out of twenty eyes achieved the objectively best-corrected levels of VSX described in Chapter 3. Potential explanations for this finding that involve the neural component of the metric are investigated in Chapters 5 and 6, while those that concern the optical component are discussed in Chapter 7

1.6.4 Chapter 5

This chapter moves towards a more individualized neural weighting function by drawing from literature and defining models of normal neural contrast sensitivity as a function of (1) spatial frequency and retinal illuminance (Trolands), and (2) spatial frequency, retinal illuminance, and age. These models are used to calculate best-corrected (sphere, cylinder, and axis) VSX at physiological pupil sizes over a range of luminance levels where the neural weighting factor is specific to retinal illuminance (or retinal illuminance and age). The optical and neural components of the metric are found to interact and to contribute to visual image quality in three different ways dependent on luminance. The ability of the metric to mimic the

trends of visual acuity with age is shown to be improved with the neural weighting function that considers both retinal illuminance and age.

1.6.5 Chapter 6

Chapter 6 describes the measurement of orientation-specific neural contrast sensitivity using a custom Maxwellian-view ophthalmic laser interferometer in six eyes with keratoconus and four typical eyes. Using these measured functions, both (optical and neural) components of VSX can be personalized to an individual eye. These data are used to inform the findings of the preceding chapters such as the objective optimization of spectacle prescriptions in Chapter 2 and the performance of eyes with ectasia wearing wavefront-guided lenses in Chapter 4.

1.6.6 Chapter 7

The final chapter summarizes and synthesize the findings of the five experimental chapters and discusses their implications from both clinical and laboratory perspectives. Unexpected findings, shortcomings of the experimental designs, and possible explanations of the results of the preceding chapters (some of which are mentioned above) are discussed in the context of potential future investigations.

Chapter 2: Is an objective refraction optimized using the visual Strehl ratio better than a subjective refraction?

Reprinted with modifications from:[29] Hastings GD, Marsack JD, Nguyen LC, Cheng H, Applegate RA. Is an objective refraction optimized using the visual Strehl ratio better than a subjective refraction? Ophthalmic Physiol Opt (2017) 37: 317–325. doi: 10.1111/opo.12363

2.1 Abstract

PURPOSE

To prospectively examine whether using the visual image quality metric, visual Strehl (VSX), to optimize objective refraction from wavefront error measurements can provide equivalent or better visual performance than subjective refraction and which refraction is preferred in free viewing.

METHODS

Subjective refractions and wavefront aberrations were measured on 40 visually-normal eyes of 20 subjects, through natural and dilated pupils. For each eye a sphere, cylinder, and axis prescription was also objectively determined that optimized visual image quality (VSX) for the measured wavefront error. High contrast (HC) and low contrast (LC) logMAR visual acuity (VA) and short-term monocular distance vision preference were recorded and compared between the VSX-objective and subjective prescriptions both undilated and dilated.

RESULTS

For 36 myopic eyes, clinically equivalent (and not statistically different) HC VA was provided with both the objective and subjective refractions (undilated mean ±SD was –0.06 ±0.04 with both refractions; dilated was –0.05 ±0.04 with the objective, and –0.05 ±0.05 with the subjective refraction). LC logMAR VA provided by the objective refraction was also clinically equivalent and not statistically different to that provided by the subjective refraction through

both natural and dilated pupils for myopic eyes. In free viewing the objective prescription was preferred over the subjective by 72% of myopic eyes when not dilated.
For four habitually undercorrected high hyperopic eyes, the VSX-objective refraction was more positive in spherical power and VA poorer than with the subjective refraction.

CONCLUSIONS

A method of simultaneously optimizing sphere, cylinder, and axis from wavefront error measurements, using the visual image quality metric VSX, is described. In myopic subjects, visual performance, as measured by HC and LC VA, with this VSX-objective refraction was found equivalent to that provided by subjective refraction, and was typically preferred over subjective refraction. Subjective refraction was preferred by habitually undercorrected hyperopic eyes.

2.2 Introduction

Here we assert that an ideal objective refraction should result in a prescription that provides an individual observer with equivalent or better visual acuity (VA) than a subjective refraction and, when free viewing the world, the observer evaluates their view of the world as equal or preferable to that provided by the subjective refraction.

To achieve such a goal the objective refraction needs to respect the fact that the visual system has two key components: the optics that form the retinal image and the neural processing that transforms the retinal image into a visual percept.

Subjective refraction has historically been unique among methods of refraction in considering both components by asking the observer to choose between a series of two lens options; the goal being to optimize VA while the eye is refracted to the hyperfocal distance. However, the clinical subjective refraction is a variable process[31–34] for a variety of reasons including adaptation to a prior prescription as well as examiner prompting and the patient's interpretation of the given choices. These problems are compounded when conducting studies across different subjects and refractionists.

Most objective methods of refraction evaluate the optical component of the visual system to determine a sphere, cylinder, and axis (SCA) prescription. Although wavefront sensors provide the most comprehensive descriptions of the eye's optics and have been found more precise than subjective refraction,[34] on their own they do not consider the neural processing component. However, by utilizing visual image quality metrics, an estimate of the neural processing component can be incorporated with the optical component for the objective determination of ocular prescriptions. (To differentiate these metrics from those that quantify retinal image quality alone, the term *visual image quality* was coined to indicate inclusion of neural processing.)[15]

One visual image quality metric, called the visual Strehl ratio (VSX), has been shown to be predictive of subjective best focus [15,19] and well correlated with change in visual performance as measured by VA [20,22,24] independent of pupil size and underlying wavefront error (WFE).[24] Based on these prior studies[20,22,24,35] and capitalizing on the precision of wavefront sensing[34,36]

we expect VSX will be useful in identifying a refraction that provides equivalent if not better VA than a subjective refraction and an equal or preferable percept when viewing the world. Furthermore, given the clinical wisdom that patients can and do adapt to new prescriptions (particularly when the changes are relatively small), such objective methods of refraction would not be influenced by factors that can skew subjective refraction, such as adaptation to a habitual prescription.[37]

Numerous studies[15,19,21,38–41] have processed wavefront error measurements using image quality metric methodologies (both metrics of visual image quality and retinal image quality) to identify a SCA prescription. In contrast to methods that use only second-order[42,43] or other specific Zernike terms such as primary spherical aberration and coma,[15,44–46] metric-based methods consider the combination[8] of all aberrations in the eye when optimizing retinal image quality.[15,38,40]

Unfortunately, most previous works using WFE data have generally been limited to the difference between the dioptric powers of the wavefront and subjective refractions (generally comparing the spherical equivalents of the refractions, and many were retrospective). As a result, any comparison of the relative visual performance of these prescriptions has hitherto needed to be loosely inferred from the dioptric difference (typically in power vector[47] space). This is unfortunate because visual acuity is the outcome measure of subjective refraction. It is also problematic because dioptric spaces are not visually uniform spaces, that is, aberrations can interact differently to increase or decrease retinal image quality.[6–8] To the best of our knowledge, a prospective and double-blind comparison of visual performance of individual normal eyes with

wavefront refraction and subjective refraction remains unreported (although Jinabhai et al.[46] apparently measured VA through both such prescriptions in normal control eyes, they did not report it). Furthermore, subjects' preferences between the two types of refraction remain unreported.

Therefore here, we sought to prospectively and in a double-blind manner examine (1) whether using the visual image quality metric VSX to optimize objective refraction from a wavefront error measurement could provide VA (the outcome measure of subjective refraction) that is equivalent, or better than, traditional gold standard subjective refraction and (2) which refraction the observer preferred for both natural and dilated pupil conditions.

2.2 Methods

Prior to data collection, the nature and possible consequences of the study were explained to each subject. University of Houston Institutional Review Board-approved informed consent was signed by each subject, and the research followed the tenets of the Declaration of Helsinki. Forty visually-normal eyes (of 20 subjects) with well-correctable vision were examined. All subjects were recruited from the University of Houston, College of Optometry; mean age ± standard deviation (SD) was 26.4 ±4.8 years, and all had a habitual refractive prescription of greater than 1 D (range was +7.00 to –7.00 D sphere and 0.00 to –1.75 D cylinder).

Uncorrected wavefront error measurements were collected first through each eye's natural pupil in mesopic conditions (COAS HD, http://abbottmedicaloptics.com): A minimum of

four measurements were recorded (described up to the 10th Zernike radial order and corrected for longitudinal chromatic aberration) of which three were selected that had the maximum number of spots, smallest central reflection, and no clipping of image by lashes. The coefficients of the three measurements were mathematically averaged (for the largest common pupil size) to define the WFE for each eye, which in turn was used to determine the optimized refraction (as described below). Directly thereafter, subjective refraction was performed using a phoropter by one of two experienced clinicians, starting from an autorefractor output; sphere and cylinder were adjusted in 0.25 D steps and axis was resolved to the nearest degree (astigmatic components were determined with Jackson crossed-cylinders). According to the prescribed clinical convention, the endpoint of subjective refraction was the maximum plus that retained best VA (a hyperfocal refraction). As is the clinical custom (and consistent with conditions under which WFEs were measured) subjective refractions were conducted in a dark room and no attempt was made to fix natural pupil diameters.

High contrast (HC; –100% Weber contrast) and low contrast (LC; –25% Weber contrast) VA were measured monocularly with each of the two prescriptions (VSX-objective and subjective) in trial frames positioned at a 12 mm vertex distance. Twelve different ETDRS (logMAR) charts were generated using Visual Optics Laboratory Professional software (version 7.4, Sarver and Associates Inc.) and presented on a high resolution LCD monitor (M253i2, https://www.totoku.com) at a luminance of 380 cd/m^2. Three charts of each contrast were randomly selected and read monocularly with each prescription and the average of the three acuities was taken as the VA for that eye and condition. Letter-by-letter scoring[48] was performed where 0.02 logMAR credit was given for every letter read correctly, and subjects read until they

had accrued five missed letters.[49] After HC and LC VAs were recorded for each prescription, each subject was asked to monocularly view a distant natural scene (out of a hallway window) and to evaluate whether they could appreciate any difference between the two prescriptions and, if so, to rate how strongly they preferred one over the other on a seven point Likert scale. During the acuity measurements as well as during the short-term preference evaluation, the investigator and the subject were masked as to which prescription was the objective and which was the subjective. The prescription with which each subject viewed first and second was randomized.

When each subject had completed all of the abovementioned measurements, pupils were dilated with 1 drop of tropicamide 1% and, when the iris had been rendered unresponsive to light (typically after 20 minutes), the entire protocol was repeated.

2.2.1 Optimization method for objective refraction

The method employed identified the SCA combination (sphere and cylinder to the nearest 0.25 D, and axis in 2° increments) that provided the best image quality (VSX) for the measured WFE by performing a simulated through-focus experiment.[15,21,40] All calculations were performed using custom Matlab software (https://www.mathworks.com). A range of dioptric powers was selected over which visual image quality would be evaluated; this consisted of the 15142 SCA combinations between +3.00 and –2.00 D sphere (in 0.25 D steps) and 0 to –2.00 D cylinder (in 0.25 D steps at 2° axis steps). Previous modelling[50] demonstrated this range to be appropriate for visually-normal eyes. Because subjects' refractive errors varied, the range of applied powers was displaced and centered on the dioptric equivalent of the Zernike defocus term for each subject. For instance, for a –5.00 D myopic subject, the range of applied SCA

powers ranged from –2.00 D to –7.00 D sphere and 0 to –2.00 cylinder. These SCA combinations were propagated from a 12 mm vertex distance back to the pupil plane[51,52], mathematically converted into Zernike terms,[47,53] and each added individually to the uncorrected second-order Zernike terms of the WFE thereby generating 15142 "corrected" WFEs. VSX was calculated (using equation A23 from Thibos et al.[15] included below) for each of the "corrected" WFEs and the SCA combination that corresponded to the greatest VSX value was identified as providing best visual image quality and was selected as the objective prescription. Briefly, VSX is calculated[15] by comparing the point-spread function (PSF) of the eye with the diffraction-limited PSF for the same pupil size, where both PSFs are weighted by the inverse Fourier transform of the neural contrast sensitivity function determined with interference fringes.[16]

$$VSX = \frac{\int_{psf} PSF\,(x,y) N(x,y) dxdy}{\int_{psf} PSF_{DL}\,(x,y)\, N(x,y) dxdy}$$

2.3 Results

Results are presented and discussed separately for myopic and hyperopic eyes. All standard deviations were calculated using ANOVA and components of variance analyses to account for the dependence of right and left eyes.[54,55] Similarly, p-values were calculated using split-plot ANOVAs.[54,55]

2.3.1 Myopic eyes

2.3.1.1 Visual acuity

Figures 2.1 and 2.2 show scatter plots and limits of agreement plots that compare the HC logMAR VA recorded with the VSX-objective prescription to that recorded with the subjective refraction.

Figure 2.1 (A) and (B) correspond to typical clinical conditions (that is, HC measures of VA through natural (undilated) pupils) and show that for almost all myopic eyes the VSX objective refraction provided VA that was clinically and statistically equivalent to that provided by subjective refraction. The actual HC undilated VAs of myopic subjects with the objective prescription were all around 20/20 (0.00 logMAR) or better (mean –0.06 ±0.04), as can be seen in Figure 2.1(A). There was no significant difference in HC VA (paired t-test, p=0.67) with the two refractions (mean difference 0.00 ±0.04). The strong agreement between the VAs recorded with the two prescriptions can also be seen in (B) where mean difference is plotted as the middle blue line and is less than one letter.

When dilated (therefore all measurements were through identical fixed pupils for each subject), myopic subjects also achieved good HC VA with the objective prescription (mean –0.05 ±0.05) and there was no significant difference (paired t-test, p=0.99) between the HC VA with the subjective and objective refractions (mean difference 0.00 ±0.04), as can be seen in Figure 2.2.

The LC logMAR VA data are presented in Table 2.1. Through both natural and dilated pupils, the LC VA with the two prescriptions were not significantly different (mean difference undilated –0.02 ±0.07 and dilated –0.01 ±0.06).

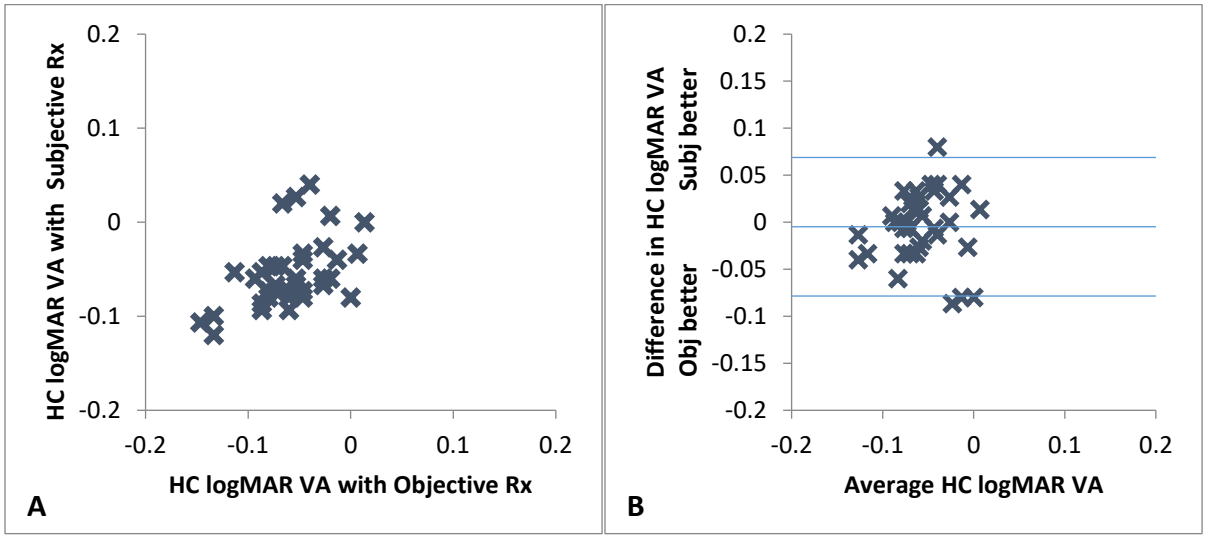

Figure 2. 1 (A) Scatter plot and (B) limits of agreement plots comparing the high contrast (HC) logMAR VA recorded with the VSX-optimized-objective refraction to that recorded with the subjective refraction through natural pupils for myopic eyes (n=36). The values of the mean differences illustrated here, as well as their standard deviations, can be found in Table 2.1.

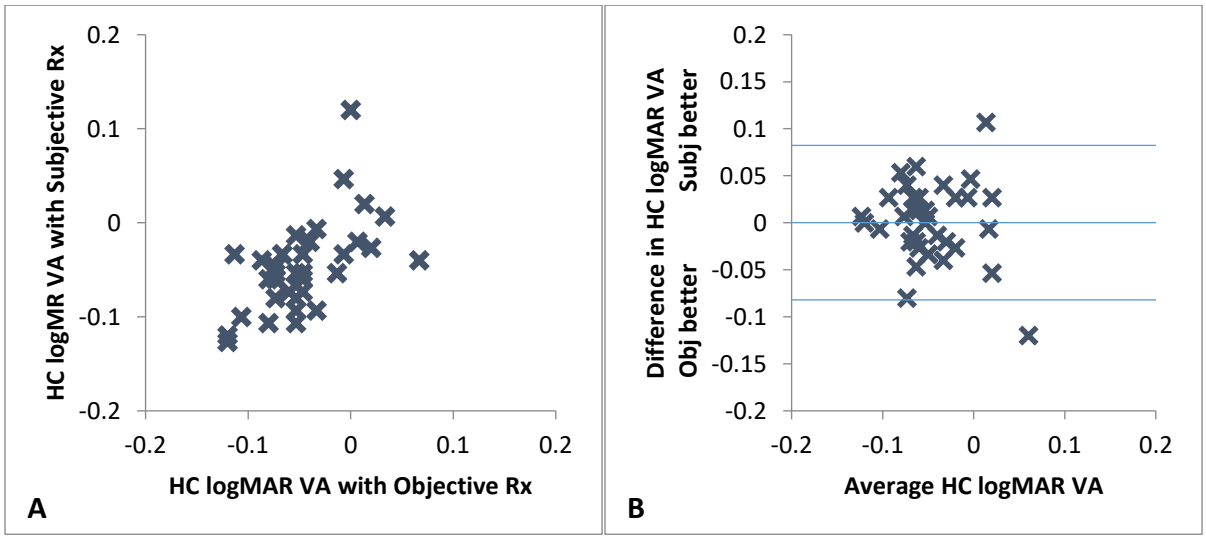

Figure 2. 2 (A) Scatter plot and (B) limits of agreement plots comparing the high contrast (HC) logMAR VA recorded with the VSX-optimized-objective refraction to that recorded with the subjective refraction through dilated pupils for myopic eyes (n=36). The values of the mean differences illustrated here, as well as their standard deviations, can be found in Table 2.1.

2.3.1.2 Short-term preference

Figure 2.3 illustrates the short-term distance vision preference between the two prescriptions for myopic eyes. When viewing through natural pupils (A) 72% of myopic eyes preferred the objective prescription. When dilated (B), 47% of eyes preferred the objective prescription, 16% judged them to be equivalent, and 36% preferred the subjective.

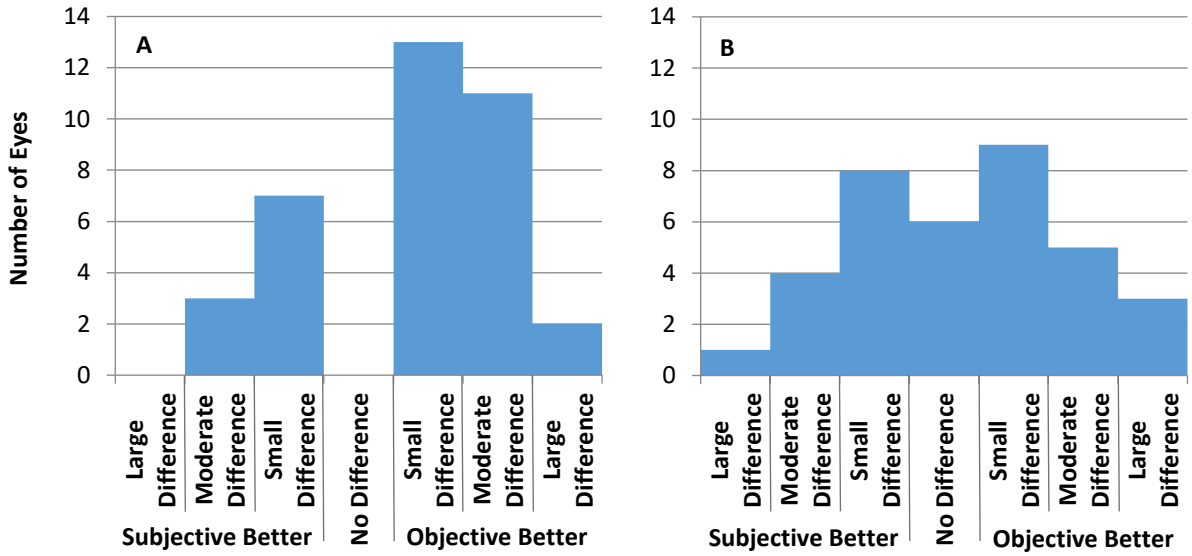

Figure 2. 3 Frequency histograms of short-term monocular preference comparison between the VSX-optimized-objective prescription and the subjective prescription for myopic eyes. The objective prescription was preferred by 72% of myopic eyes when viewing through natural pupils (A). When dilated (B), 47% of myopic eyes preferred the objective refraction while 16% judged them to be equivalent to the subjective refraction.

2.3.2 Hyperopic eyes

2.3.2.1 Visual acuity and short-term preference

We report the hyperopic eyes because the result was fundamentally different than for myopic eyes, even though the number of eyes studied is too small for meaningful statistical analysis. Four habitually undercorrected high hyperopic eyes were examined – one subject's habitual spectacle prescription was R: +7.25 D, L: +5.75 D, while the other subject's was

approximately +3.00D in both eyes. The objective refraction generally did not provide equivalent VA to the subjective refraction. All four high hyperopic eyes preferred the subjective refraction over the objective when undilated and dilated.

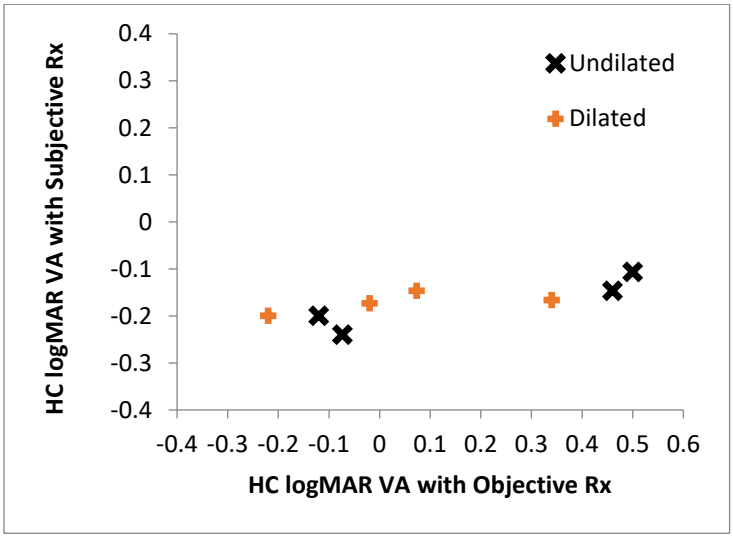

Figure 2. 4 For four habitually undercorrected hyperopic eyes, comparison of the high contrast (HC) logMAR VA recorded with the VSX-optimized-objective refraction to that recorded with the subjective refraction through natural pupils (black crosses) and dilated pupils (red plusses).

2.4 Discussion

We sought to examine whether using the visual image quality metric VSX to optimize objective refraction from a wavefront error measurement could provide visual performance equivalent, or better than, traditional subjective refraction. Visual acuity was selected as the primary measure for this comparison because it is the most common outcome measure of refraction and is what subjective refraction is intended to optimize. Numerous studies have evaluated the test-retest variability of HC logMAR VA; the average SD of six studies summarized by Raasch et al.[56] was ±2.56 letters (±0.05 logMAR); while that of another five

adult studies compared by Manny et al.[57] was ±3.97 letters (±0.08 logMAR). Typical statistical practice defines a 95% confidence interval as ±2 SD (approximately one line of logMAR VA). Here we elected a stricter criterion and defined *clinically* equivalent HC logMAR VA as differences less than ±2.5 letters (±0.05 logMAR).

2.4.1 Hyperopic eyes

The VSX-objective prescription did not provide equivalent or better VA than subjective refraction for the two habitually undercorrected high hyperopic subjects examined. For both hyperopic subjects, the wavefront sensor measured higher levels of hyperopia than the subjective refraction (and the habitual prescription); however, the astigmatism components were very similar across the two refractions. When not dilated, the VSX-objective prescription was over 1.00 D more positive in spherical power than the subjective, for three of the four eyes. Despite accommodation being largely relaxed when dilated, the difference for three of the four hyperopic eyes was still over 0.75 D, with the objective being more positive than the subjective. Although four high hyperopic eyes is a limited sample size from which to form conclusions we believe, that being young and habituated to a constant level of accommodation (one subject had even functioned unaided until high school), these subjects did not relax their tonic level of accommodation during the ~20 minutes of VA and preference testing and, consequently, performed poorly with the much the more positive objective prescription.

Tonic accommodation as a result of habitually undercorrected hyperopia remains a challenge for objective and subjective methods of refraction, and care needs to be taken when examining hyperopic subjects particularly in rare cases of hyperopia as high as those examined

here. Most other studies of metric-based refraction have either examined only myopic subjects[38,39] or mild hyperopic subjects with spherical equivalent[21,41] or spherical power[40] of +1.75 D or less. The rarity of such high hyperopic subjects means that they form a small proportion of clinical cases and also limits the extent to which this finding can be explored at this time.

2.4.2 Myopic eyes

The VSX-objectively determined prescription met the ±2.5 letters visual performance hypothesis of being equivalent to the subjective refraction in nearly all myopic eyes, both through natural pupils and when dilated. Figure 2.5 shows the number of myopic eyes that were within the ±2.5 letters SD reported by Raasch et al,[56] as well as the number of eyes that performed better with either of the refractions. These findings demonstrate that equivalent visual performance can be objectively provided for myopic eyes from either dilated or undilated WFE measurements by using VSX as a refraction optimization metric even though pupil diameter might vary when undilated as it would in clinical practice.

While VA was clinically and statistically equivalent for myopic eyes, both through natural pupils and when dilated, in both conditions the majority of these eyes preferred the objective prescription over the subjective in a short-term comparison. This finding is consistent with the observation[23] that a just noticeable difference in blur can be perceived well before a change in VA occurs. These preference data suggest that subjects were able to discern a noticeable difference in image quality with the objective refraction and expressed it in their preference. The difference in image quality (logVSX) between the objective and subjective

refractions was greater than the JND in perceived blur determined by Ravikumar et al.[23] for all 36 myopic eyes when not dilated, and for 32 of the 36 eyes when dilated.

The best VAs of the subjects examined here are on average a few letters worse than what has been reported for the same age group.[58] This is possibly due to our predominantly myopic sample and particularly the number of significantly myopic eyes;[59–61] 10 eyes had ≥5 D of myopia.

Table 2. 1 Summary of the mean logMAR VA with each prescription as well as the difference in VA (objective – subjective). Split-plot ANOVAs found none of the differences to be statistically significant for myopic eyes.

Pupil	**Visual Acuity**		**Objective VA Mean ±SD**	**Subjective VA Mean ±SD**	**Difference Mean ±SD**
Undilated	High Contrast	n=40	–0.03 ± 0.13	–0.07 ± 0.05	0.03 ± 0.14
		Myopic n=36	–0.06 ± 0.04	–0.06 ± 0.04	0.00 ± 0.04
		Hyperopic n=4	0.19 ± 0.41	–0.17 ± 0.07	0.37 ± 0.34
	Low Contrast	n=40	0.07 ± 0.16	0.04 ± 0.07	0.03 ± 0.18
		Myopic n=36	0.04 ± 0.05	0.05 ± 0.06	–0.02 ± 0.07
		Hyperopic n=4	0.36 ± 0.48	–0.09 ± 0.07	0.44 ± 0.41
Dilated	High Contrast	n=40	–0.04 ± 0.08	–0.06 ± 0.06	0.02 ± 0.10
		Myopic n=36	–0.05 ± 0.04	–0.05 ± 0.05	0.00 ± 0.04
		Hyperopic n=4	0.04 ± 0.26	–0.17 ± 0.02	0.22 ± 0.24
	Low Contrast	n=40	0.11 ± 0.10	0.09 ± 0.08	0.02 ± 0.13
		Myopic n=36	0.09 ± 0.06	0.10 ± 0.07	–0.01 ± 0.06
		Hyperopic n=4	0.30 ± 0.22	–0.02 ± 0.02	0.32 ± 0.21

Dioptric differences between the two refractions are included here for comparison with other studies, despite the many different metric[15,21,38–41], wavefront refraction[42–46], and subjective refraction[41] methodologies used in the past. However, when stating dioptric values, bear in mind

that while a particular VSX value quantifies visual image quality essentially independent of pupil size, a particular dioptric value does not, for instance, –1 D affects vision very differently when viewing through small and large pupils.[62,63]

The objective and subjective refractions were converted from sphere, cylinder, and axis into power vectors[47] and the subjective refractions components were subtracted from the objective.

Astigmatism components have generally been found very similar between wavefront and subjective refractions[15,39,40,44–46], and that was also true here; the mean differences in the astigmatic components (J_0 and J_{45}) were all less than one-tenth of a diopter (as can be seen in Table 2.2).

Very few studies have performed undilated comparisons of the spherical equivalent (M) component of wavefront refractions. Using metrics Iskander[40] found differences in M that ranged between –0.31 and –0.62 D, while, calculating refraction from coefficient terms, Zhu et al.[45] found –0.39 D. The mean difference in M for undilated myopic eyes found here was –0.65 D (and for all eyes was –0.48 D). When dilated, that difference was more than halved, –0.26 D for myopic eyes (and –0.16 D for all eyes), which is consistent with other metric-based studies, such as Teel et al.[41] who found –0.24 D, and Kilintari et al.[39] where most differences ranged between –0.17 and –0.36 D; as well as other methods of wavefront refraction, such as Jinabhai et al.,[46] where differences were around –0.19 D.

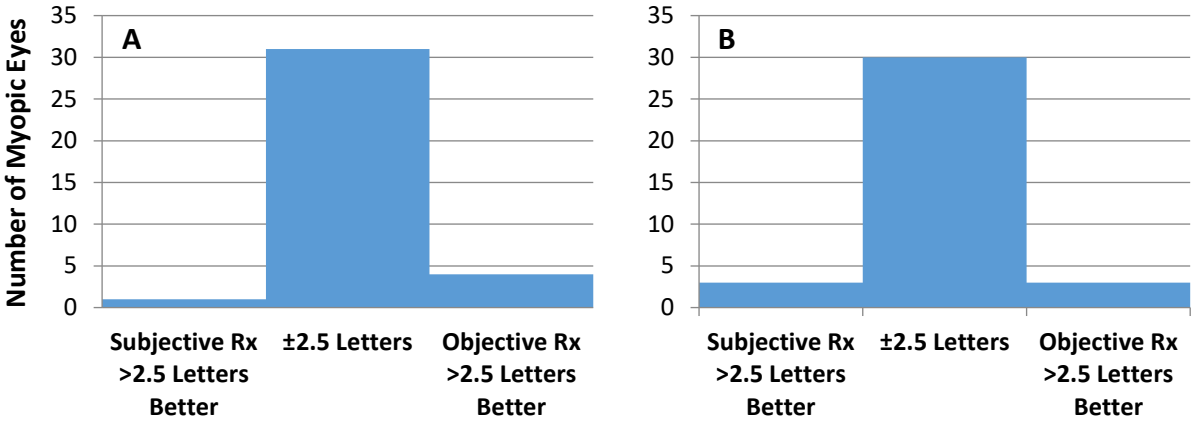

Figure 2. 5 Frequency histograms for myopic eyes of the difference in HC logMAR VA between the VSX-objective and the subjective prescriptions when (A) not dilated and (B) dilated. Clinically equivalent VAs were defined as differences less than 2.5 letters.

Table 2. 2 Summary of dioptric component differences (VSX-objective – subjective).

Pupil		M	J_0	J_{45}	Euclidean Separation
Undilated	n=40	–0.48 ± 0.68	0.07 ± 0.16	–0.03 ± 0.10	0.74 ± 0.42
	Myopic n=36	–0.65 ± 0.35	0.07 ± 0.17	–0.03 ± 0.10	0.69 ± 0.34
	Hyperopic n=4	1.09 ± 1.08	0.03 ± 0.12	–0.02 ± 0.08	1.17 ± 0.94
Dilated	n=40	–0.16 ± 0.40	–0.03 ± 0.14	–0.02 ± 0.10	0.40 ± 0.23
	Myopic n=36	–0.26 ± 0.25	–0.02 ± 0.15	–0.02 ± 0.10	0.36 ± 0.19
	Hyperopic n=4	0.75 ± 0.32	0.00 ± 0.08	–0.02 ± 0.12	0.76 ± 0.31

Because chromatic aberration was accounted for, and Kilintari et al.[39] found very little improvement in the accuracy of wavefront refractions using polychromatic metrics rather than monochromatic or by accounting for the Stiles-Crawford effect, remaining explanations for the dioptric difference between wavefront and subjective refractions include: That the infrared (IR) light used in wavefront sensors reflects from structures deeper than the apertures of the photoreceptors[64] – this can only perhaps be mitigated by custom modification of an instrument.[21] Accommodation during measurement (instrument myopia) could play a role when not dilated,

however, the hyperopic subjects examined here evidently managed to relax their accommodation much more while being measured than when viewing a letter chart.

We believe the mantra of ending subjective refraction on the most positive prescription that does not reduce VA also contributes to this finding because, as pointed out by Thibos et al.,[15] image quality metrics identify the centre of the depth of focus (maximum image quality) while subjective refraction finds the most positive end of the depth of focus.

Although maximizing the usable range of depth of focus might be sound practice as patients approach presbyopia, the method used here provided equivalent VA to the subjective refraction in myopic eyes, and our short-term preference data (as described above) suggests that maximising visual image quality is preferred by younger eyes.

While this study supports the possibility of prescribing refraction directly from an objective measurement for myopic eyes, and may be particularly useful for patients that provide poor subjective refraction responses, there are some limitations to the study: A relatively small sample of 40 young eyes (20 individuals) was used; although the reduced accommodative ability associated with presbyopia would likely improve the accuracy and precision of objective refraction, this remains to be demonstrated. The technique was not evaluated on low hyperopic eyes. Currently, the objective refraction does not incorporate binocular balancing that might be necessitated by anisometropia. Despite not being given any opportunity to adapt to the objective prescription, the majority of eyes preferred that prescription through natural pupils. Allowing subjects time to adapt could inform any broader advocacy of this method and also speak to the

typically challenging cases of adaptation such as the high undercorrected hyperopic eyes examined here, as well as first-time cylinder wearers.

2.5 Conclusions

A method of simultaneously optimizing sphere, cylinder, and axis from a wavefront error measurement, using the visual image quality metric VSX, was described. In myopic subjects, visual performance, as measured by VA, with this VSX-objective refraction was prospectively found to be equivalent to that provided by subjective refraction, and was preferred over subjective refraction by the majority of myopic eyes. The four habitually undercorrected hyperopic eyes examined here, preferred and benefitted from subjective refraction.

Chapter 3: Normative best-corrected values of the visual image quality metric VSX as a function of age and pupil size.

Reprinted with modifications from:[30] Hastings GD, Marsack JD, Thibos LN, Applegate RA. Normative best-corrected values of the visual image quality metric VSX as a function of age and pupil size. J. Opt. Soc. Am. A. (2018) 35(5):732-739. https://doi.org/10.1364/JOSAA.35.000732.

3.1 Abstract

The visual image quality metric the Visual Strehl ratio (VSX) combines a comprehensive description of the optics of an eye (wavefront error) with an estimate of the photopic neural processing of the visual system, and has been shown predictive of subjective best focus and well correlated with change in visual performance. Best-corrected visual image quality was determined for 146 eyes and the quantitative relation of VSX, age, and pupil size is presented, including 95% confidence interval norms for age groups between 20 and 80 years and pupil diameters from 3 to 7 mm. These norms were validated using an independently collected population of wavefront error measurements. The best visual image quality was found in young eyes at smaller pupil sizes. Increasing pupil size caused a more rapid decrease in VSX than increasing age. These objectively determined benchmarks represent the best theoretical levels of visual image quality achievable with a sphere, cylinder, and axis correction in normal eyes and can be used to evaluate both traditional and wavefront-guided optical corrections provided by refractive surgery, contact lenses, and spectacles.

3.2 Introduction

The optical quality of the eye has been studied in increasing detail and complexity from geometric schematic eyes[52,65] and dioptric refractive error,[66,67] to optical metrics such as line spread functions,[68–70] point spread functions (PSFs),[71,72] modulation transfer functions (MTFs),[16,73–76] root mean square (RMS) wavefront error (WFE),[76,77,4] and metrics of retinal image quality.[15,38–40]

Normative references are essential to the use of these various metrics as benchmarks in scientific and clinical enquiry. A widely used set of normative values, for instance, is that of RMS WFE and higher order aberrations (HOAs) as a function of pupil size and age,[4] which has, for example, been used in studies of traditional[78] and wavefront-guided[79,80] contact lens corrections, reading speed,[81] intra-ocular lenses (IOLs),[82] and the optical properties of the cornea.[83]

Although satisfactory in many cases, a drawback of this normative dataset is that RMS WFE does not consider the visual interaction of aberrations.[15,53] Figure 3.1 illustrates an example where the addition (interaction) of aberrations causes an increase (worsening) in RMS WFE, but actually results in an improvement in image quality. For the same reason, the calculation of equivalent dioptric defocus from RMS[53] can be misleading. Moreover, any description of the quality of an eye in diopters is generally troublesome because the visual effect of diopters varies with pupil size, that is, the same dioptric refractive error causes much larger retinal blur and has a more detrimental effect on vision at large pupil sizes than at small pupils.[62,63]

Some studies have published normative results for the MTF of the eye: Artal et al.[73] used two age-groups of five subjects and one pupil size, while Guirao et al.[75] used larger samples from three age-groups and three pupil sizes, and others[84,85] have modelled MTFs across pupil sizes and age. Although the MTF metric combines the effect of all aberrations on contrast transfer, it considers neither the sensitivity and limits of the neural processing of the visual system, nor phase errors, which have been shown to influence visual quality.[86,87]

The evolution of optical metrics, such as the MTF, to include consideration of the neural processing of the visual system gave rise to visual image quality metrics,[15,38,39,88,89] which combine a comprehensive description of the optics of an eye – provided by wavefront sensing – with a measure of the neural transfer function of the human visual system.

Therefore, the purpose of this paper is to provide normative best-corrected values for a visual image quality metric, which incorporates both the optical and neural components of the visual system, as a function of pupil size and age. Given the reported variability of subjective methods of refraction,[32–34] these benchmarks are determined objectively – therefore unaffected by subjective performance and adaptation – and represent the best theoretical level of visual image quality (as measured by VSX) that is achievable with a sphere, cylinder, and axis (SCA) correction in a normal eye.

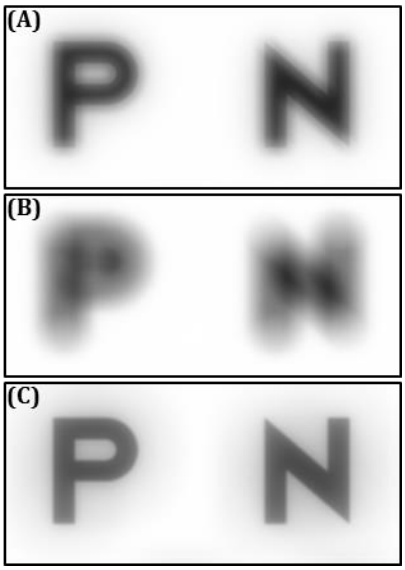

Figure 3. 1 The shortcoming of root mean square (RMS) wavefront error (WFE) is that it does not capture the visual interaction of aberrations. (A) Spherical aberration alone, RMS = 0.200 μm. (B) Defocus alone, RMS = 0.451 μm. (C) Spherical aberration + defocus, RMS = 0.493 μm. Note that with the addition of these aberrations RMS WFE increases (worsens), while image quality actually improves.

The particular metric that will be presented is the visual Strehl ratio (VSX), which has been shown predictive of subjective best focus,[15,19] well correlated with change in visual acuity (VA),[20,22,24] and able to identify a sphere, cylinder, and axis (SCA) prescription that performs equivalently to subjective refraction,[29] independent of pupil size and underlying WFE.[24] We have calculated VSX according to its original definition (equation A23 from Thibos et al.;[15] also included below). As shown in equation (1), VSX is the ratio of the volume under the weighted PSF of an eye at a given pupil size to the volume under the weighted diffraction-limited PSF for the same pupil size. The weighting function in both cases is the inverse Fourier transform of the photopic neural contrast sensitivity function (nCSF) determined using interference fringes.[16] In this form, VSX ranges from 0 to 1, with 1 being best.

It has been suggested[17,18] that visual image quality metrics should be normalized using the neurally weighted PSF for a diffraction-limited 3 mm pupil diameter irrespective of the pupil size of the eye (this metric could be referred to as VSX*). The virtues of VSX and VSX* are considered in the Discussion, however their values were found to be very similar and, therefore, data from the original definition of VSX are presented throughout the Results.

$$VSX = \frac{\int_{psf} PSF\,(x,y)N(x,y)dxdy}{\int_{psf} PSF_{DL}\,(x,y)\,N(x,y)dxdy}$$

3.3 Methods

The study followed the tenets of the Declaration of Helsinki and University of Houston Institutional Review Board approval.

Wavefront error data collected during the Texas Investigation of Normal and Cataract Optics (TINCO) study were analyzed. Collection of the TINCO data and description of subjects are described in detail elsewhere;[4,90] briefly, the TINCO study investigated the aberration structure of normal healthy eyes as crystalline lens opalescence increases naturally with aging. Subjects with cortical and / or posterior subcapsular cataracts graded (independently by five masked clinicians) as >2 according to The Lens Opacities Classification System III (LOCS-III) [91] were excluded, as were subjects with any ocular pathology or abnormality (such as strabismus or amblyopia), previous ocular surgery, or neurological or systemic condition that affected the visual system. The preferred eyes of 146 normal subjects between the ages of 20 and 80 years of age were dilated with one drop of tropicamide 1% and one drop of neosynephrine 5%. Wavefront error measurements were recorded using a custom built Shack-Hartmann wavefront sensor over the maximum dilated pupil, described by a 10th radial order normalized Zernike polynomial fit, and algebraically scaled down (concentrically using the center of the dilated pupil) to 7mm, 6mm, 5mm, 4mm, and 3mm pupil diameters.[92] It has been shown that scaling down from a larger pupil size is preferable to re-fitting the wavefront error over a smaller pupil using fewer points.[93] Two eyes did not dilate to a 6 mm pupil diameter, and an additional 32 eyes did not dilate to 7 mm. The number of subjects per pupil size and age group is shown in Table 3.1.

For each eye at each pupil size, the second-order defocus term was mathematically compensated for the shift due to chromatic aberration from the measured 840 nm to the desired 555 nm by extrapolating the flattening portion of the hyperbolic equation defined in reference[94] to 840 nm. Validation of this extrapolation has been confirmed experimentally.[95,96] Changes in HOAs due to change in wavelength have been found to be non-uniform,[97] rendering a single adjustment factor inappropriate. However, these changes in HOAs have also been shown to be insignificant,[95,98] and therefore no other terms were adjusted.

The SCA combination (sphere and cylinder to the nearest 0.25 D, and axis in 2° increments) that maximized visual image quality (VSX) was then objectively identified using a simulated through focus experiment as previously described,[29] by calculating VSX for a set of 95454 SCA prescriptions. Although this meant that eyes with low astigmatism were sampled at small dioptric increments, our intention was to frame the analyses using units (sphere, cylinder, and axis) that were clinically available and familiar rather than using units of one of the mathematically uniform dioptric spaces. Consequently, instead of searching axis in increments that varied with cylinder magnitude, the highest accuracy, that is 2°, specified by the American National Standards Institute (ANSI Z80.1-2015)[99] was used as the axis increment for all eyes.

Subjects' refractive errors varied from +4.75 to –6.75 D sphere and 0 to -3.50 D cylinder. Younger eyes tended to be slightly more myopic than older eyes, but both spherical and astigmatic refractive errors were generally well distributed across age groups.

Table 3. 1 Number of Subjects per Pupil Diameter (mm) and Age Group (years)

Age Group	Mean Age ± SD	Maximum Age	Minimum Age	Subjects per Pupil Size		
				3, 4, 5	6	7
20–29	25.2 ± 2.3	29.8	21.6	20	20	18
30–39	35.0 ± 2.4	38.7	30.1	18	18	15
40–49	45.2 ± 2.8	49.9	40.5	32	32	29
50–59	54.4 ± 2.9	58.7	50.5	32	31	18
60–69	62.9 ± 1.9	67.4	60.3	21	20	16
70–79	72.9 ± 2.4	78.4	70.0	23	23	16
		Total Count		146	144	112

Means and 95% confidence intervals for SCA best-corrected VSX were determined for each pupil size and age group. The mean best-corrected VSX, as well as the base 10 logarithm of VSX (logVSX), for each unique age group and pupil size combination were used to determine the multiple (two-element) regression of VSX (and logVSX) as a function of age and pupil size.

Towards normative validation of these data, best-corrected VSX was calculated for an independently collected WFE dataset (the Rochester Ocular Wave Aberration Study; Porter el al.[100]) of 218 normal eyes that spanned a similar age range (21 to 65 years old). These WFEs underwent a similar defocus correction for chromatic aberration (from 780 to 555 nm)[94] and the resultant SCA best corrected image quality values were compared with the confidence intervals of the TINCO dataset.

3.4 Results

The quantitative relationship between visual image quality, pupil size, and age, shown in Figure 3.2, agrees with the prevailing qualitative clinical understanding of how these variables interact. Best VSX was found in young eyes (20 to 30 years old) at small pupil diameters (3mm), and VSX decreased as age increased and as pupil size increased, with pupil size causing a more rapid decrease. Both pupil size and age had statistically significant influence on visual image quality ($p<0.0001$), and the multiple regressions for the mean and 95% confidence intervals of the three variables were

$$\text{mean logVSX} = 0.414 - (0.122*\text{pupil size}) - (0.005*\text{age}) \quad (2)$$

$$\text{upper 95\% CI} = 0.501 - (0.104*\text{pupil size}) - (0.005*\text{age}) \quad (3)$$

$$\text{lower 95\% CI} = 0.321 - (0.140*\text{pupil size}) - (0.006*\text{age}). \quad (4)$$

In the above regressions, as well as in Figure 3.2, logVSX is used rather than VSX, because logVSX has been shown to have a linear relationship with logMAR VA.[24] The regressions for the upper and lower confidence intervals facilitate the calculation of normative best SCA corrected visual image quality ranges for any pupil size and age. Corresponding multiple regressions for VSX can be found in the Appendix 2a.

The full set of best-corrected VSX and logVSX results as a function of pupil size and age, including means, standard deviations, maximum and minimum values, and 95% confidence intervals are presented in reference format in Tables 3.2 and 3.3 of the Appendix.

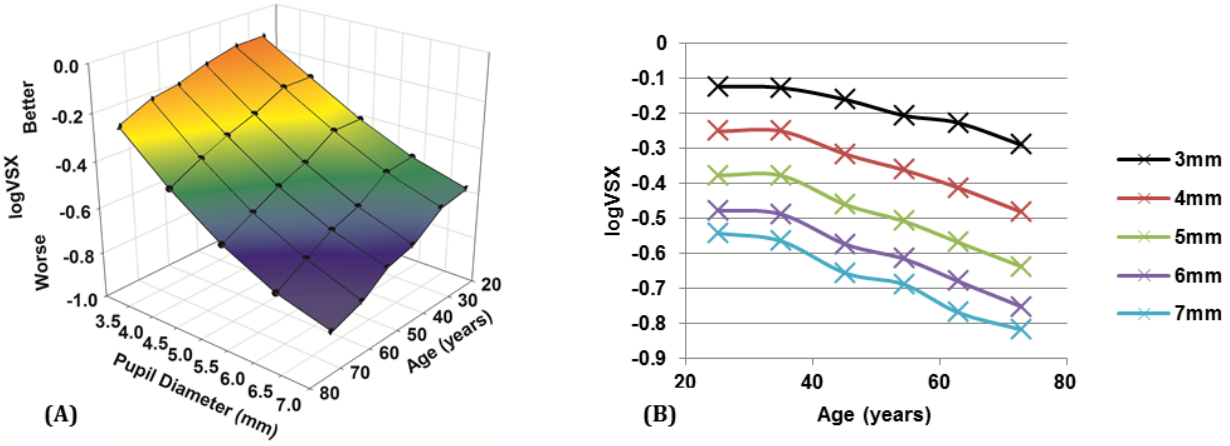

Figure 3. 2 (A) Quantitative relationship between best-corrected visual image quality (logVSX), pupil diameter, and age. Black circles are the mean logVSX for the corresponding pupil sizes and means of each age group. (B) Two-dimensional depiction of the same data as in (A). Best visual image quality (logVSX) was found in young eyes (20 to 30 years old) and at small pupil diameters, and decreased as age increased and pupil size increased, with pupil size causing a more rapid decrease.

Best-corrected logVSX values determined for an independently collected set of WFE data[100] from 218 eyes at a 5.7 mm pupil diameter are shown (as black circles) in Figure 3.3 along with the 95% confidence interval determined for the TINCO dataset at 5.7 mm using the regressions provided in equations (2), (3), and (4). No statistically significant difference was found between datasets: The best-corrected logVSX values of 95.4% of the independently measured eyes (208 eyes) were within the 95% confidence interval defined by the TINCO dataset; and as expected for normative data, the remaining eyes were split almost equally above and below the confidence interval (2.8% (6 eyes) above and 1.8% (4 eyes) below).

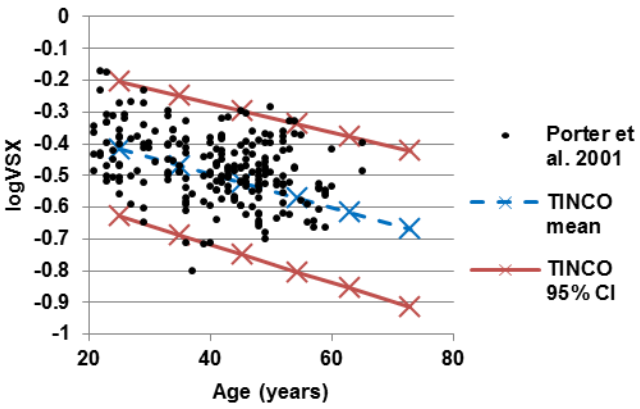

Figure 3. 3 Best-corrected logVSX for an independently collected set of WFE data (the Rochester Ocular Wave Aberration Study96) from 218 eyes at 5.7 mm pupil diameter (black circles) and mean and 95% confidence interval determined from the TINCO dataset. Best-corrected logVSX of 95.4% of these independently measured eyes were within the TINCO 95% confidence interval.

3.5 Discussion

We have presented mean and confidence interval values for the objectively determined best-corrected visual image quality (VSX) provided to normal eyes by sphere and cylinder prescriptions, as a function of pupil size and age, and have validated these normative values using a large independently collected dataset.[100] The means and confidence intervals provided here constitute a normative reference with which the visual image quality of an individual eye at a given age and pupil size can be compared and has the potential to be useful in sample size calculations as well as the design and manufacture of ophthalmic products across different correction modalities.

3.5.1. Comparison with other studies

A cross sectional reference of normative values of VSX is given by Thibos,[101] where visual image quality was calculated for 1000 simulated eyes generated from a statistical model[102] and for 100 real eyes (from the Indiana Aberration Study).[53] Unfortunately the age distribution of the 100 real eyes was very homogeneous – most were in the 20 to 29 and 30 to 39 age groups and the statistical model[102] was based on the same sample. Metric values were presented for a 6 mm pupil diameter.

The mean ±SD logVSX values were –0.51 ±0.19 for the 100 real eyes and –0.55 ±0.21 for the 1000 simulated eyes, which are similar to the corresponding values of this study, –0.48, –0.49, and –0.58, for the 20 to 30, 30 to 40, and 40 to 50 age groups respectively (see Table 3.2).

The findings of this study were also in general agreement with the literature: Best visual image quality was found in young eyes and at small pupil sizes, which confirms findings of optical metrics such as higher order (HO) RMS,[4] and MTF,[73,75] as well as measures of total visual performance (combining the optical and neural components) such as contrast sensitivity (CSF) (see Owsley[103] for a review) and VA.[58]

The literature is divided on the cause of the abovementioned decrease in overall visual performance with age. Some studies[12,14,76] suggest that neural changes have a significant contribution, while others[73,104,105] suggest that optical changes are primarily responsible and that neural changes are insignificant.

Certain optical changes, such as scatter due to crystalline lens opalescence, increase with age[90] and are not captured by VSX. Although large amounts of scatter could be expected to reduce retinal image quality,[106,107] visual acuity has been shown to be largely unaffected by scatter.[107] We believe the effect of scatter on the interpretation of the present data to be minimal because subjects with cortical and / or posterior subcapsular cataracts graded as >2 according to LOCS-III were excluded, and the data agreed with an independently collected wavefront error set with a similar age distribution. A full description of the nature and degree of lens opaciification present in the TINCO subjects can be found in Table 4 of Applegate et al.[4]

The photopic neural transfer function used in the calculation of VSX is derived from the nCSF of Campbell and Green,[16] which was measured on a 27 year old subject. Given the uncertainty in the stability of the neural processing with age, all visual image quality metrics should be framed as describing the optical quality of an eye in terms of the sensitivity of a healthy normal visual system. Work is underway in our laboratory to evaluate the personalization of these metrics for eyes that are not considered healthy or normal.

3.5.2. Are these normative levels of visual image quality clinically achievable?

The eyes analyzed here (both the TINCO eyes and the eyes from Porter et al.[100]) underwent an objective simulated through focus refraction that identified the SCA combination that optimized VSX. This method has been shown to provide equivalent VA to subjective refraction.[29] The question arose as to whether the normative confidence intervals presented here establish benchmarks of visual image quality that would be achievable with other SCA

combinations not optimized for VSX but still considered clinically acceptable, given the variability of clinical subjective refraction.[32–34]

Towards this end, for each of the 218 eyes from Porter et al.[100] all SCA combinations (sphere and cylinder in 0.25 D steps and axis in 2° steps) that provided VSX better than the lower 95% confidence interval of the TINCO norms were identified. The mean ±SD number of prescriptions was 264 ±183; the median was 240. (The four eyes that did not surpass the TINCO lower 95% confidence interval had zero SCA combinations for this analysis.) In other words, although adaptation and other factors can influence subjective refraction, for the majority of these eyes there are many SCA combinations (in addition to the one that optimized VSX) that would provide a VSX level within the 95% TINCO confidence intervals. However, the number of prescriptions in this group is dependent on the dioptric increments that are used (for instance, fewer SCA combinations would correct an eye to within the 95% confidence interval if axis was sampled in 5° steps). Consequently, the dioptric distance from the best SCA correction to the TINCO lower 95% confidence interval was estimated (using power vectors[47]), by calculating the dioptric difference between the best SCA combination (that optimized VSX) and the "worst" SCA prescription that still corrected an eye to within the confidence interval. The mean ±SD dioptric distance was 0.41 ±0.23 D; the median was 0.36 D. Despite that dioptric spaces are not visually uniform and a given dioptric difference could have different visual interactions with the underlying aberrations of different eyes, this Euclidean dioptric distance provides an indication of how dioptrically different a refraction can be from the optimal objective refraction and still provide an eye with visual image quality within the TINCO 95% confidence interval norms. It is

also likely that eyes with high astigmatism will have fewer SCA combinations that correct them to within the normative levels of visual image quality presented here.

The SCA prescriptions that maximized VSX for the TINCO eyes generally did not change by a clinically significant amount across the range of pupil sizes examined. The mean variability (SD) of the spherical and astigmatic components (in power vectors)[47] across all 148 eyes were less than 0.08 D. This is consistent with the finding that subjective refraction of normal eyes does not vary significantly across pupil sizes.[108]

The VSX metric presented here describes monochromatic visual image quality, which would be degraded by chromatic aberration in natural viewing conditions. Chromatic aberration of the eye has been shown to be essentially constant across studies and populations.[94] Although the use of polychromatic metrics has been advocated,[109] they have been found to not provide a significant benefit over monochromatic metrics.[39]

While the VSX metric tracks subjective image quality for pupil sizes greater than 3 mm, it may not accurately describe subjective visual image quality over smaller pupil diameters. At such small pupil sizes, the diffraction-limited PSF (the denominator) used in normalizing the metric is significantly deteriorated by diffraction, while the aberrations of normal eyes (the numerator) are also greatly reduced. As a result, metric values may approach 1 (excellent) while visual image quality is actually quite poor due to diffraction. In these situations, normalizing the metric (VSX*) to a constant pupil size, such as 3 mm, as has been done for other visual image quality metrics,[17,18] could provide a more realistic assessment of visual image quality.

However, for pupil sizes greater than 3 mm (such as the normative data presented here) renormalizing to a 3 mm pupil diameter (VSX*) was only minimally different to the VSX values. Renormalization increased the metric value as the numerator pupil size increased, but the maximum increase was less than 5 % of the VSX value. This increase was small chiefly due to the effect of the neural weighting of the PSFs in the calculation of VSX and VSX*. Thus the choice between fixed and variable pupil size for normalization is of no practical importance for computing VSX for pupil sizes greater than 3 mm. However, other metrics that do not incorporate a visual or neural weighting, such as the traditional Strehl ratio, are more affected by the choice of reference pupil size. In those metrics, normalization by a fixed standard may be preferred in applications where absolute image quality is more important than image quality relative to a standard that varies with pupil size.

3.6 Conclusions

The quantitative relation of SCA best corrected visual image quality (logVSX), pupil size, and age is presented and 95% confidence interval norms are provided for pupil size from 3 to 7 mm and for age groups between 20 and 80 years, as well as regression equations for the calculation of logVSX at any individual age and pupil size. These objectively determined benchmarks represent the best theoretical levels of visual image quality that normal eyes can achieve with conventional sphere, cylinder, and axis corrections and can be useful in evaluating both traditional and wavefront-guided optical corrections across different modalities.

Table 3. 2 Best-corrected VSX values as a function of pupil diameter (mm) and age (years)

Age	Pupil Diameter	Mean VSX ± SD	Upper 95% CI	Lower 95% CI	Max VSX	Min VSX
20–29	3	0.762 ± 0.111	0.979	0.545	0.919	0.531
20–29	4	0.574 ± 0.116	0.801	0.346	0.745	0.331
20–29	5	0.432 ± 0.099	0.625	0.238	0.584	0.229
20–29	6	0.344 ± 0.084	0.509	0.179	0.491	0.173
20–29	7	0.294 ± 0.068	0.428	0.161	0.412	0.159
30–39	3	0.757 ± 0.114	0.980	0.535	0.922	0.484
30–39	4	0.578 ± 0.138	0.849	0.306	0.859	0.341
30–39	5	0.434 ± 0.122	0.674	0.194	0.724	0.264
30–39	6	0.338 ± 0.102	0.538	0.137	0.575	0.207
30–39	7	0.283 ± 0.087	0.454	0.112	0.470	0.170
40–49	3	0.701 ± 0.116	0.929	0.473	0.877	0.497
40–49	4	0.496 ± 0.114	0.720	0.272	0.680	0.307
40–49	5	0.356 ± 0.086	0.525	0.188	0.496	0.206
40–49	6	0.275 ± 0.067	0.407	0.143	0.385	0.156
40–49	7	0.228 ± 0.057	0.340	0.115	0.325	0.129
50–59	3	0.640 ± 0.148	0.929	0.351	0.876	0.370
50–59	4	0.457 ± 0.147	0.745	0.169	0.798	0.230
50–59	5	0.331 ± 0.124	0.573	0.088	0.646	0.155
50–59	6	0.257 ± 0.094	0.441	0.072	0.506	0.118
50–59	7	0.213 ± 0.066	0.341	0.084	0.387	0.140
60–69	3	0.601 ± 0.097	0.790	0.412	0.773	0.468
60–69	4	0.395 ± 0.083	0.559	0.231	0.585	0.261
60–69	5	0.277 ± 0.068	0.410	0.145	0.444	0.165
60–69	6	0.215 ± 0.054	0.320	0.110	0.354	0.126
60–69	7	0.175 ± 0.046	0.265	0.086	0.296	0.104
70–79	3	0.525 ± 0.116	0.753	0.297	0.785	0.352
70–79	4	0.342 ± 0.095	0.527	0.156	0.551	0.190
70–79	5	0.240 ± 0.076	0.389	0.092	0.421	0.128
70–79	6	0.185 ± 0.059	0.301	0.069	0.325	0.097
70–79	7	0.158 ± 0.049	0.254	0.063	0.267	0.098
All Ages	3	0.661 ± 0.143	0.941	0.380	0.922	0.352
All Ages	4	0.469 ± 0.142	0.748	0.190	0.859	0.190
All Ages	5	0.341 ± 0.118	0.572	0.110	0.724	0.128
All Ages	6	0.266 ± 0.094	0.451	0.081	0.575	0.097
All Ages	7	0.226 ± 0.078	0.378	0.074	0.470	0.098

Table 3. 3 Best-corrected logVSX values as a function of pupil diameter (mm) and age (years)

Age	Pupil Diameter	Mean logVSX ± SD	Upper 95% CI	Lower 95% CI	Maximum logVSX	Minimum logVSX
20–29	3	-0.123 ± 0.067	0.000	-0.255	-0.037	-0.275
20–29	4	-0.251 ± 0.096	-0.062	-0.439	-0.128	-0.480
20–29	5	-0.377 ± 0.111	-0.160	-0.594	-0.233	-0.641
20–29	6	-0.477 ± 0.118	-0.246	-0.709	-0.309	-0.761
20–29	7	-0.543 ± 0.107	-0.333	-0.753	-0.386	-0.799
30–39	3	-0.126 ± 0.070	0.000	-0.264	-0.035	-0.316
30–39	4	-0.250 ± 0.104	-0.047	-0.454	-0.066	-0.467
30–39	5	-0.377 ± 0.115	-0.152	-0.602	-0.140	-0.579
30–39	6	-0.488 ± 0.120	-0.253	-0.723	-0.241	-0.685
30–39	7	-0.565 ± 0.125	-0.320	-0.811	-0.328	-0.770
40–49	3	-0.160 ± 0.074	-0.016	-0.305	-0.057	-0.304
40–49	4	-0.317 ± 0.104	-0.113	-0.520	-0.168	-0.512
40–49	5	-0.461 ± 0.111	-0.243	-0.680	-0.305	-0.685
40–49	6	-0.575 ± 0.113	-0.353	-0.797	-0.414	-0.808
40–49	7	-0.657 ± 0.117	-0.429	-0.886	-0.488	-0.890
50–59	3	-0.206 ± 0.105	0.001	-0.412	-0.057	-0.432
50–59	4	-0.362 ± 0.139	-0.089	-0.635	-0.098	-0.639
50–59	5	-0.508 ± 0.157	-0.201	-0.815	-0.190	-0.811
50–59	6	-0.616 ± 0.151	-0.320	-0.913	-0.296	-0.930
50–59	7	-0.689 ± 0.123	-0.448	-0.930	-0.412	-0.853
60–69	3	-0.227 ± 0.069	-0.091	-0.362	-0.112	-0.330
60–69	4	-0.412 ± 0.090	-0.236	-0.589	-0.233	-0.583
60–69	5	-0.569 ± 0.104	-0.364	-0.774	-0.352	-0.782
60–69	6	-0.680 ± 0.108	-0.468	-0.892	-0.451	-0.900
60–69	7	-0.770 ± 0.111	-0.553	-0.987	-0.528	-0.983
70–79	3	-0.290 ± 0.097	-0.101	-0.479	-0.105	-0.453
70–79	4	-0.482 ± 0.120	-0.247	-0.717	-0.259	-0.720
70–79	5	-0.638 ± 0.132	-0.380	-0.897	-0.376	-0.894
70–79	6	-0.753 ± 0.134	-0.491	-1.016	-0.487	-1.011
70–79	7	-0.819 ± 0.129	-0.565	-1.073	-0.574	-1.010
All Ages	3	-0.191 ± 0.100	0.000	-0.386	-0.035	-0.453
All Ages	4	-0.349 ± 0.136	-0.083	-0.615	-0.066	-0.720
All Ages	5	-0.493 ± 0.152	-0.195	-0.791	-0.140	-0.894
All Ages	6	-0.603 ± 0.155	-0.299	-0.906	-0.241	-1.011
All Ages	7	-0.671 ± 0.149	-0.379	-0.963	-0.328	-1.010

3.7 Appendix

3.7.1 Regressions

These multiple regressions allow the calculation of normative VSX (mean and 95% confidence interval (CI)) values for any particular pupil size and age. The corresponding regressions for logVSX are presented in the Results section.

VSX

mean VSX = 1.148 – (0.108*pupil size) – (0.004*age) (5)

upper 95% CI = 1.529 – (0.137*pupil size) – (0.005*age) (6)

lower 95% CI = 0.766 – (0.079*pupil size) – (0.003*age) (7)

Chapter 4: Comparison of Wavefront-Guided and Best Conventional Scleral Lenses after Habituation in Eyes with Corneal Ectasia.

Reprinted with modifications from:[110] Hastings GD, Applegate RA, Nguyen LC, Kauffman MJ, Hemmati RT, Marsack JD. Comparison of Wavefront-Guided and Best Conventional Scleral Lenses after Habituation in Eyes with Corneal Ectasia. Optom Vis Sci (2019) 96(4):238–247. doi:10.1097/OPX.0000000000001365.

4.1 Abstract

SIGNIFICANCE

Visual performance with wavefront-guided (WFG) contact lenses has only been reported immediately after manufacture without time for habituation, and comparison has only been made with clinically unrefined predicate conventional lenses. We present comparisons of habitual corrections, best conventional scleral lenses, and WFG scleral lenses after habituation to all corrections.

PURPOSE

To compare, in a cross-over design, optical and visual performance of eyes with corneal ectasias wearing dispensed best conventional scleral lens corrections and dispensed individualized WFG scleral lens corrections.

METHODS

Ten subjects (20 eyes) participated in a randomized cross-over study where best conventional scleral lenses and WFG scleral lenses (customized through the 5th radial order) were worn for eight weeks each. These corrections, as well as each subject's habitual correction and normative data for normal eyes, were compared using (1) residual higher-order aberrations (HORMS), (2) visual acuity (VA), (3) letter contrast sensitivity (CS), and (4) visual image quality (logVSX). Correlations were performed between Pentacam biometric measures and gains provided by WFG lenses.

RESULTS

Mean HORMS reduced 48% from habitual to conventional, and 43% from conventional to WFG. Mean logMAR VA improved from habitual (+0.12) to conventional (–0.03) and further with WFG (–0.09); six eyes gained >1 line with WFG over conventional. Area under CS curve improved 26% from habitual to conventional and 14% from conventional to WFG. Eyes achieving normal levels: HORMS: conventional 40%, WFG 85%; VA: conventional 50%, WFG 85%; CS: conventional 60%, WFG 90%. LogVSX improved 16% from habitual to conventional and 25% further with WFG. Reduction in aberrations with WFG lenses best correlated with posterior cornea radius of curvature.

CONCLUSIONS

Visual performance was superior to that reported with non-habituated WFG lens wear; with WFG lenses HORMS and logVSX significantly improved, allowing more eyes to reach normal levels of optical and visual performance than with conventional lenses.

4.2 Introduction

Decreased visual performance in corneal ectasias such as keratoconus is predominantly optical in origin, typically resulting from bilaterally-asymmetric elevated higher-order aberrations caused by the rotationally-asymmetric irregular profiles of anterior and posterior corneal surfaces.[111–113] Onset of most ectatic conditions is during adolescence and these individuals usually experience normal visual stimulation throughout critical periods of development and undergo typical neural development. Hence, if the aberrated optics of these

eyes can be appropriately corrected, normal levels of visual performance are expected to recover after habituation to the improved retinal image.

Current standards of care for corneal ectasias are rigid corneal or scleral lenses, which partially mask anterior cornea irregularities through approximate refractive index matching of the post-lens tear film and cornea, and by providing a new optically well-formed first surface for the eye. Those refractive indices are, however, not perfectly matched and residual anterior corneal surface aberrations remain, as do aberrations from the irregular posterior corneal surface[111–113] which cannot be masked by rigid contact lenses.

Wavefront-guided contact lens technology is designed to specifically target the unique aberrations of individual eyes, particularly the elevated levels of residual aberrations experienced by highly aberrated eyes wearing conventional contact lenses.[112,114–116]

While customized wavefront-guided contact lenses have been manufactured and demonstrated with varying levels of efficacy in laboratory settings,[117–121,79,122–124,80] and studied using simulations and theoretical modelling,[125–133] those studies that measured visual performance with these lenses[117–121,79,122–124,80] did so immediately after manufacturing and fitting the lenses without allowing time for the visual systems of the wearers to habituate to the new percept.

Previous studies compared wavefront-guided lenses with habitual or conventional lenses that served as predicate stepping-stones (for wavefront-guided lenses) and were not necessarily

clinically optimized in terms of their fit and optics.[79,80,120,121,123] In some studies, sphero-cylindrical components of the wavefront-guided lenses have been corrected using spectacle trial lenses before evaluating visual performance[121,123,124] and, consequently, lenses were not dispensed.

Allowing the visual system time to adapt is common clinical practice when dispensing progressive addition lenses, large changes in prescriptions, high cylinders, or after ocular surgery. Likewise, when highly aberrated eyes are acutely corrected (without providing time for adaptation) with adaptive optics, visual performance is improved, but not to normal levels,[134] and further gains are only achieved after habituation or training.[135]

Given that the visual system is adapted to its habitual aberration structure,[37,134] and given the considerable reduction in aberration magnitude imparted by wavefront-guided lenses (in this study and others[80,123]) along with the reversal[112,113] in key aberrations (such as coma) associated with directional blur, patients should habituate to the corrections before visual performance is evaluated. While visual performance reported with wavefront-guided lenses has been improved, we postulate it has hitherto remained worse than normal (despite reduced levels of aberration[79,122,123,80,136]) due to insufficient habituation time and / or the interaction of residual aberrations being detrimental to visual image quality.

As wavefront-guided technology becomes more accessible, it is important to present controlled comparisons of state of the art wavefront-guided scleral lenses with the best conventional scleral lenses prescribed in practice. In fact, first achieving clinically typical

performance with best conventional scleral lenses is an essential prerequisite in appreciating any real gains in performance provided by wavefront-guided lenses and in identifying which eyes would benefit most from wavefront-guided lenses over conventional lenses.

Therefore, this paper presents comparison of three corrections: (1) the subject's habitual correction, (2) a best conventional scleral lens, (3) and a best individualized wavefront-guided scleral lens, after lenses were dispensed and worn as part of daily life by eyes with corneal ectasias, which allowed approximately eight weeks of habituation to each new correction in a cross-over manner. This comparison is presented in terms of (1) residual higher-order root mean square (RMS) wavefront error, (2) high contrast visual acuity, (3) letter contrast sensitivity, and (4) the visual image quality metric logVSX (the logarithm of the visual Strehl ratio). Correlations between ocular biometric measures and the reduction in higher-order aberrations provided by the wavefront-guided lenses over conventional lenses are examined.

4.3 Methods

This research adhered to the tenets of the Declaration of Helsinki. Prior to data collection, the nature and potential consequences of the study were explained to each subject and University of Houston Institutional Review Board approved informed consent was signed.

4.3.1 Subjects

Ten subjects (nine male, one female) with corneal ectasia were recruited; nine were diagnosed with bilateral keratoconus and one with bilateral pellucid marginal degeneration.

These conditions characteristically present with bilaterally-asymmetric disease severities,[114,137] and the ectasias of some fellow eyes were quite mild (these eyes stood to benefit less from wavefront-guided lenses than more severe ectasias). Nonetheless, both eyes of each subject (20 eyes) were included because each eye presented unique optical and fitting challenges. Appropriate statistical methods[54,55] (see Results) were used to account for any dependency between right and left eyes of each individual.

Table 1 classifies the severity of the subjects in terms of the ABCD Keratoconus Grading System,[138] which incorporates anterior ("A") and posterior ("B") corneal radii of curvature and thinnest pachymetry ("C"), all determined by Topometric KC Staging software on the Pentacam HR (Oculus Inc., Arlington WA), as well as best-corrected distance VA ("D"). Grading ranges from 0 (normal) to 4 (most severe).

Five subjects used spectacles for the habitual correction measurements; three used contact lenses on both eyes (two wore sclerals, one wore hybrids); one used a toric soft lens on one eye and was unaided in the other; and one subject performed the habitual correction measurements unaided. Mean (± SD) age of the subjects was 34.4 ±11.1 years (range: 24 to 55). Inclusion criteria: no corneal scarring over the central 7 mm of the pupil and unremarkable systemic and other ocular health.

4.3.2 Performance measures

Performance measures were recorded monocularly.

4.3.2.1 Higher-order root mean square wavefront error

Three wavefront error measurements recorded using a COAS HD wavefront sensor (Johnson and Johnson Vision, Santa Ana CA) and described by a 10^{th} radial order normalized Zernike polynomial fit, were averaged over a common dilated pupil size.

4.3.2.2 Visual acuity

High contrast visual acuity was measured in a darkened room and calculated with per-letter scoring, terminating after five missed letters, as the mean of three unique ETDRS logMAR charts displayed with –100% Weber contrast (Display++ monitor; Cambridge Research Systems, Kent UK) and background luminance of 116 cd/m^2 (Minolta LS-110, Konica Minolta, Ramsey, New Jersey).

4.3.2.3 Letter contrast sensitivity

Using the same monitor and darkened room, letter contrast sensitivity was measured using letter sizes having fundamental-spatial frequencies of 4, 8, and 16 cycles per degree (20/150, 20/75, and 20/37.5 respectively) and area under the log contrast sensitivity function curve[139] was calculated. For each letter size, contrast threshold was estimated to the nearest 0.2 log unit, after which three measures of contrast threshold were determined using rows of unique Sloan letters that began at a contrast level 0.4 log units above the initial estimate and reduced in steps of 0.1 log units per line until five letters were missed.

4.3.2.4 The logarithm of the visual Strehl ratio (logVSX)

Visual image quality was quantified using logVSX,[15] a single value metric combining comprehensive description of the optics (here, wavefront error of an eye wearing a correction) with a measure of the neural processing of the visual system. LogVSX has been shown predictive of subjective best focus,[15,19] and able to identify spectacle prescriptions equivalent to subjective refraction.[29] Change in logVSX has been well correlated with change in logMAR visual acuity.[22,24]

VSX ranges from 0 (worst) to 1 (best). The (base 10) logarithm of 1 is 0, thus, the closer the value of logVSX to 0 (the less negative the value), the better the visual image quality. LogVSX was calculated from mean wavefront error (of the corrected eyes) over 5 mm pupil diameters.

4.3.3 Study format and lens designs

The study protocol began with measurement of the four outcomes using the habitual correction. Thereafter, fitting (but not necessarily dispensing) of conventional scleral lenses commenced, which involved adjusting the designs of the lenses to provide healthy, comfortable fits that were rotationally and translationally stable, and to refine sphere, cylinder, and axis.

The macro design of the conventional and wavefront-guided scleral lenses is described in detail elsewhere.[80] Briefly, lenses were manufactured at the Visual Optics Institute, University of Houston, College of Optometry, using a DAC 2X-ALM OTT ophthalmic lens lathe (DAC

International, Carpinteria CA) and Boston XO material (Bausch and Lomb, Rochester NY). Overall diameter ranged from 17 to 18.1 mm. The front surface was aspheric, designed to render the lens free of spherical aberration when on the eye and included a 10 mm central optic zone. The posterior surface contained six curves; the fifth curve was a toric annulus designed to impart rotational stability.[140,141]

After allowing 30 minutes for settling on the eye, lens engravings were monitored to quantify lens rotation and the orientation of the peripheral toric annulus was adjusted in subsequent lens designs to compensate for the observed rotation.[80,141] When a stable and correctly-oriented lens with a clinically acceptable fit was achieved, the location of the pupil center relative to the geometric center of the lens was measured such that the wavefront-guided prescription could be offset in opposite xy-directions relative to the lens center to compensate. Most scleral lenses rested inferior and temporal relative to the center of the pupil[123] and, consequently, most wavefront-guided prescriptions were offset superior and nasal relative to the lens center (Figure 4.1). Thresholds for tolerable lens movements are inversely proportional to the magnitudes of wavefront-guided prescriptions,[125,126,130,132,133] and therefore varied across the range of ectasia severities included here.

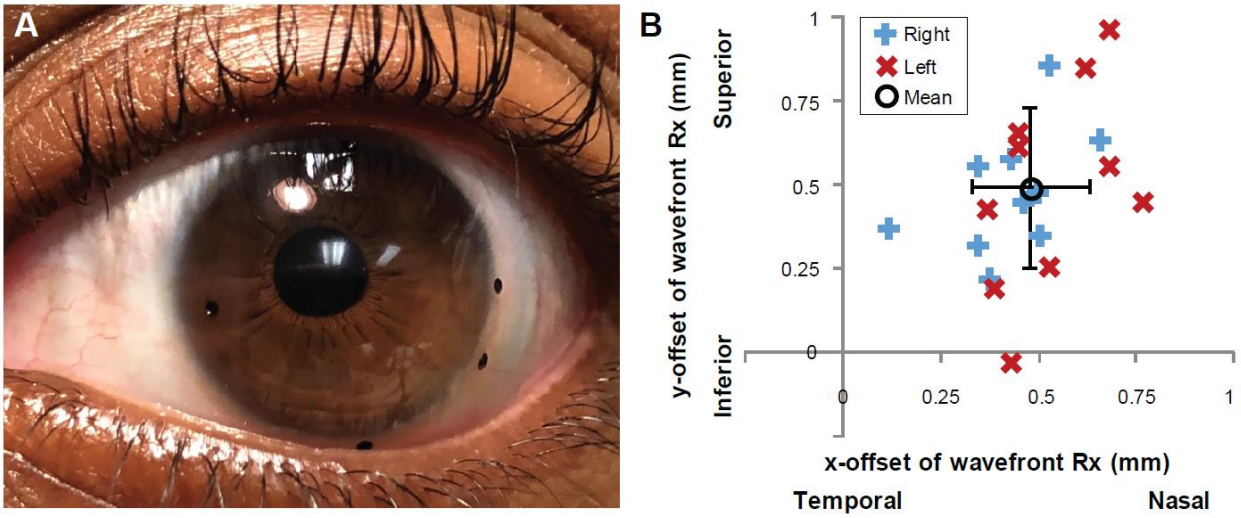

Figure 4. 1 (A) Scleral lens positioned inferiorly and temporally with a small amount of anti-clockwise rotation on a left eye. (B) Distribution of xy-offsets of wavefront-guided prescriptions (relative to the geometric lens center (0,0)) to compensate for lens displacement. Offset of the wavefront-guided prescription compensates for lens misalignment and positions the prescription over the center of the pupil, while observed rotation is corrected by rotation of a peripheral posterior toric curve.

Table 4. 1 Severity of ectasia according the ABCD system[138] of the right and left eyes of each subject, where stage 0 is least severe and stage 4 is most severe. Dimensions: A: anterior radius of curvature; B: posterior radius of curvature; C: thinnest pachymetry; D: best corrected distance vision with each correction.

	S 01		S 02		S 03		S 04		S 05		S 06		S 07		S 08		S 09		S 10	
Dimension	R	L	R	L	R	L	R	L	R	L	R	L	R	L	R	L	R	L	R	L
A:	1	0	4	1	3	4	2	2	2	4	0	0	0	0	2	2	2	2	0	0
B:	2	2	4	2	3	4	2	2	3	4	1	1	0	2	4	4	4	3	0	2
C:	0	0	1	0	2	3	1	1	0	0	0	0	1	2	0	0	2	1	0	0
D (habitual):	0	0	1	0	1	1	0	0	1	2	2	1	1	1	1	1	1	0	0	0
D (conventional):	1	0	0	1	0	1	0	0	1	1	0	1	0	0	1	0	0	1	0	0
D(wavefront):	0	0	0	0	0	0	0	1	1	1	0	0	0	0	0	0	0	0	0	0

Wavefront-guided lenses were designed using the macro parameters of the stable conventional lens. Residual wavefront error was measured through the stable lens after dilation (one drop 1% tropicamide, one drop 2.5% phenylephrine), and an offset wavefront-guided

prescription targeting residual aberrations up to the fifth Zernike radial order[142] was imparted into the anterior lens surface.

Median diameter of the wavefront-guided prescription was 8 mm (mean 7.84 mm); this was limited on the low end by the maximum dilated pupil size, and the wavefront error measurements for eyes with larger pupils were scaled[2] down to 8 mm.

At this point, a cross-over study design was initiated where each subject wore a best conventional scleral lens daily for approximately eight weeks and a wavefront-guided scleral lens daily for an additional eight weeks. This provided an opportunity for the visual system of each subject to habituate to the retinal image formed by each lens in their everyday environment, and follow-up visits provided opportunities (if needed) for refinement of the optics and the fit of each lens (which necessitated manufacture of new lenses). Subjects generally conformed to the eight week time period; some subjects wore a lens type for slightly longer, for example, due to travel or work obligations, illness, or natural disaster (hurricane Harvey). The order of lens wear was randomized; three subjects wore conventional lenses first and seven wore wavefront-guided lenses first. Some subjects that wore the wavefront-guided lenses first, expressed such substantial unhappiness during the conventional lens (second) part of the cross-over that we will re-evaluate this randomization during future studies. One subject did not complete the conventional lens part of the cross-over, but still wore the wavefront-guided lens for eight weeks.

At the final visit with each lens, visual acuity and contrast sensitivity were measured with the lenses through natural pupils, and residual wavefront error was measured over dilated pupils.

4.4 Results

Both statistical and clinical significance are considered. All standard deviations were calculated using ANOVA and components of variance analyses to account for any dependence of right and left eyes.[54,55] Similarly, p-values were calculated using split-plot ANOVAs.[54,55] Plots for individual eyes use lines to track each eye across the three (categorical) corrections and any given eye is consistently represented by the same color, symbol, and line across all four outcomes. The best conventional lens for 18 eyes was spherical and for two eyes was sphero-cylindrical.

4.4.1 Higher-order root mean square wavefront error

Higher-order RMS results were scaled[2] to a 5 mm pupil diameter to better agree with habitual physiological pupil sizes and pupil sizes during visual acuity and contrast sensitivity measures, and are presented up to the 6th radial order.

Mean ±SD higher-order RMS wavefront error decreased from the habitual correction (0.886 ±0.589 μm, mean across modalities) to conventional lenses (0.458 ±0.238 μm), and further decreased to within normal limits with wavefront-guided lenses (0.260 ±0.077 μm) (Figure 4.2). These represent statistically significant reductions of 48% (P = .02) from habitual to conventional, 43% (P = .004) from conventional to wavefront-guided, and 71% (P = .001) from habitual to wavefront-guided. Note the reduction in variability with wavefront-guided lenses.

The unique reduction in higher-order RMS wavefront error for each eye may be better appreciated as the percentage of eyes within age-matched normal (normal eye)[77] limits: 15% of eyes were within normal limits wearing the habitual correction; 40% with best conventional scleral lenses; and 85% with wavefront-guided lenses. A representative example of higher-order wavefront error maps (across unaided and the three corrections) for one subject with moderate keratoconus is shown in Figure 4.3.

Reduction in higher-order aberrations by wavefront-guided lenses over conventional lenses was best correlated (Figure 4.4) with posterior corneal radius of curvature (dimension "B")[138] ($R^2 = 0.75$) followed by the mean severity grading (averaging across dimensions ABC and D for the conventional lens) ($R^2 = 0.62$).

4.4.2 Visual acuity

Mean ±SD logMAR visual acuity improved from the habitual correction (+0.09 ±0.18, mean across modalities) to conventional lenses (–0.03 ±0.09), and improved further with wavefront-guided lenses (–0.09 ±0.10) (Figure 4.5). Disease severity dimension "D" (best corrected distance visual acuity) thus varies dependent on which correction (habitual, conventional, wavefront-guided) is used; for example, subjects in each severity grade of "D" (0:1:2:3:4) were 8:10:2:0:0 with habitual, 12:8:0:0:0 with conventional, and 17:3:0:0:0 with wavefront-guided corrections.

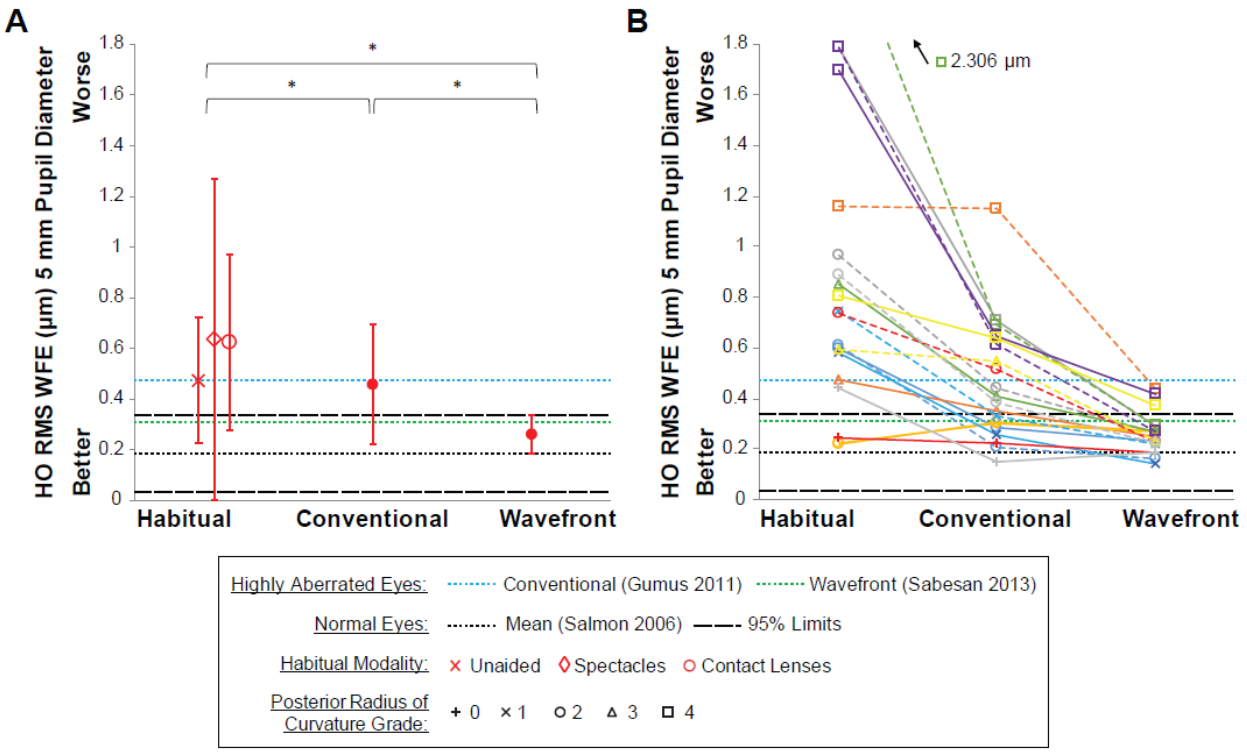

Figure 4. 2 Higher-order root mean square (HO RMS) wavefront error (WFE) across the three corrections for (A) the mean of all eyes and (B) all individual eyes. Error bars are one standard deviation. In (B) two eyes of a subject are plotted in the same color; right eyes solid; left eyes dashed; symbols indicate severity grade of posterior radius of curvature.[138] The 95% limits for normal eyes (Salmon and van de Pol[77]) are plotted as well as mean levels for eyes with keratoconus wearing conventional scleral lenses (Gumus et al.[116]) and wavefront-guided scleral lenses (Sabesan et al.[123]). Study data is scaled[2] in the Discussion for comprehensive comparison with literature; here available data for contact lens related norms have been approximated to a common 5mm using the ratio of pupil sizes.

Mean improvements from habitual to conventional and from habitual to wavefront-guided were statistically significant (P = .048 and P = .007 respectively). Mean improvement from conventional to wavefront-guided was not (P = .07), however, from an individual perspective, six eyes showed clinically significant improvements of greater than one line of logMAR visual acuity and substantially more eyes reached normal[58] levels: habitual correction 25%; conventional lenses 50%; wavefront-guided lenses 85%.

4.4.3 Letter contrast sensitivity

At each fundamental spatial frequency, the majority of eyes improved in letter contrast sensitivity from the habitual correction to conventional scleral lenses, and improved further with wavefront-guided lenses.

Mean ±SD area under the log contrast sensitivity function[139] (Figure 4.6) improved from the habitual correction (11.07 ±3.48, mean across modalities) to conventional lenses (13.91 ±2.20), and improved further with wavefront-guided lenses (15.82 ±2.34). These correspond to significant gains of 26% (P = .009) from habitual to conventional and 43% (P < .001) from habitual to wavefront-guided. The 14% gain from conventional to wavefront-guided was not significant (P = .09). Eyes within normal limits: habitual correction 30%; conventional lenses 60%; wavefront-guided lenses 90%.

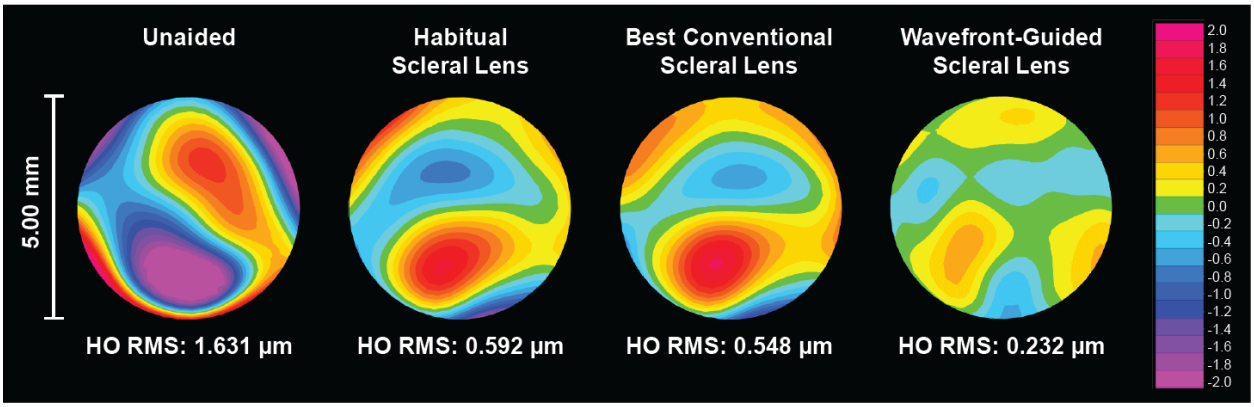

Figure 4. 3 Higher order wavefront error maps for the left eye (corresponding to the dashed yellow line in Figure 4.2B) of a 33 year old male subject with moderate keratoconus.

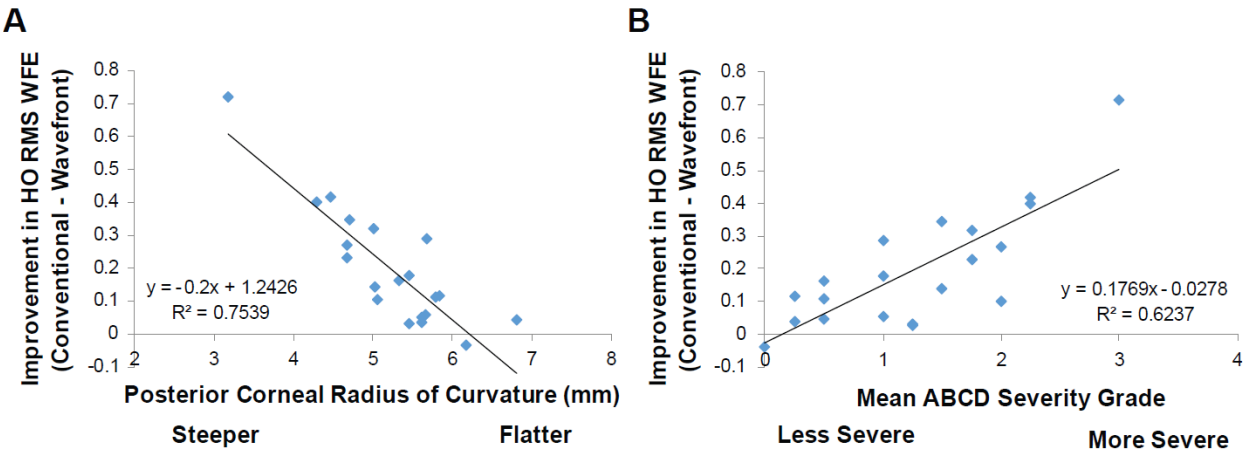

Figure 4. 4 Biometric measures that correlated best with improvement in higher-order root mean square (HO RMS) wavefront error (WFE) from best conventional lenses to wavefront-guided lenses were (A) posterior corneal radius of curvature and (B) mean severity of ectasia[138] (average across severity dimensions "A" anterior corneal radius of curvature, "B" posterior corneal radius of curvature, "C" thinnest pachymetry (all measured with a Pentacam), and "D" distance visual acuity with the best conventional lens).

4.4.4 The logarithm of the visual Strehl ratio (logVSX)

A similar pattern of gains was found for logVSX (Figure 4.7): mean ±SD metric value improved from the habitual correction (–1.55 ±0.48, mean across modalities) to conventional lenses (–1.31 ±0.51), and improved further with wavefront-guided lenses (–0.98 ±0.27). Wavefront-guided lenses provided 37% and 25% statistically significant ($P < .0001$ and $P = .019$ respectively) better visual image quality than the habitual and conventional corrections. The 16% improvement from habitual to conventional was not significant ($P = .11$). While the pattern of results for logVSX agrees with the other outcomes and best visual image quality was provided by the wavefront-guided lenses, the majority (18) of eyes did not reach the high logVSX levels theoretically obtained by objectively best-correcting normal eyes.[30]

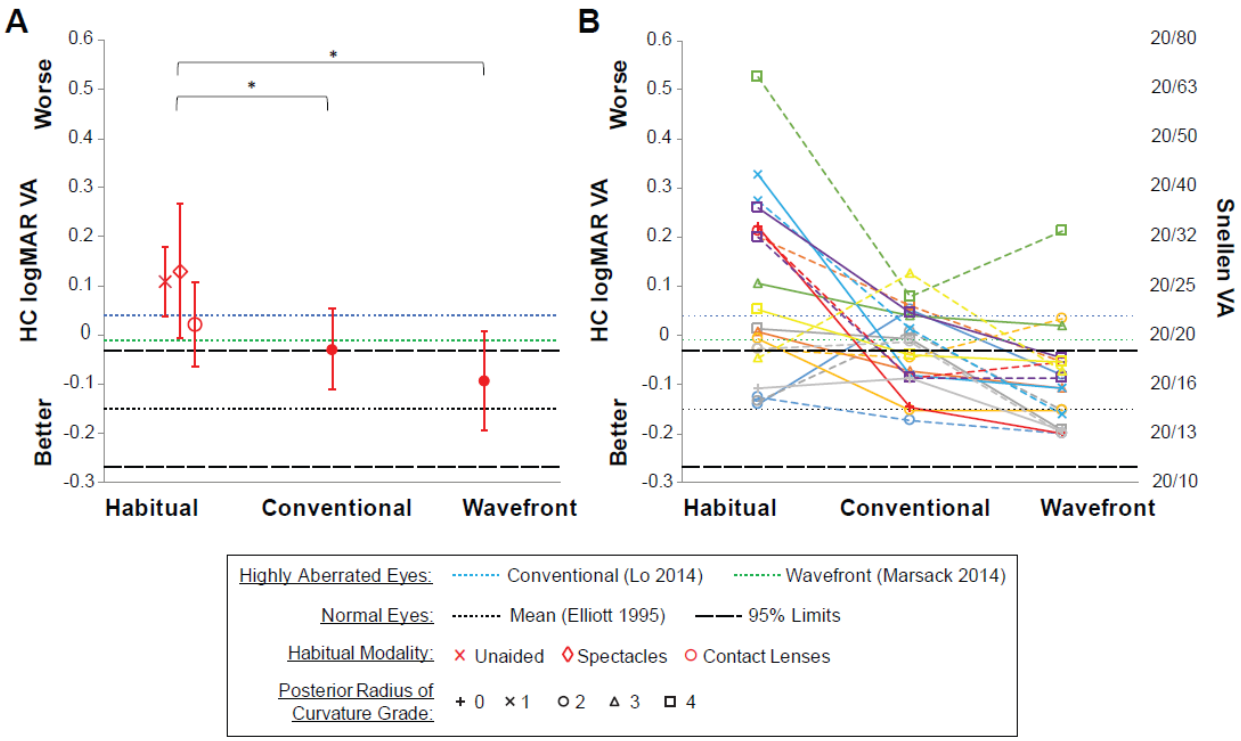

Figure 4. 5 High contrast (HC) logMAR visual acuity (VA) across the three corrections for (A) the mean of all eyes and (B) all individual eyes. Error bars are one standard deviation. In (B) two eyes of a subject are plotted in the same color; right eyes solid; left eyes dashed; symbols indicate severity grade of posterior radius of curvature.[138] Age-matched 95% limits for normal eyes (Elliott et al.[58]) are plotted as well as levels for eyes with keratoconus wearing conventional (Lo et al.[143]) and wavefront-guided scleral lenses (Marsack et al.[80]).

4.5 Discussion

This study sought to determine the benefit of transferring individuals with corneal ectasia from their habitual correction to best conventional scleral lenses and to personalized wavefront-guided lenses by dispensing each type of lens and allowing approximately eight weeks of habituation to the retinal image formed by each.

4.5.1 Best conventional scleral lenses

Achieving equivalent, or better than, clinically representative performance with best conventional scleral lenses is an essential prerequisite in appreciating any gains in performance provided by wavefront-guided lenses.

Mean residual levels of higher-order RMS wavefront error with best conventional lenses (0.30 μm over a 4 mm pupil; 0.46 μm over 5mm; 0.58 μm over 6mm) were equivalent to, or better than, reports of highly aberrated eyes wearing conventional scleral lenses[80,116,123] or corneal rigid gas permeable lenses.[112,114,115] Similarly, best conventional scleral lenses provided mean visual acuity (–0.03) better than or equivalent to reports of highly aberrated eyes wearing conventional scleral lenses[144] or corneal rigid gas permeable lenses.[145] Despite differences in methodology discussed below, letter contrast sensitivity with the best conventional scleral lenses was also equivalent to that of highly aberrated eyes wearing corneal rigid gas permeable lenses.[146] In this study, the magnitudes and distributions of residual higher-order aberrations, through best conventional lenses, interacted such that all eyes remained outside the objectively optimized logVSX levels of best-corrected normal eyes.[30]

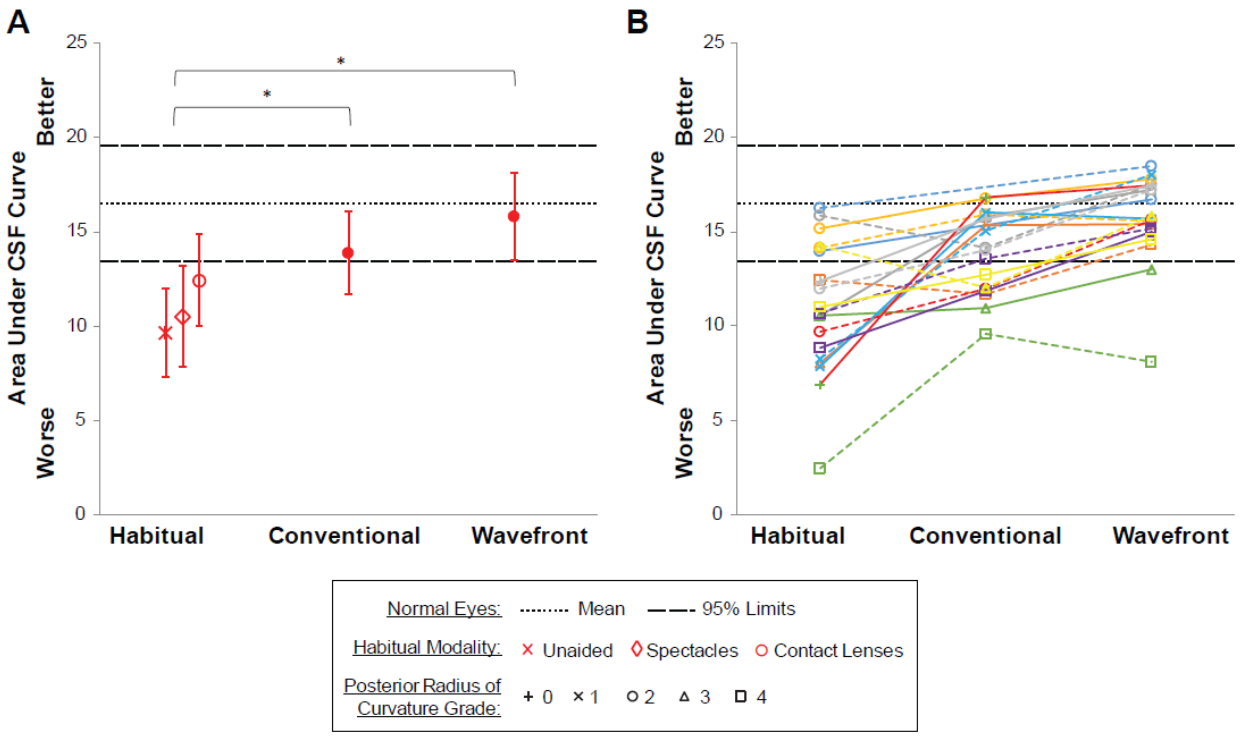

Figure 4. 6 Area under the log contrast sensitivity function (CSF) across the three corrections for (A) the mean of all eyes and (B) all individual eyes. Error bars are one standard deviation. In (B) two eyes of a subject are plotted in the same color; right eyes solid; left eyes dashed; symbols indicate severity grade of posterior radius of curvature.[138] Age-matched 95% limits for normal eyes were measured on the same instrument system.

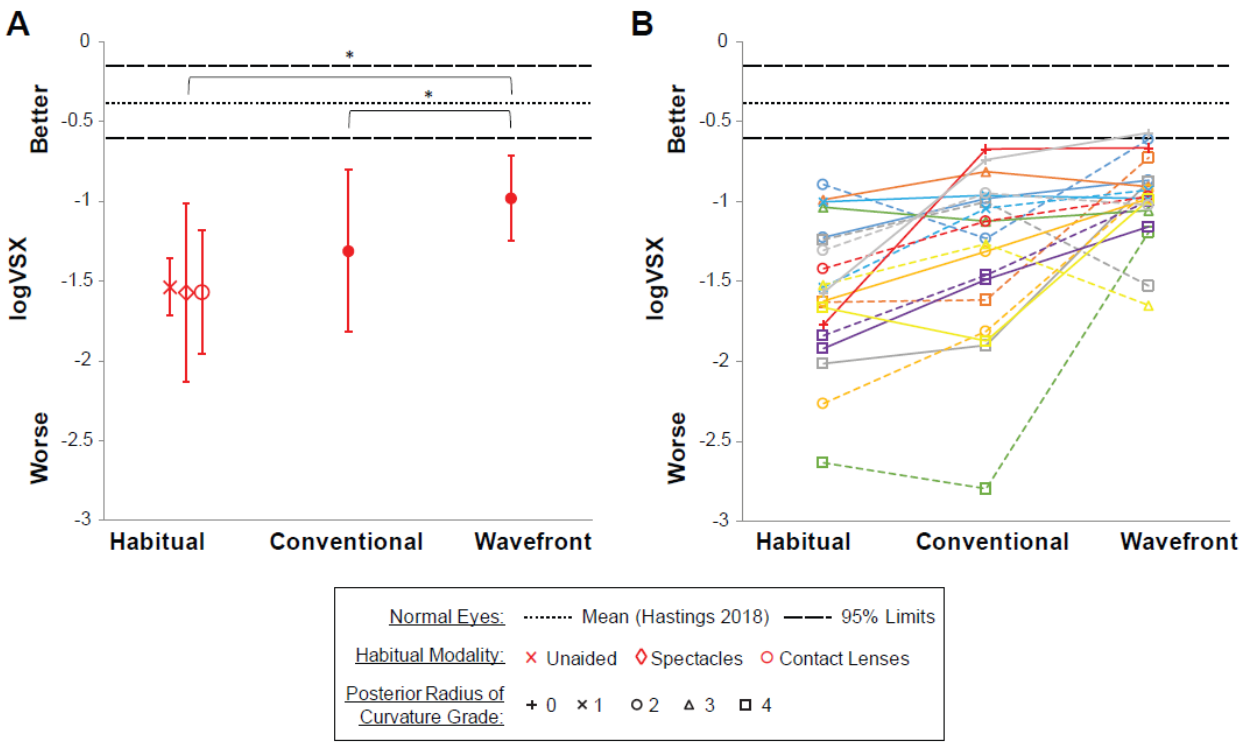

Figure 4. 7 Visual image quality metric logVSX (the visual Strehl ratio) across the three corrections for (A) the mean of all eyes (B) all individual eyes. Error bars are one standard deviation. In (B) two eyes of a subject are plotted in the same color; right eyes solid; left eyes dashed; symbols indicate severity grade of posterior radius of curvature.[138] Age-matched 95% limits are for objectively best-corrected normal eyes (Hastings et al.[30]).

4.5.2 Comparison of wavefront-guided lenses with other studies

Comparisons are made with (1) attempts to correct measured aberrations of real eyes and (2) benchmark modalities of clinical practice.

4.5.2.1 Higher-order root mean square wavefront error

Mean higher-order RMS levels with wavefront-guided lenses reported here (0.19 µm over a 4 mm diameter pupil; 0.26 µm over 5mm; 0.33 µm over 6mm) are statistically equivalent to previous reports of wavefront-guided scleral lenses,[80,123] significantly better than reports of wavefront-guided soft lenses,[120–122] better than that of conventional scleral lenses in this study

and others,[80,116,123] and better than reports of highly aberrated eyes wearing corneal rigid gas permeable lenses.[112,114,115]

4.5.2.2 Visual acuity

Visual acuity is a variable subjective quantity[56] that can be relatively insensitive to visual blur,[147] which could have contributed to lack of significance in gain between best conventional and wavefront-guided lenses. Nonetheless, mean logMAR visual acuity with wavefront-guided lenses in this study (–0.09) is clinically equivalent or better than other reports of scleral wavefront-guided lenses,[80,123] better than wavefront-guided soft lenses,[117,122,124] better than that conventional scleral lenses in this study and elsewhere,[144] and better than reports of highly aberrated eyes wearing corneal rigid gas permeable lenses.[145] These differences may be due to habituation.

4.5.2.3 Letter contrast sensitivity

Letter contrast sensitivity was compared with performance of well-corrected normal eyes on the same instrument system. Firstly, because common letter contrast sensitivity charts[148] typically only test one low spatial frequency (1 to 2 cycles per degree). Secondly, contrast sensitivity with wavefront-guided lenses[117,123] or corneal rigid gas permeable lenses,[146] has been studied using sine-wave gratings. While the fundamental frequencies of letter and sine-wave stimuli can be equivalent, sine-wave gratings are insensitive to phase errors present in normal[149] – and amplified in highly aberrated – eyes[150] that can affect visual perception.[87]

Sabesan et al.[123] presented change in contrast sensitivity with wavefront-guided lenses as a multiple of contrast sensitivity with conventional lenses. This can be bias the performance of the wavefront-guided lenses because the conventional lenses were unrefined predicate lenses, as has been common practice.[79,80,120,121] Overall, we found an opposite pattern of contrast sensitivity results in that performance with wavefront-guided lenses in this study gained more at higher spatial frequencies than at lower spatial frequencies. Comparing with their Figure 4.5, mean log contrast sensitivity reported here was equivalent for 4 cycles per degree (1.64 ±0.14); significantly better for 8 cycles per degree (1.41 ±0.19); and mean log contrast sensitivity reported here for 16 cycles per degree (1.01 ±0.25) was significantly better than at the highest spatial frequency (12 cycles per degree) they reported. These differences may be due to habituation.

4.5.2.4 The logarithm of the visual Strehl ratio (logVSX)

Wavefront-guided lenses were designed to correct measured residual aberrations from the second through fifth radial orders. Although the total magnitude (RMS) of higher-order aberrations was reduced to within normal levels for 85% of eyes, the distribution and magnitude of individual aberration terms residual through the wavefront-guided lenses interacted visually such that logVSX for the majority of eyes did not reach the objectively optimized levels of best-corrected normal eyes.[30] Considering, the realistic variability of subjective refraction, 14 eyes reached the logVSX limits (–0.580 ±0.239; 5 mm pupil diameter) calculated from the typical subjective refraction of 200 young normal eyes.[151]

This indicates that further improvement in visual quality is possible as wavefront-guided corrections continue to be improved and might involve, for example, targeting particular aberrations such that the residual distributions of higher-order aberrations better resemble those of normal eyes.

4.5.3 Who will benefit most from wavefront-guided lenses?

Health care is evolving towards personalized treatments tailored to the individual needs of each specific patient. Wavefront-guided contact lenses are serving as an ophthalmic application of such individualized medicine for corneal ectasias. However, the investments of time, technology, and cost involved in fitting wavefront-guided products are greater than conventional corrections, making them more comparable to prosthetic devices. Although the choice of corrections is influenced by the visual quality expectations of an individual in addition to the investments of time and money, it is desirable – perhaps even ethically necessary – to estimate the benefits that an individual could gain from wavefront-guided lenses over conventional scleral lenses. This is pertinent given that we are in the infancy of the clinical translation of wavefront-guided lenses, which will become more widely accessible, further improved, and an option for certain individuals with normal eyes wishing to reduce higher-order aberrations.

Residual higher-order RMS wavefront error through best conventional scleral lenses best predicted ($R^2 = 0.94$) the additional reduction in higher-order aberrations achieved by wavefront-guided lenses over conventional lenses. This is not surprising because wavefront-guided lenses were designed to specifically target residual higher-order RMS wavefront error. Estimating a

patient's potential gains using residual higher-order RMS wavefront error through a conventional lens is reasonable because a best conventional lens is a prerequisite for a wavefront-guided lens. However, as visual processing is better understood and visual image quality metrics better developed, it is likely that the field should strive to optimize these metrics as opposed to simplistically targeting a reduction in aberration terms.

Of the biometric measures, posterior corneal radius of curvature best correlated ($R^2 = 0.75$) with the reduction in higher-order aberrations provided by wavefront-guided lenses, followed by mean disease severity (averaging grading dimensions A, B, C, and D for the conventional lens) ($R^2 = 0.62$), both of which can be evaluated with Pentacam software (Oculus Inc., Arlington WA).

Based on posterior corneal radius of curvature, the present sample of eyes could be divided into: (1) those of severity grades 0 and 1 (>5.7 mm) and (2) those of severity grades 2, 3, and 4 (<5.7 mm). Seventy-five percent of eyes in the first group were within normal levels of higher-order RMS wavefront error with a best conventional lens, compared with 31% of eyes in the second group. Eyes in the first group experienced a mean reduction of 0.057 μm in higher-order RMS wavefront error (5 mm pupil) with the wavefront-guided lens over the conventional, while a mean reduction of 0.233 μm was experienced by the second group. A greater sample of eyes is needed before this threshold criterion could be confidently advocated.

If these insights were followed, some eyes fit with wavefront-guided lenses in this study would not be fit in practice – these eyes experienced smaller gains with the wavefront-guided

lenses. Both eyes of each subject were fit here by experimental design to gain insights into who would benefit most. Given the bilateral-asymmetry that characterizes corneal ectasias and the current state of wavefront-guided lenses, these individuals might currently be well served wearing a wavefront-guided lens on their more severe eye and a conventional lens on the less severe eye.

Predicting the individual benefit in this way only considers the unique optical challenges presented by each eye but neglects the many traditional challenges of scleral lens fitting; both sets of challenges need to be resolved for the successful fitting of wavefront-guided lenses. In this study, as is true of clinical practice, the challenges of fitting a stable scleral lens were sometimes significant. In contrast, the incorporation of the wavefront-guided correction was relatively easy (requiring an additional two to three visits) once a stable well-fitting conventional scleral lens was achieved.

Identifying individuals that stand to benefit from wavefront-guided lenses is important because the eyes in this study that experienced substantial gains, reported the investment of time to fit wavefront-guided lenses as worthwhile, and described the gains in visual performance and quality as life-changing.

Chapter 5: Modelling neural and optical contributions to physiological visual image quality metrics as a function of age and luminance.

At the time of the dissertation, this work has been submitted for publication and is under review as: Hastings GD, Marsack JD, Thibos LN, Applegate RA. Modelling neural and optical contributions to physiological visual image quality metrics as a function of age and luminance.

5.1 Abstract

Visual image quality metrics combine comprehensive descriptions of ocular optics (from wavefront error measurements) with a measure of the neural processing of the visual system (neural contrast sensitivity). To investigate the roles and interactions of those optical and neural components in foveal physiological visual image quality as a function of age and target luminance, models of neural contrast sensitivity were constructed from literature as a function of (1) retinal illuminance (Trolands, td) and (2) retinal illuminance and age and incorporated into calculation of the visual Strehl ratio (VSX). Best-corrected VSX metric values were determined at physiological pupil sizes over target luminances of 104 to 10-3 cd/m2 for a sample of 146 eyes spanning six decades of age. Optical and neural components of the metrics interact and contribute to visual image quality in three ways: At target luminances resulting in >900 td at physiological pupil size, neural processing is constant and only aberrations (that change as pupil size changes with luminance) affect the metric. At low mesopic luminances below where pupil size asymptotes to a maximum, optics are constant (maximum pupil) and only the neural component changes with luminance. Between these two levels both optical and neural components of the metrics are affected by changes in target luminance. The model that accounted for both retinal illuminance and age allowed VSX to best track visual acuity trends as a function of age from literature.

5.2 Introduction

Visual image quality metrics [152,153] distil the visual system into two fundamental components: An optical component derived from an ocular wavefront error measurement (with or without ophthalmic correction) and a neural processing component that originated from a photopic foveal neural contrast sensitivity function measured historically with laser interferometry [154], although these measurements are also now possible with adaptive optics [155,156]. The convention of reporting wavefront error at a common pupil size [1] across individuals has meant that normative values of visual image quality as a function of age have been defined at fixed pupil sizes [30]. While these have been clinically satisfactory at the level of an individual patient, literature consistently reports decreasing visual performance with increasing age, typically measured through physiological pupils at constant luminances (examples include visual acuity [157,158] and photopic and mesopic contrast sensitivity [158–161]).

To study physiological visual image quality as a function of age and to compare it with visual performance, both (optical and neural) components of visual image quality metrics should account for the decrease in physiological pupil size with age (senile miosis). Treatment of the optical component is trivial as methods exist to scale [162] monochromatic wavefront error from a maximum dilated pupil size to a predicted [163] physiological pupil sizes. However, the neural component is more challenging, firstly, because decreasing physiological pupil size with age results in decreasing effective retinal illuminance (Trolands, td) and literature agrees that neural processing (specifically, neural contrast sensitivity) varies with retinal illuminance [9–11]. Secondly, there is the consideration of whether neural processing (at a constant retinal

illuminance) decreases with age due to neuron loss or worsening signal to noise; relevant literature (which is divided on this second topic) is summarized in the Discussion and, in the absence of a definitive understanding of the impact of age, we study both cases here.

To investigate the interactions and contributions of the optical and neural components of visual image quality metrics as a function of age and target luminance we combine (1) predictions of physiological pupil size, (2) scaling of wavefront error aberrations, and models of neural contrast sensitivity, constructed from literature, as functions of (3a) spatial frequency and retinal illuminance and (3b) spatial frequency, retinal illuminance, and age (decade age-groups). In doing so, visual image quality metrics provide an additional perspective from which to examine the roles and interactions of optical and neural factors as target luminance and age change. We find that these components interact and contribute to visual image quality differently over three luminance domains.

5.3 Methods

5.3.1 Wavefront error, target luminance, physiological pupils, and retinal illuminance (Trolands)

Data were collected during the Texas Investigation of Normal and Cataract Optics study (referred to here as Applegate et al. [164]), which followed the tenets of the declaration of Helsinki and obtained signed informed consent approved by the University of Houston Institutional Review Board. Briefly, Applegate et al. (2007) studied the change in wavefront aberration structure as crystalline lens opalescence increased naturally with age. Individuals with cortical and / or posterior subcapsular cataracts graded as >2 on The Lens Opacities Classification

System III (LOCS-III) [165] were excluded, as were applicants with any previous ocular surgery, pathology, or abnormality (such as strabismus or amblyopia).

Wavefront error was measured over maximum dilated pupils (one drop 1% tropicamide and one drop 5% neosynephrine) of the preferred eyes of 146 normal healthy individuals between 20 and 80 years of age using a custom Shack-Hartmann wavefront sensor. Resulting wavefront errors were fit with a 10^{th} radial order normalized Zernike polynomial expansion.

Measured wavefront errors were scaled [162] to physiological pupil sizes predicted [163] over a range of photopic and mesopic target luminances (–3 to +4 in 1 log cd/m^2 increments; 10^{-3} cd/m^2 being the lower bound of cone sensitivity [166]). (The term m*esopic* is used despite neural contrast sensitivity and visual image quality in this paper being confined to the (rod-free) fovea because foveal cones are still functional at these luminance levels.[166]) Inputs to the physiological pupil size calculations were *binocular* (rather than *monocular*) viewing and a 60° adapting field [163]. Additionally, target luminance of 160 cd/m^2 was evaluated for comparison with specific literature. A small proportion of eyes did not dilate to the physiological pupil sizes predicted for low target luminances (see Appendix 1) – in these cases the maximum dilated pupil size was used instead to avoid scaling aberrations to larger pupil sizes than was measured. Accommodation could decrease pupil size beyond that which is predicted by luminance and age; throughout this paper we assume accommodation to be relaxed. Retinal illuminance for each eye at each target luminance was calculated as the product of target luminance and predicted physiological pupil area.

5.3.2 Models of neural contrast sensitivity as a function of spatial frequency, retinal illuminance, and age

Neural contrast sensitivity data for six retinal illuminances between 0.9 and 9000 td were extracted from Figure 1 of Xu et al. (2017) (replotted in our Figure 5.1A) and fit with a two-dimensional regression using *polyfitn* [167] in Matlab (The Mathworks, Inc); $R^2 = 0.9958$, degrees of freedom remaining = 319, RMS error of fit = 0.046 log neural contrast sensitivity. Xu et al. (2017) derived their data from measurements made by Rovamo, Mustonen, and Näsänen (1994) and had scaled the functions to agree with the 500 td function of a 27 year old from Campbell and Green (1965) that was historically used in visual image quality metrics. When incorporating an age-related factor, these functions (from Xu et al. (2017)) were taken as representing the 20 to 29 year old age-group across different levels of retinal illuminance.

Neural contrast sensitivity data for decade age-groups at one retinal illuminance (160 td) were extracted from Figure 3 of Nameda, Kawara, and Ohzu (1989) and are shown in our Figure 5.2A. At each spatial frequency, the sensitivities of the 30 to 39, 40 to 49, 50 to 59, and 60 to 69 age groups were each divided by that of the 20 to 29 year old group to generate decade age-group multipliers relative to the 20 to 29 years group (Figure 5.2B). At each spatial frequency the multipliers were linearly extrapolated in Matlab to determine an age-multiplier for the >70 year old age-group. Linear extrapolation was used because change in neural contrast sensitivity with age was approximately linear (within each spatial frequency; [13,169]) and is in agreement with anatomical [170–173] and performance measures [158,174,157] that change approximately linearly with age.

5.3.3 Visual image quality metric: The visual Strehl ratio (VSX)

The contents of this paper are applicable to any visual image quality metric that incorporates a neural contrast sensitivity weighting function. To illustrate the developments made here, the visual Strehl ratio (VSX) [153] is used. Historically, VSX has been calculated as the ratio of the volume of the point spread function (PSF) of an eye (determined from a wavefront error measurement at a specific pupil size) to the volume of the diffraction-limited PSF for the same pupil size, where both PSFs are first weighted by the inverse Fourier transform of a neural contrast sensitivity function from Campbell and Green (1965). More recently, using a constant denominator, such as a diffraction-limited 3 mm pupil, across all eyes has been advocated [175,176] and we employed such normalization here.

Despite that VSX (like other visual image quality metrics) incorporated a single neural contrast sensitivity measurement drawn by eye through method-of-adjustment data from one 27 year old individual in 1965, it has been shown predictive of subjective best focus [153,177–179], able to predict sphere, cylinder, and axis spectacle prescriptions that performed equivalently to subjective refraction [25,180], and has been used to evaluate conventional and wavefront-guided contact lenses [110]. Changes in the logarithm of VSX have been well correlated with changes in visual performance [181] and especially with logMAR visual acuity [147,182] independent of underlying pupil size and wavefront error.

To respect how the neural contrast sensitivity weighting function of the metric changes with retinal illuminance as well as with both retinal illuminance and age, we define two

modifications of VSX which are presented in parallel throughout the paper. The metric referred to as *VSX(td)* is calculated as:

(1)

$$\boldsymbol{VSX(td)} = \frac{\iint \boldsymbol{PSF_{(Eye)}(x,y)} \cdot \boldsymbol{N_{(Trolands)}(x,y,t)dxdy}}{\iint \boldsymbol{PSF_{DL(3mm)}(x,y)} \cdot \boldsymbol{N_{(900td)}(x,y)dxdy}}$$

where $PSF_{(Eye)}$ is at the physiological pupil size to which the wavefront error was scaled, the neural weighting function (*N*) in the numerator is specific to the retinal illuminance (product of physiological pupil size and target luminance) of the condition, $PSF_{DL(3mm)}$ is for a diffraction-limited 3mm pupil diameter, and the neural weighting function in the denominator is from the (maximum) neural contrast sensitivity function defined at 900 td.

The metric referred to as VSX(td,a) is defined as:

(2)

$$\boldsymbol{VSX(td,a)} = \frac{\iint \boldsymbol{PSF_{(Eye)}(x,y)} \cdot \boldsymbol{N_{(Trolands,Age)}(x,y,t,a)dxdy}}{\iint \boldsymbol{PSF_{DL(3mm)}(x,y)} \cdot \boldsymbol{N_{(900td,20-29y/o)}(x,y)dxdy}}$$

where $PSF_{(Eye)}$ and both parts of the denominator are the same as VSX(td) above, and the neural weighting function in the numerator is specific to both retinal illuminance and the age of the eye.

5.3.4 Metric calculations

Simulated through-focus experiments using VSX(td) and VSX(td,a) were performed. For each scaled wavefront error (including higher- and lower-order aberrations) of each of the 146

eyes at the physiological pupil sizes predicted for each target luminance, a spherical dioptric value was calculated from second-order Zernike defocus. Around this value, a range of sphere, cylinder, and axis prescriptions was mathematically applied that spanned: sphere from –1.50 D to +1.50 D in 0.25 D steps (centered on the second-order Zernike defocus) and cylinder from 0 up to –1.50 D beyond the second-order Zernike cylinder in 0.25 D steps and 2 degree axis increments. This resulted in at least 7000 prescriptions being objectively applied to the wavefront error of each eye at each predicted physiological pupil size condition. Best-corrected metric values were taken as the maximum metric value obtainable with any of these sphere, cylinder, and axis combinations.

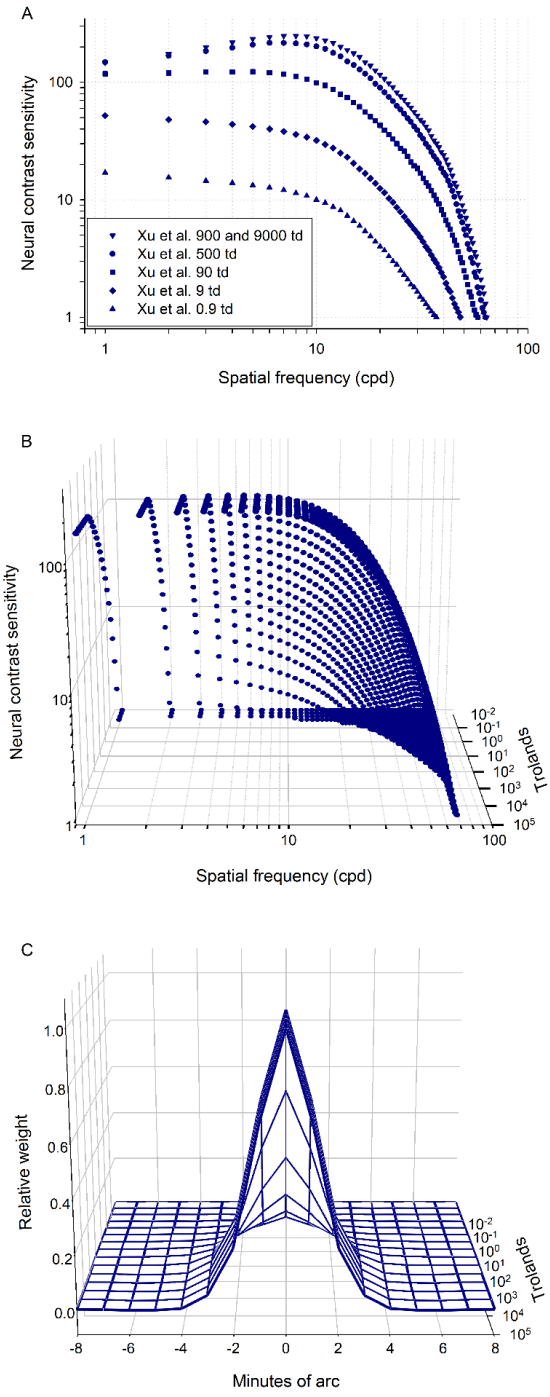

Figure 5. 1 (A) Neural contrast sensitivity functions at six retinal illuminance levels from Xu et al. (2017) that were fit with a two-dimensional regression to form (B) the model of neural contrast sensitivity as a function of spatial frequency (cycles per degree) and retinal illuminance (Trolands). (C) Neural weighting functions used in the VSX(td) metric, obtained via inverse Fourier transform of the functions in (B). [There is an animated version of this image in the submitted manuscript.]

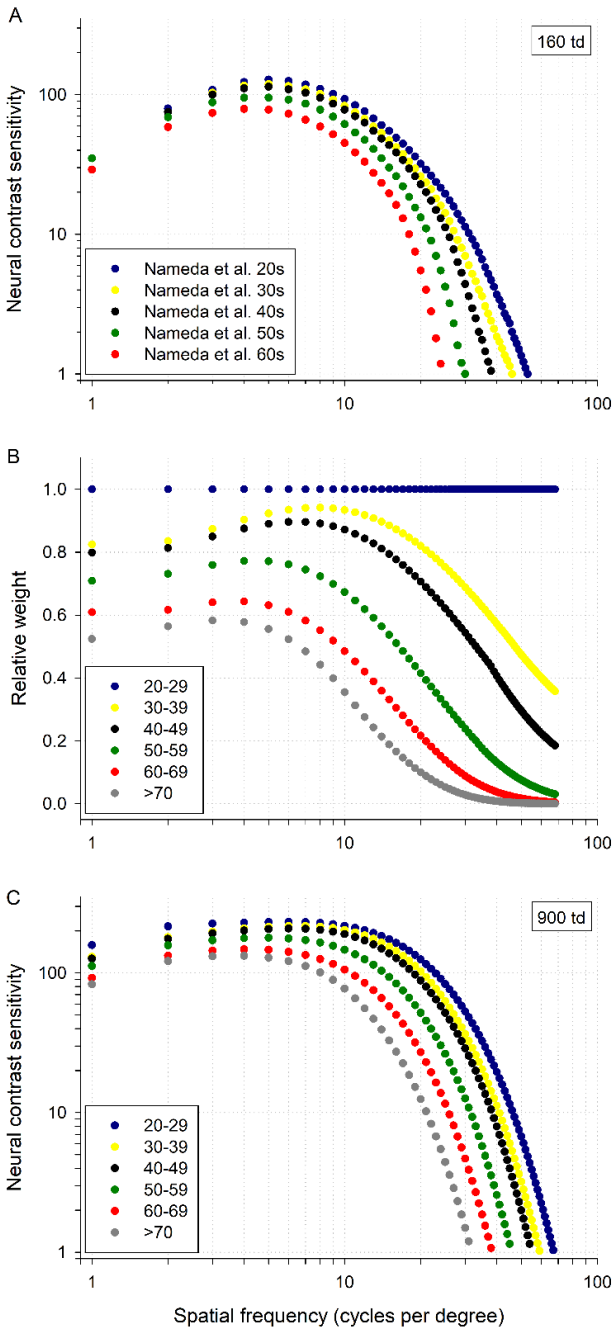

Figure 5. 2 (A) Neural contrast sensitivity functions at 160 td from Nameda et al. (1989) for decade age-groups were divided (at each spatial frequency) by the sensitivity of the 20s age-group to derive (B) decade age-group multipliers as a function of spatial frequency, which weight the model defined in Equation 3 and Figure 5.1 and determine the neural contrast sensitivity functions that (after Fourier transform) are used in the VSX(td,a) metric. The age-group multipliers in (B) are numerically defined in Appendix 2. Panel (C) shows an example of the function for 900 td being weighted for all age-groups – the function labelled as 20-29, is the function at 900 td in Figure 5.1B.

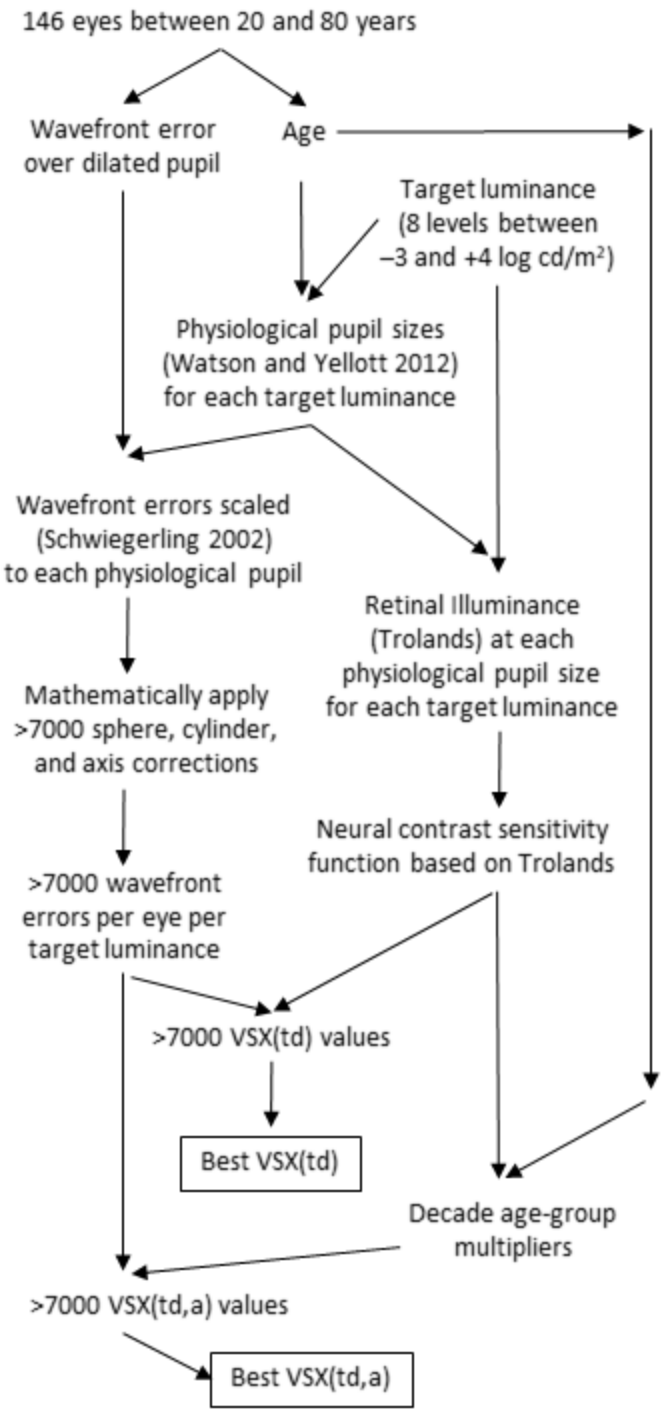

Figure 5. 3 Flow diagram of methods beginning with measured wavefront error and culminating in best-corrected visual image quality metric values for VSX (td) and VSX(td,a).

5.4 Results

5.4.1 Physiological pupil size and retinal illuminance

Decreasing (or increasing) luminance always results in decreased (increased) retinal illuminance at all ages despite the compensatory enlargement (decrease) of pupil size. Calculated physiological pupil diameters ranged from 2.47 mm for the oldest eye (78.4 years) at the brightest target luminance (10^4 cd/m^2), to 8.05 mm for the youngest eye (21.8 years) at the dimmest target luminance (10^{-3} cd/m^2).

5.4.2 Models of neural contrast sensitivity as a function of spatial frequency, retinal illuminance, and age

The model of neural contrast sensitivity fit using *polyfitn* [167] and used in VSX(td) calculations is defined as:

(3)

$$\begin{aligned}\log nCS(t,f) = {} & -0.009t^4 - 0.020t^3f + 0.062t^3 + 0.013t^2f^2 + 0.107t^2f \\ & - 0.203t^2 - 0.115tf^3 + 0.209tf^2 - 0.142tf + 0.62t - 0.934f^4 \\ & + 2.490f^3 - 2.668f^2 + 0.869f^1 + 1.221f\end{aligned}$$

where *nCS* is neural contrast sensitivity, *t* is retinal illuminance (log Trolands), and *f* is spatial frequency (log cycles per degree). Matlab script (to greater decimal precision) for the above equation is included in Appendix 2. This model and the associated inverse Fourier transforms (PSF weighting functions) are shown in Figure 5.1 B and C for the range of Troland values that result from target luminance values of 10^{-3} to 10^4 cd/m^2 at physiological pupil sizes.

The weighting functions used in the VSX(td,a) metric each started with calculation of a neural contrast sensitivity function at a specific retinal illuminance using Equation 3 (the same function used in the VSX(td) metric). Thereafter, that function was weighted at each spatial frequency by the relevant decade age-group multiplier (based on the age of the eye), as shown in Figure 5.2. Numeric definitions of the age-multipliers are included in Appendix 2. The resulting (weighted) neural contrast sensitivity function (specific to retinal illuminance and age) underwent an inverse Fourier transform and was incorporated into the numerator of Equation 2.

5.4.3 Relative contributions of optical and neural metric components as a function of target luminance

Physiological visual image quality is determined by the interaction and relative contributions of the optical and neural components of the metric in three ways defined by target luminance. These are identical for VSX(td) and VSX(td,a). In Figure 5.4, lines designating the transition of these three zones are superimposed on the data described in the next section.

At high photopic target luminances that result in greater than or equal to 900 td retinal illuminance at physiological pupil sizes, the neural component is constant [9,183]. As luminance changes above this level, visual image quality is influenced solely by changes in the optical component, that is, optical aberrations that increase (or decrease) with the increase (decrease) in pupil size in response to decreasing (increasing) luminance. This luminance bracket varied with age: The target luminance at which 900 td was reached and neural processing became constant

decreased with increasing age and spanned from 10^4 cd/m^2 to approximately $10^{1.58}$ cd/m^2 in the youngest eyes and to $10^{1.98}$ cd/m^2 in the oldest eyes. This is indicated by red lines in Figure 5.4.

On the opposite end of the target luminance range, at levels below those where maximum physiological pupils occur, the optical component is constant as luminance decreases further (because pupil size is already at a maximum) and visual image quality is influenced only by changes in the neural processing component, which decreases with the decrease in luminance (Figure 5.4). Scotopic physiological pupil unrest (hippus) in alert individuals is on the order of 0.25 mm [184], therefore in this modelling maximum pupil diameter was taken as being within 0.25 mm of the physiological pupil diameter defined by the Watson and Yellott (2012) model at 10^{-4} cd/m^2. This point also varied with age, occurring at approximately $10^{-1.38}$ and $10^{-0.56}$ cd/m^2 for 20 and 80 year old eyes respectively, and is indicated by blue lines in Figure 5.4.

Between high photopic luminances producing 900 td and low mesopic luminances that result in maximum physiological pupil sizes, both optical and neural components change when target luminance changes and both influence visual image quality. This is the region between the blue and red lines in Figure 5.4. As target luminance decreases within this range, physiological pupil size increases, which increases aberrations, and retinal illuminance decreases, which reduces the neural contrast sensitivity function (as shown in Figure 5.1).

Over the ranges modelled here, as target luminance decreases, the role of the optical component in physiological visual image quality decreases as age increases. That is, (1) the high luminance point at which neural processing is no longer constant and begins to depend on

luminance, occurs sooner as age increases, and (2) the point where the optical component becomes constant and only luminance-driven changes in the neural component affect physiological visual image quality also decrease as age increases. In summary, the neural component plays an increasing relevant role as age increases.

5.4.4 Best-corrected physiological visual image quality

In agreement with the prevailing qualitative clinical understanding of visual quality, best VSX(td) and VSX(td,a) occurred in young eyes at high photopic luminances (small physiological pupils). When the neural weighting function only accounted for retinal illuminance (VSX(td)), visual image quality was relatively constant across age for all target luminances (Figure 5.4A). The addition of age-specific weighting to the neural component (VSX(td,a)) resulted in a decrease in visual image quality with age that was more gradual at high target luminances and more pronounced as luminance decreased (Figure 5.4B).

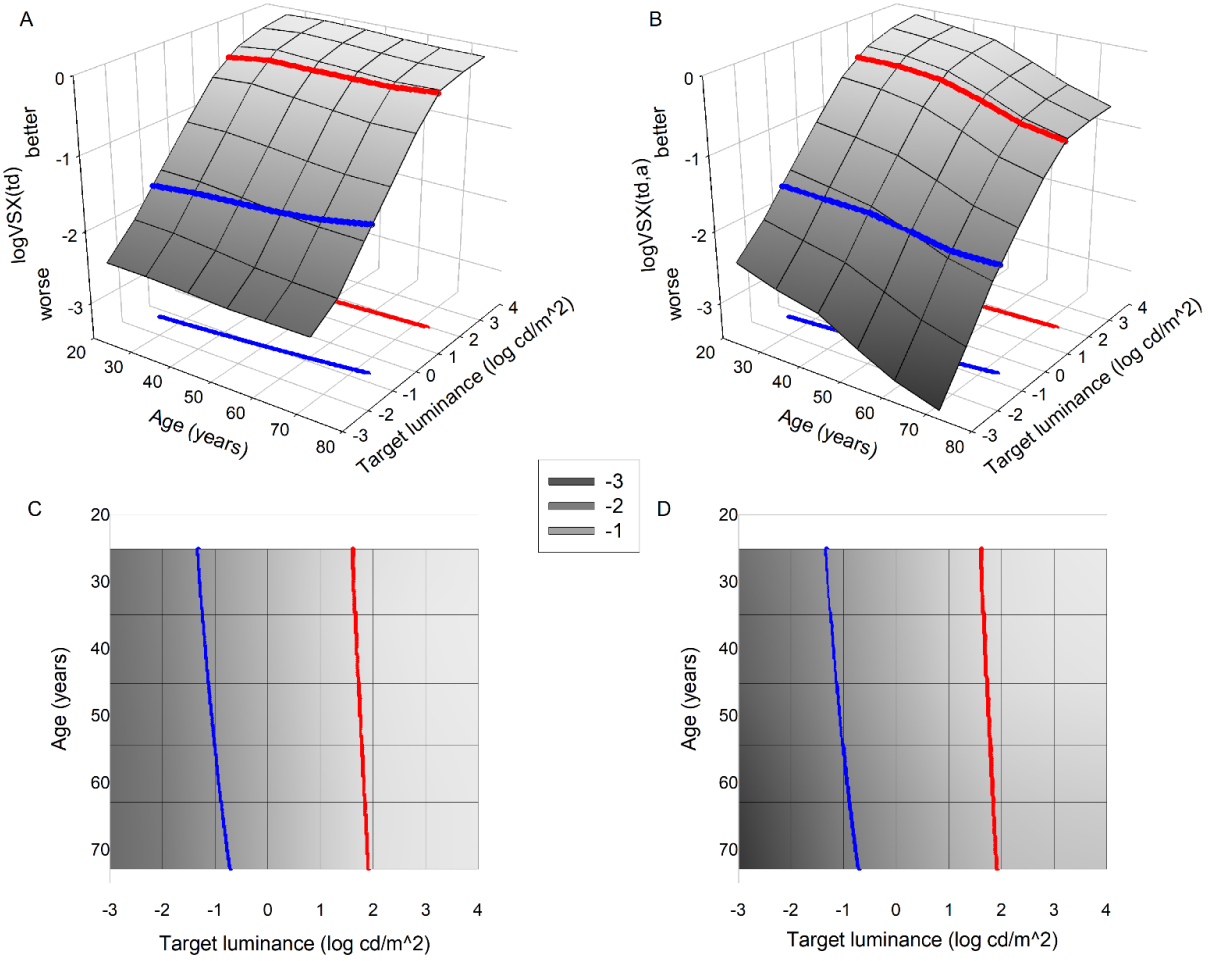

Figure 5. 4 Mean best-corrected visual image quality for each decade age-group and target luminance where the metrics were calculated at the physiological pupil size [163] of each subject for each luminance and the neural weighting function (from Figures 5.1 and 5.2) was specific to (A and C) retinal illuminance and (B and D) retinal illuminance and age. Above the red lines on each surface, target luminance results in retinal illuminance (not shown; product of target luminance and physiological pupil area) of at least 900 td at physiological pupil sizes; here neural contrast sensitivity is constant as target luminance changes and only optical aberrations affect visual image quality. Below the blue lines on each surface are low mesopic luminances that cause maximum physiological pupils; here optics are constant (maximum pupil) as luminance changes and only neural processing affects visual image quality. At target luminances between those two lines, optical and neural factors both change as luminance changes. Panels (C) and (D) show top-views of (A) and (B) and illustrate the effects of senile miosis: 900 td and maximum physiological pupil sizes occur at higher luminance as age increases, meaning that as luminance changes, the role of the optical component decreases with age, while the neural component becomes more relevant with increasing age.

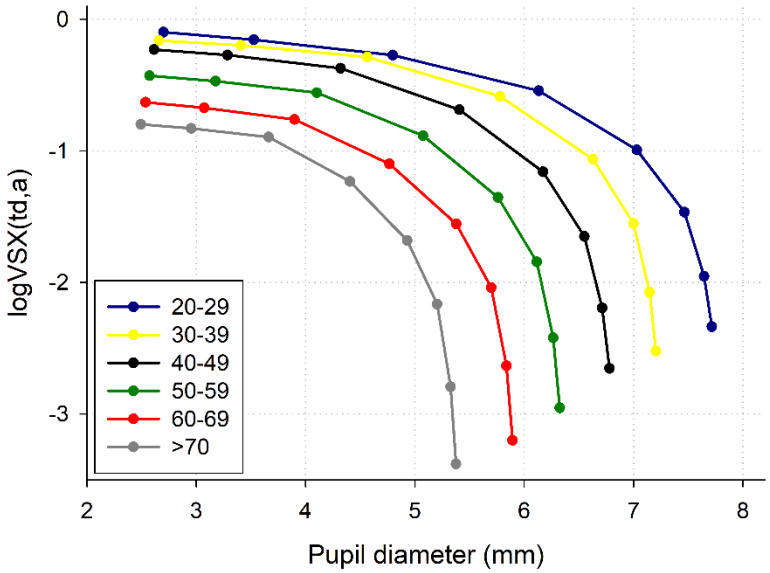

Figure 5. 5 Best-corrected logVSX(td,a) as a function of physiological pupil diameter. For any age-group, as pupil size increases (abscissa) in response to decreasing luminance (corresponding to the eight points on each line, but not explicitly shown), the logVSX(td,a) metric value decreases due to increasing aberrations and a worsening neural weighting function (lower retinal illuminance). When physiological pupil size asymptotes to a maximum, the optics remain essentially constant (maximum pupil) as luminance decreases further, and the neural weighting function is responsible for the further decrease in visual image quality (ordinate).

5.5 Discussion

We sought to describe physiological visual image quality as a function of target luminance as well as of target luminance and age. Towards this end, physiological pupil sizes were calculated for a large dataset of eyes, wavefront error aberrations were scaled to those physiological pupil sizes, and two models of neural contrast sensitivity were developed from literature and used to modify the calculation of the visual image quality metric VSX.

5.5.1 Comparison with literature: Models of neural contrast sensitivity

The models should be taken as representing mean neural contrast sensitivity and there will undoubtedly be variability in the performance of individuals. It is challenging to unify the literature on neural contrast sensitivity – even if comparisons are limited to laser interferometry studies (and methods such as adaptive optics are not considered) – because the sophistication of technology has evolved significantly over time and certain characteristics of the systems (such as coherence fractions [185]) were frequently not considered or reported. Most studies of neural contrast sensitivity were performed at a single retinal illuminance level and often this value, as well as the ages of subjects, were not reported.

The models presented here were constructed using data from Xu et al. (2017) (scaled to match Campbell and Green (1965)) and Nameda et al. (1989) and show good agreement (Figure 5.6A) with neural contrast sensitivity curves at various retinal illuminances from Kawara and Ohzu (1977), Coletta and Sharma (1995), and Still (1989). The model corresponds to approximately the best performance reported by Dressler and Rassow (1981) at 1000 td and the worst performance reported by Williams (1985) at 500 td; in Figure 5.6B, mean data from both studies are compared with the model. The neural contrast sensitivity functions measured by Williams (1985) were better than all literature with which they compared themselves, and Dressler and Rassow pooled data across six decades, which likely contributed to the lower levels they reported. The models, like the data upon which they are based [9], agree with other literature [183] that neural contrast sensitivity is constant at retinal illuminances above 900 td.

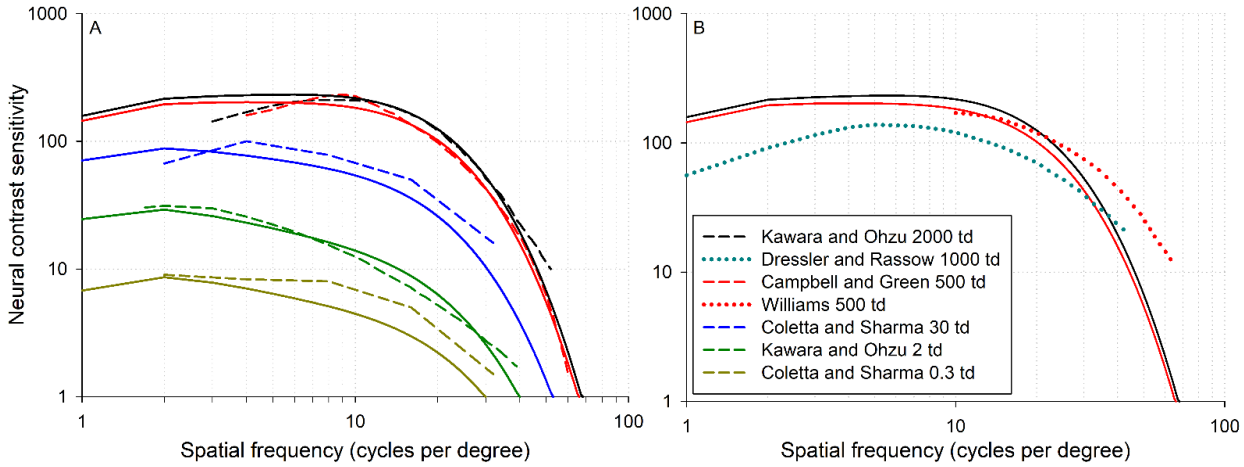

Figure 5. 6 Comparison of the model (solid lines) with neural contrast sensitivity functions at (A) five retinal illuminance levels from Figure 5 of Kawara and Ohzu (1977), Figure 5 of Campbell and Green (1965), and Figures 2d and 2g of Coletta and Sharma (1995) and (B) from Figure 5 of Williams (1985) and Figure 5 of Dressler and Rassow (1981). Model curves are for the 20-29 year old group; the Campbell and Green (1965) curve is for a 27 year old; Kawara and Ohzu (1977) and Coletta and Sharma (1995) did not specify ages; the mean age of six subjects from Williams (1985) was 36 years; and Dressler and Rassow (1981) pooled data from six age-group decades.

5.5.2 Comparison with literature: Best-corrected physiological visual image quality

Best-corrected (sphere, cylinder, and axis) metric values as functions of age (for physiological pupils) at 160 cd/m2 were compared with best-corrected (sphere, cylinder, and axis) visual acuity recorded with physiological pupils and target luminances of 160 [157] to 200 [158] cd/m^2. We desire metrics that mimic the relative change in performance with age, therefore, the actual performance (such as the minimum angle of resolution (MAR) or logMAR) for all ages have been normalized to that of the 20 to 29 year old group.

Figure 5.7 plots the relative change in three metrics with age. Here, aberrations for each Applegate et al. (2007) eye have been scaled to their predicted physiological pupil size for 160 cd/m^2 (there is not a substantial difference in pupil size or retinal illuminance between 160 and 200 cd/m^2) and the conventional optical Strehl ratio (no neural weighting) has been included to

illustrate the isolated effect of aberrations (only the optical component; no neural component) at physiological pupil sizes.

While none of the metric curves track the age-related change perfectly, the VSX(td,a) curve (weighting the optical component with a retinal illuminance and age-specific neural function) performs better than both VSX(td) (only considers retinal illuminance in the weighting function) and the conventional Strehl ratio. Potential explanations of the difference between VSX(td,a) and the performance data are discussed in the limitations section.

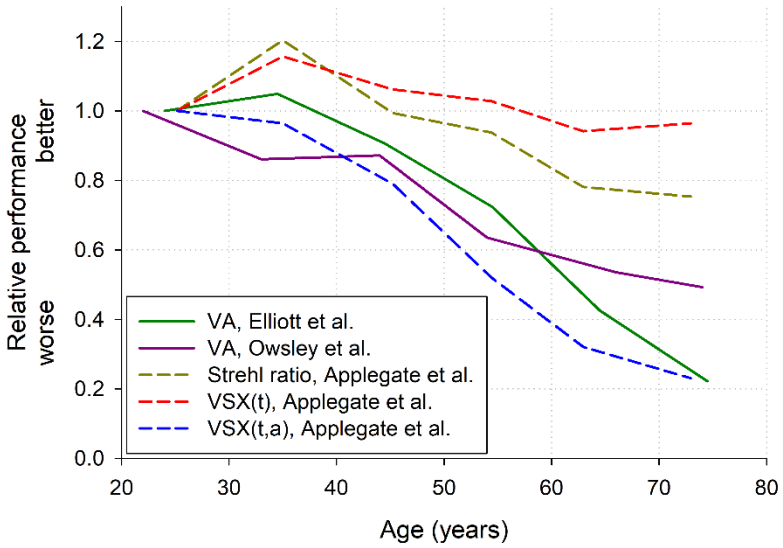

Figure 5. 7 Best-corrected (sphere, cylinder, and axis) metric values as a function of age for physiological pupil sizes at 160 cd/m2 compared with visual acuity [157,158]. VSX(td,a) (weighting the optical component with a retinal illuminance and age-specific neural function) tracked the change in performance with age better than VSX(td) (only accounting for retinal illuminance in the neural component) and the conventional optical Strehl ratio (no neural weighting).

5.5.3 Interaction and roles of optical and neural factors

The modelling presented above most closely resembled physiological visual performance as a function of age when both the optical and neural components of the visual image quality metric VSX respected changes with age. Moreover, those findings suggested that the role of the neural component becomes increasingly important as age increases. However, the relative contribution of optical and neural factors to the senescence of visual performance is a matter of some division in the literature. This may be partly due to some confusing classification terminology. Here we summarize some areas of literature with respect to the optical and neural components of the metrics and the modelling presented.

1. Ocular wavefront aberrations are an optical factor that literature generally agrees increases with age at a fixed pupil size [188–192,164]. Some studies [189,190,164] suggest this increase is mitigated by decreasing physiological pupil size, while others found the biggest optical differences between young and old eyes at small and medium pupil sizes [190], and that senile miosis did not bring older eyes to the level of young eyes [191]. Literature is divided on whether the increase in aberrations with age can [188,191,192] or cannot [189,164] account for the decrease in overall visual performance.

   The aberrations of the Applegate et al. (2007) eyes increased with age at any fixed pupil size (greater for larger fixed pupils). For physiological pupil sizes at high luminance levels aberrations increased slightly with age, and at lower luminances decreased slightly with age. Aberrations were not measured by Elliott et al. (1995) or Owlsey et al. (1983) (Figure 5.7).

2. Ocular scatter is another purely optical factor that literature generally agrees increases with age [193,194] due to inhomogeneties and increased density of ocular media [195,196]. Some literature expects scatter to reduce contrast sensitivity at all spatial frequencies [159], and some found reduced low-contrast visual acuity [197] while others [198] found little to no effect of scatter on visual acuity.

   The Applegate et al. (2007) dataset excluded individuals with cortical and / or posterior subcapsular cataracts graded as >2 on The Lens Opacities Classification System III (LOCS-III) [165]. Both reports of best-corrected visual acuity (Elliott et al. (1995) and Owsley et al. (1983)) with which the present modelling is compared (Figure 5.7) employed strict clinical screenings for pathology and eyes with substantial opacification were also excluded.

3. Decreases and shifts in transmission [199–201] (due to media opacification and absorption) combined with senile miosis produce lower retinal illuminance with age. This is frequently considered optical because it is caused primarily by the pupil, despite that the origin is neural – as shown when pupil size is constant [9,202] or irrelevant (such as with Maxwellian-view interferometry [10,11]) and retinal illuminance is varied.

   Using various methods to mimic the retinal processing of older eyes during contrast sensitivity testing, some studies found retinal illuminance accounted for a substantial

amount [158,203,204] of age-related differences, while others controlled for retinal illuminance and attributed differences to neural processing [161,205–209].

The present study incorporated age-related neural contrast sensitivity interferometry data [169] into the weighting function of a visual image quality metric, however, interferometry at constant retinal illuminance has also returned conflicting results: Some studies found no difference with age [27,187] but did not present specific data to that effect; Burton, Owsley, and Sloane (1993) found a small difference between young and old subjects and others [13,159,169] found a more significant difference with age. Williams (1985) re-measured subject "DG" from Campbell and Green (1965) and found very little change over time from 27 to 48 years old, however the latter measurements were on a technologically-superior interferometry system and used improved psychophysical methods that both might have compensated for age-related changes.

Other methods that essentially bypass the ocular optics such as contrast sensitivity through adaptive optics correction [155] and displacement threshold hyperacuity [211] have found differences between young and old eyes that were attributed to neural changes.

4. Loss of structure does not necessarily translate to loss of function, however, an anatomical loss (or deterioration) of retinal and cortical neurons with age has been noted: Retinal ganglion cells are lost with age [171,212]. Although change to the morphology of foveal cones has been found [213], cone numbers [172,173] and RPE densities [172] are largely unchanged with age. Loss of visual cortical cells with age has been shown anatomically

[170] and corroborated by ERG and VEP [174]. While neural noise might increase with age, this has not been very extensively studied [208,209].

5.5.4 Limitations and applications

While more delineated models have been developed [214,215], visual image quality metrics consider the visual system in terms of two (optical and neural) components. Here, additional simplifications were employed: Monochromatic metrics were calculated; ocular chromatic aberration is relatively constant with age [216,217] and the models presented here could readily be incorporated into polychromatic metric calculations [218], however, spectral composition of the light reaching the retina may vary with age [199,200]. We were unable to find reports of how the *oblique effect* [219,220] (reduced sensitivity to obliquely oriented gratings) varies with retinal illuminance or age – this might be expected, given that it is thought to be cortical in origin [221]. Previous incorporation of the oblique effect into visual image quality metrics [222] did not significantly improve the metrics and this effect was not modelled here.

Physiological pupil sizes were predictions around which variability would be expected and would also be affected by accommodation. This variability would affect both the scaled aberrations (of the optical component) as well as retinal illuminance (which substantially affects the neural weighting function). Potential variability across individuals motivated the definition of the neural age-multipliers in decade age-groups rather than interpolating to obtain a continuous function. In the same manner that neural contrast sensitivity functions for the older age groups were defined relative to the 20-29 year old group, the entire model could be shifted and defined relative to a measured function of an individual.

The models of neural contrast sensitivity utilized by the present modelling should be considered unaffected by Piper's law, that is, being measured using a stimulus of sufficient extent (sufficient number of cycles) so as to be independent of stimulus area. We feel this to be a reasonable assumption given that the data of Xu et al. (2017) were made to agree with that of Campbell and Green (1965), which was measured using a 30 stimulus and, therefore, at least 30 cycles were visible for all spatial frequencies tested. Literature has shown that spatial summation, and by extension, contrast sensitivity suffers when fewer than approximately eight [223] or ten [224] cycles are visible. Therefore, the modelling may not be representative of tasks that involve very small targets where spatial details are insufficiently represented. Similarly, while Hoekstra et al. (1974) found that the critical number of cycles varied with target luminance, they found the critical number of cycles decreased (fewer visible cycles were necessary) with decreasing luminance. At all luminances tested by Hoekstra et al. (ranging from 2 to 600 cd/m2) the critical number of cycles appeared (from their Figure 1) to occur at fewer than 10 cycles.

The objective determination of the best-corrected refractive state performed here was likely less variable than a subjectively determined best-correction [226,227], however, the visual acuity data with which the metric values were compared, would have been affected by subjective variability [228,229]. That, in these comparisons, VSX(td,a) predicted a greater decrease in visual performance with age than either of the actual performance datasets (Elliott et al. (1995) and Owsley et al. (1983)), might agree with the criticism [210] that Nameda et al. (1989) did not employ adequate screening for pathology in their elderly patients. While the neural weighting component of visual image quality metrics such as VSX constrains the PSF to the approximate sampling and

processing limits of the visual system, a ceiling effect has been noted in how these metrics track visual performance at excellent levels of high contrast visual acuity [230,231]. In these cases, the metric value can be sensitive to improvements in image quality while visual acuity is unchanged at its physiological maximum.

Nevertheless, the VSX(td,a) metric that explicitly considered both retinal illuminance and age in the neural weighting component, tracked the relative change in visual acuity with age better than VSX(td), which only considered age insofar as it affects retinal illuminance via senile miosis. Although others [13] found comparable results to Nameda et al. (1989), the present comparisons may suggest that age-specific neural weighting of the model is appropriate in principle, but that a lesser decrease with age (than that found by Nameda et al. (1989)) should be used. An ideal dataset would have contained aberrations, best-corrected performance, and a measure of neural processing such as neural contrast sensitivity, as a function of retinal illuminance and age, all on the same individuals – unfortunately this was not available. When combining and comparing data from multiple sources, making manual modifications, say, to the weighting functions, could easily have been erroneously influenced by an idiosyncrasy of another dataset and, therefore, this was not done. In contrast, we sought to base the models in literature.

Ultimately, the models of neural contrast sensitivity presented here can easily be incorporated into existing visual image quality metric calculations (Appendix 2) as well as into other modelling of foveal vision and visual processing. While the Campbell and Green (1965) function has been adequate at high photopic levels, the presented models allow the neural

weighting component of visual image quality metrics to better respect how retinal illuminance and age impact the neural contrast sensitivity function.

5.6 Conclusions

Physiological visual image quality was modelled as a function of target luminance and age, where the optical component (aberrations) of the metric was scaled to physiological pupil sizes and two models of neural contrast sensitivity as a function of (1) retinal illuminance and (2) retinal illuminance and age were constructed from literature and incorporated into the metric calculation. The optical and neural components of the metric interacted in three ways that depended on luminance and the role of the neural component became increasingly relevant as age increased. Weighting the optical component with a neural function that considered both retinal illuminance and age allowed objectively best-corrected metric values at physiological pupil sizes to track measured best-corrected visual acuity as a function of age better than a model that only accounted for retinal illuminance and better than a purely optical model (no neural weighting).

5.7 Appendix 1: Calculated and actual dilated pupil diameters (mm)

Table 5. 1 Calculated and actual dilated pupil diameters. All mean ± SD pupil sizes are diameters expressed in mm. At target luminances between 4 and 1 log cd/m^2, the dilated pupil size of each eye was greater than the calculated physiological pupil size [163]. At lower target luminances, a small proportion of eyes did not dilate to the calculated pupil size and the actual dilated pupil size was used instead to avoid scaling aberrations to a larger pupil size than was measured.

	Age group	**20-29**	**30-39**	**40-49**	**50-59**	**60-69**	**70-79**
	Total eyes	20	18	32	32	21	23
4 log cd/m^2	Calculated pupil	2.70 ± 0.01	2.66 ± 0.01	2.61 ± 0.01	2.57 ± 0.01	2.54 ± 0.01	2.49 ± 0.01
3 log cd/m^2	Calculated pupil	3.53 ± 0.03	3.41 ± 0.03	3.41 ± 0.03	3.29 ± 0.03	3.18 ± 0.03	3.07 ± 0.02
2 log cd/m^2	Calculated pupil	4.80 ± 0.05	4.56 ± 0.06	4.32 ± 0.07	4.10 ± 0.07	3.90 ± 0.05	3.66 ± 0.06
1 log cd/m^2	Calculated pupil	6.13 ± 0.08	5.78 ± 0.09	5.41 ± 0.10	5.08 ± 0.10	4.77 ± 0.07	4.41 ± 0.09
0 log cd/m^2	Calculated pupil	7.07 ± 0.10	6.63 ± 0.11	6.17 ± 0.13	5.76 ± 0.13	5.38 ± 0.09	4.93 ± 0.11
	Actual pupil	7.03 ± 0.15	6.63 ± 0.11	6.17 ± 0.13	5.76 ± 0.13	5.38 ± 0.09	4.93 ± 0.11
	Mean difference	0.04	0.00	0.00	0.00	0.00	0.00
	Eyes that actual pupil < calculated	2	2	0	0	0	0
–1 log cd/m^2	Calculated pupil	7.56 ± 0.11	7.08 ± 0.12	6.57 ± 0.14	6.12 ± 0.14	5.70 ± 0.10	5.20 ± 0.12
	Actual pupil	7.47 ± 0.29	7.00 ± 0.17	6.55 ± 0.16	6.11 ± 0.15	5.70 ± 0.10	5.20 ± 0.12
	Mean difference	0.10	0.08	0.02	0.00	0.00	0.00
	Eyes that actual pupil < calculated	3	4	2	1	0	0
–2 log cd/m^2	Calculated pupil	7.78 ± 0.12	7.28 ± 0.12	6.75 ± 0.14	6.28 ± 0.15	5.84 ± 0.10	5.33 ± 0.12
	Actual pupil	7.64 ± 0.35	7.15 ± 0.24	6.71 ± 0.19	6.26 ± 0.17	5.84 ± 0.10	5.33 ± 0.12
	Mean difference	0.14	0.13	0.04	0.01	0.00	0.00
	Eyes that actual pupil < calculated	4	5	3	3	1	0
–3 log cd/m^2	Calculated pupil	7.87 ± 0.12	7.36 ± 0.13	6.82 ± 0.15	6.34 ± 0.15	5.90 ± 0.10	5.38 ± 0.13
	Actual pupil	7.72 ± 0.38	7.20 ± 0.27	6.78 ± 0.21	6.32 ± 0.18	5.89 ± 0.10	5.38 ± 0.12
	Mean difference	0.16	0.15	0.04	0.02	0.01	0.00
.	Eyes that actual pupil < calculated	4	6	3	3	1	0

5.8 Appendix 2: Matlab code to generate neural contrast sensitivity as a function of retinal illuminance and age

```
% nCSF_model.m
%
% Permission is granted to use this code for research purposes only.
%
% Publications based on this code should cite the original source:
% Hastings GD, Marsack JD, Thibos LN, Applegate RA. Modelling neural and
% optical contributions to physiological visual image quality metrics as a
% function of age and luminance. xx
%
% This script generates neural contrast sensitivity functions (nCSFs)
% specific to age and retinal illuminance (Trolands).
% Data were incorporated from:
% Xu R, Wang H, Thibos L, Bradley A. JOSA (A) 2017;34:481-92, and
% Nameda N, Kawara T, Ohzu H. Optom Vis Sci 1989;66:760-5,
% and fit using:
% polyfitn, written by John D'Errico, accessed at:
% https://www.mathworks.com/matlabcentral/fileexchange/34765-polyfitn
%
% Operation: run as script; modify the "troland" and "age" variables in
% lines 27 and 28 as needed; if no age-specific weighting is desired,
% input an age between 20 and 29;
%
%
%%

% define inputs
trolands = 500;
age = 25;
spat_freq_array = 0:68;

% fit was best using log spatial frequency and log Trolands
log_spat_freq_array = log10(spat_freq_array);

% above 900td, nCSF is constant
if trolands > 900
    log_trolands = log10(900);
else
    log_trolands = log10(trolands);
end


%% hard-coded results of running polyfitn
%%

model_terms =[...
    4   0
    3   1
    3   0
    2   2
    2   1
    2   0
    1   3
    1   2
    1   1
    1   0
    0   4
    0   3
    0   2
```

```
    0   1
    0   0
    ];

coefficients =[...
    -0.008885018
    -0.020354839
    0.061913598
    0.01312143
    0.107014577
    -0.203086197
    -0.11541031
    0.208645549
    -0.141587645
    0.620001945
    -0.933535687
    2.489686204
    -2.667968721
    0.869141735
    1.220563819
    ];

%%
log_ncs_array(1:size(log_spat_freq_array,2)) = zeros;

%% here a neural contrast sensitivity z-value is calculated from x and y;
%% log spatial frequency contributes to x and log Trolands contributes to y
%%

% loop that goes through each spatial frequency
for loop1 = 1:size(log_spat_freq_array,2)

    log_spat_freq = log_spat_freq_array(1,loop1);

    log_ncs = 0;
    cumulative_term_value = 0;

    % loop that calculates single nCS value
    for loop2 = 1:size(model_terms,1)
        x_value = (log_trolands^(model_terms(loop2,1)));
        y_value = (log_spat_freq^(model_terms(loop2,2)));
        term_value = x_value*y_value*coefficients(loop2);
        cumulative_term_value = cumulative_term_value + term_value;
    end

    if cumulative_term_value >= 0
        log_ncs = cumulative_term_value;
    else
        log_ncs = 0;
    end

    % write to storage array
    log_ncs_array(loop1) = log_ncs;

end

%% end of log fit

% convert to linear neural contrast sensitivity output
ncs_array = 10.^log_ncs_array;

% extrapolate the first nCS element (corresponding to 0 cpd) from the peak
% of the nCSF back to zero
[max_ncs index_ncs] = max(ncs_array);
```

```
% cannot extrapolate for 0 cpd if the peak is at 1 cpd
if index_ncs == 2
    warning('peak of nCSF is at 1 cpd; double-check extrapolation');
end

if max_ncs > 2
    zero_cpd_ncs = interp1([spat_freq_array(2:index_ncs)],...
        [ncs_array(2:index_ncs)],[0],'linear','extrap');
    ncs_array(1) = zero_cpd_ncs;
elseif max_ncs <= 2
    ncs_array(1) = 1;
end

%%
% age-multipliers defined from 0 to 68 cpd to agree with input
if age <30
    age_multiplier = ones(1,69);
elseif age >= 30 && age <40
    age_multiplier =
[0.814087639,0.824355959,0.835354525,0.873760474,0.903262953,0.922946774,0.934736731,0
.940470769,0.941585945,0.939166100,0.934027270,0.926788705,0.917925223,0.907804760,0.8
96715246,0.884884018,0.872491984,0.859684090,0.846577150,0.833265769,0.819826876,0.806
323221,0.792806104,0.779317526,0.765891883,0.752557332,0.739336879,0.726249263,0.71330
9681,0.700530366,0.687921082,0.675489516,0.663241612,0.651181849,0.639313468,0.6276386
70,0.616158774,0.604874359,0.593785378,0.582891257,0.572190978,0.561683152,0.551366079
,0.541237801,0.531296145,0.521538763,0.511963163,0.501923353,0.492497569,0.483425692,0
.474681988,0.466242960,0.458087130,0.450194837,0.442548065,0.435130286,0.427926326,0.4
20922237,0.414105186,0.407463364,0.401149760,0.395043761,0.389138838,0.383428729,0.377
907423,0.372569154,0.367408390,0.362419823,0.357598361];
elseif age >= 40 && age <50
    age_multiplier =
[0.788617117,0.798662769,0.813147535,0.849556031,0.875127701,0.889855940,0.896100055,0
.895956784,0.891032641,0.882527844,0.871340435,0.858148218,0.843468006,0.827697728,0.8
11146463,0.794056083,0.776617026,0.758979966,0.741264525,0.723565882,0.705959813,0.688
506599,0.671254060,0.654239948,0.637493842,0.621038660,0.604891866,0.589066459,0.57357
1761,0.558414073,0.543597203,0.529122905,0.514991247,0.501200901,0.487749402,0.4746333
54,0.461848600,0.449390372,0.437253413,0.420614239,0.406313820,0.392755731,0.379880880
,0.367636161,0.355973747,0.344850478,0.334227326,0.324068935,0.314343215,0.305020991,0
.296075691,0.287483079,0.279221008,0.271269215,0.263609129,0.256361022,0.249412730,0.2
42750601,0.236361690,0.230233721,0.224355052,0.218714637,0.213301996,0.208107180,0.203
120746,0.198333728,0.193737613,0.189324312,0.185086142];
elseif age >= 50 && age <60
    age_multiplier =
[0.688228592,0.708637940,0.730735980,0.759066439,0.771554676,0.770939410,0.760890838,0
.744271765,0.723170881,0.699099181,0.673153959,0.646136603,0.618634891,0.591080614,0.5
63790378,0.536994881,0.510860209,0.485503522,0.461004748,0.437415380,0.414765165,0.393
067219,0.372321979,0.352520260,0.333645640,0.315676322,0.298586600,0.282348003,0.26693
0200,0.252301706,0.238430442,0.225284165,0.212830806,0.201038734,0.187942745,0.1767030
52,0.166289836,0.156625695,0.147642155,0.139278465,0.131480575,0.124200268,0.117394415
,0.111024346,0.105055301,0.099455964,0.094079858,0.089024619,0.084269661,0.079795798,0
.075585145,0.071621025,0.067887882,0.064371205,0.061057452,0.057933979,0.054988984,0.0
52211441,0.049591052,0.047118191,0.044783863,0.042579656,0.040497703,0.038530646,0.036
671598,0.034914115,0.033252162,0.031680089,0.030192602];
elseif age >= 60 && age <70
    age_multiplier =
[0.601363500,0.608810398,0.616257296,0.640001723,0.643144178,0.631450680,0.610007062,0
.582472062,0.551397538,0.518553150,0.485162194,0.452064390,0.419827980,0.388827691,0.3
59299636,0.331380441,0.305135427,0.280579083,0.257690049,0.236422119,0.216712364,0.198
487118,0.181666395,0.166167122,0.151905499,0.138798695,0.126766050,0.115729894,0.10561
6095,0.096628121,0.088269768,0.080741577,0.073946725,0.067801591,0.062233692,0.0571799
87,0.052585463,0.048401967,0.044587218,0.040997442,0.037712173,0.034704418,0.031949671
,0.029425674,0.027112206,0.024990889,0.023045014,0.021259383,0.019620169,0.018114787,0
.016731780,0.015460711,0.014292072,0.013217196,0.012228181,0.011317821,0.01047954,0.00
```

```
9707334,0.008995725,0.008339707,0.007734706,0.007176542,0.006661393,0.006185764,0.0057
46455,0.005340539,0.004965335,0.004618388,0.004297449];
elseif age >=70
    age_multiplier =
[0.497925795,0.523784693,0.563948023,0.582654706,0.577290040,0.555446998,0.523084116,0
.484372560,0.442190006,0.398519691,0.354725539,0.312607937,0.275422870,0.242661010,0.2
13796209,0.188364909,0.165958691,0.146217717,0.128824955,0.113501082,0.100000000,0.088
1048870,0.0776247120,0.0683911650,0.0602559590,0.0530884440,0.0467735140,0.0412097520,
0.0363078050,0.0319889510,0.0281838290,0.0248313310,0.0218776160,0.0192752490,0.016982
4370,0.0149623570,0.0131825670,0.0116144860,0.01023293,0.009015711,0.007943282,0.00699
8420,0.006165950,0.005432503,0.004786301,0.004216965,0.003715352,0.003273407,0.0028840
32,0.002540973,0.002238721,0.001972423,0.001737801,0.001531087,0.001348963,0.001188502
,0.001047129,0.000922571,0.000812831,0.000716143,0.000630957,0.000555904,0.000489779,0
.000431519,0.000380189,0.000334965,0.000295121,0.000260016,0.000229087];
else
    disp('age error');
    return
end

% weight nCSF by the age_multiplier
ncs_array = ncs_array.*age_multiplier;

% for clarity, output arrays
output_spat_freq = spat_freq_array;
output_ncs = ncs_array;

%plot(output_spat_freq,output_ncs);

%%
disp('done model');
```

Chapter 6: Personalizing the neural weighting component of visual image quality metrics

Hastings GD, Schill AW, Hu C, Coates DR, Applegate RA, Marsack JD.

(in preparation)

6.1 Abstract

PURPOSE

Eyes with keratoconus have displayed better performance (such as visual acuity) than would be expected from their aberrations (prominently coma), which cause rotationally asymmetric blur. This study sought to measure neural contrast sensitivity functions of eyes with keratoconus, compare them to those of typical eyes, and evaluate their potential impact in the clinical applications of visual image quality metrics, such as optimizing objective refraction and comparing corrections and predicting performance across ophthalmic correction modalities.

METHODS

Using a custom ophthalmic interferometer that bypassed the optics of an eye, sinusoidal grating neural contrast sensitivity was measured in six eyes (three subjects) with keratoconus and four typical eyes (two subjects) at six spatial frequencies (2, 4, 8, 16, 22.5, 32 cycles per degree) and eight orientations (0 (horizontal), 22.5, 45, 67.5, 90, 112.5, 135, 157.5). Total experiment duration was between 24 and 28 hours per subject. Three additional typical subjects were measured at one (horizontal) orientation. Visual Strehl ratio (VSX) was calculated using neural weighting functions of each individual eye as well as a rotationally symmetric (model) function from literature and used to identify an optimal objective spectacle refraction in all eyes and evaluate wavefront-guided scleral lens corrections in eyes with keratoconus.

RESULTS

Neural contrast sensitivity of typical eyes agreed with levels from literature at the same retinal illuminance (15 Trolands) and generally showed the oblique effect on a linear-scale and rotational symmetry on a log-scale (ratio of major and minor radii of best ellipse fit to all orientations within each spatial frequency, mean 0.93, median 0.93; where circle = 1). Radially averaged sensitivities of eyes with keratoconus were 20% (lowest SFs) to 60% (highest SFs) lower than typical eyes and showed marked rotational asymmetry (mean 0.84; median 0.86) and substantial reductions (generally proportional to disease severity) in specific orientations.

For eyes with keratoconus, across wavefront-guided scleral lenses and spectacles, VSX was better (both $p = 0.046$; Wilcoxon matched pairs) when weighted using the measured neural contrast sensitivity functions than when using a rotationally symmetric model function. Spectacle VSX for typical eyes did not statistically differ ($p = 0.068$).

Optimal objective sphero-cylindrical corrections did not differ clinically for any eyes across the different neural weighting functions (mean ±SD Euclidean dioptric difference 0.13 ±0.18 D).

CONCLUSIONS

Neural contrast sensitivity functions of eyes with keratoconus differed from typical eyes and appeared to mitigate some effects of the rotationally asymmetric optics of eyes with keratoconus when calculating VSX, whereas a rotationally symmetric function overestimated the detrimental effects of aberrations on vision. Optimal objective sphero-cylindrical corrections were clinically equivalent irrespective of the neural contrast sensitivity function used.

6.2 Introduction

Chapter 4 described the evolution of scleral lens corrections to be personalized to optics (wavefront error) of an individual eye. The desire for a metric that can evaluate ophthalmic corrections across modalities has been repeatedly stated in this dissertation and, analogous to Chapter 4, this chapter describes the evolution of such metrics to be personalized to an individual eye.

Visual image quality metrics[153] distil the visual system into two fundamental (optical and neural) components. The optical component is derived from an ocular wavefront error measurement and, as such, is always specific to an individual eye. Historically, the neural component had generally used the photopic neural contrast sensitivity function measured[154] using laser interferometry in one young eye. While recent work from our laboratory (Chapter 5) developed a model of neural contrast sensitivity for typical eyes as a function of retinal illuminance and age (that allows the metrics to better respect real-world conditions), the neural component of visual image quality metrics has never truly been individualized in the same sense as the optical component.

Variability in neural contrast sensitivity across individuals with typical eyes has been noted both when measured using interferometry and adaptive optics[10,154,155,159,185,187,206,210] (as discussed in Chapter 5) however, the relevance of this variability in the context of visual image quality metrics is unknown. Neural contrast sensitivity functions of individuals with keratoconus, measured at one grating orientation, also differ from those of normal eyes.[11,27,28,156,232] As these

experiments are both time-consuming and difficult for subjects (especially those with ocular disease), all authors based their observations on fewer than five eyes.

The concept of individualizing the neural weighting function is applicable to all visual image quality metrics; the one that will be used to illustrate the work of this chapter is the visual Strehl ratio (VSX) calculated in the space domain.[153] As stated in preceding chapters, VSX has been used to evaluate and optimize spectacle[25,30] and contact lens[110,233,234] corrections because it has been shown predictive of subjective best focus[153,177–179] and changes in the logarithm of VSX have been well correlated with changes in visual performance,[181] especially with logMAR visual acuity,[147,182] independent of underlying pupil size and wavefront error. VSX has also been applied in studying highly aberrated eyes, such as those with keratoconus.[181,235]

While many interesting analyses can be performed on neural contrast sensitivity data from eyes with keratoconus (please see future directions in Chapter 7), the work described here is limited to considering whether personalizing the neural weighting function of VSX alters or explains the clinical applications and findings described in the preceding chapters. Specifically, this chapter examines whether personalizing the neural weighting function (1) changes the sphere, cylinder, and axis prescription that objectively optimizes the metric by a clinically significant amount (0.50 D), and (2) affects the metric value of eyes wearing wavefront-guided lenses (and might help explain the apparent dissonance between these eyes reaching typical levels of visual acuity and contrast sensitivity, but not reaching typical levels of VSX).

6.3 Methods

6.3.1 Subjects

Prior to data collection, the purpose and methods were explained to each subject and informed consent approved by the University of Houston Institutional Review Board was signed. This study adhered to the tenets of the declaration of Helsinki.

Three subjects (six eyes) with keratoconus, aged 44, 30, and 36, participated; disease severity, evaluated using the Topometric/KC Staging software on the Pentacam HR (Oculus Inc, Arlington, WA) is described using the ABCD[138] system in Table 6.1. Two subjects (four eyes) without keratoconus, aged 35 and 33 completed all orientations as controls and three additional typically-sighted subjects performed neural contrast sensitivity measurements (Section 6.3.3) at one orientation. Exclusion criteria included systemic conditions that could have ocular consequences as well as history of ocular surgery, trauma, or pathology other than keratoconus. Subjects were fit with a dental impression bite-bar that aligned them across wavefront error and interferometry measurements. Total experiment duration was 24 to 28 hours, divided into seven to twelve sessions on different days depending on subject fatigue and availability.

6.3.2 Wavefront error

Wavefront error was measured in a darkened room without mydriasis using a COAS HD (Johnson and Johnson Vision, Santa Ana, CA), which output a 10^{th} radial order normalized Zernike expansion corrected to 555 nm. Three measurements were recorded at the beginning and three at the end of the experiment, then pooled and averaged (per Zernike term) after being scaled down to the largest common pupil size – wherever possible, a 5 mm diameter was used, to

agree with previous chapters. Wavefront error for contact lens corrections were measured through the lenses.

Table 6. 1 Disease severities[138] of the eyes with keratoconus, where 0 is normal and 4 is the most severe. Dimension D (best corrected visual acuity) is not reported as it varies drastically depending on whether the eyes are corrected with spectacles, conventional scleral lenses, or wavefront-guided lenses. All typical eyes were graded as 0 across dimensions A, B, and C.

	(A) Anterior corneal radius of curvature[138]	(B) Posterior corneal radius of curvature[138]	(C) Thinnest pachymetry[138]
KC1 Right	1.9	2.6	1.4
KC1 Left	1.6	2.4	1.8
KC2 Right	2.8	>4.0	0.4
KC2 Left	2.8	>4.0	0.6
KC3 Right	2.3	>4.0	3.1
KC3 Left	>4.0	>4.0	>4.0

6.3.3 Ophthalmic interferometry

Sinusoidal interference fringes were generated using an amplitude-division Maxwellian-view ophthalmic interferometer similar to that of Williams[185,236] and Coletta and Sharma.[10] A floating, vibration-damped optical table helped isolated the system from vibrations that could reduce interference fringe stability. The dental impression bite-bar for each subject was mounted to a three-axis translation stage adjacent to – but not touching – the optical table.

Monochromatic light from a 543 nm helium-neon laser (Research Electro Optics, Boulder, CO) was divided into two beams with a 50/50 beam-splitter cube. Each beam was (square-wave) flickered at 500 Hz by an acousto-optic modulator (AOM) using a custom Matlab (The Mathworks Inc, Natick, MA) interface, a Rigol DG1022 function generator (Rigol Technologies, Beaverton, OR), and a two-channel fixed frequency driver (Brimrose Corp,

Sparks, MD). Contrast of the interference fringe was controlled by varying the relative phase of the AOM flicker. When the two beams were flickered in phase, they arrived at the retina at the same time and interfered for the maximum amount of time resulting in maximum contrast. When the two beams were perfectly out of phase, they did not temporally overlap on the retina, which resulted in a zero contrast uniform field (500 Hz flicker is much higher the critical fusion frequency of the human visual system). This technique allows modulation of contrast while maintaining constant retinal illuminance.[10,185,236]

Spatial frequency of the interference fringes is proportional to the separation of the point foci of each beam in the focal plane of the Maxwellian-view lens. The separation of the point foci was controlled using two mirrors equipped with micrometers that were adjusted by equal amounts to displace each beam equally and oppositely from the center of the entrance pupil in an attempt to minimize any role of the Stiles-Crawford effect. An aperture on the surface of the Maxwellian-view lens limited the interference pattern to a circular 10 degree patch.

Because the optical aberrations of eyes with keratoconus typically cause directionally-specific (rotationally asymmetric) blur, we were interested in measuring neural contrast sensitivity at many orientations. After the beams were recombined (50/50 pellicle) they passed through a dove prism, which was electronically rotated (NanoPZ-Util v1.0.2, Newport Corp, Irvine, CA) and controlled the orientation of the fringes with better than 0.25° resolution. Calibration experiments verified that rotating the coherent beams in this manner did not alter contrast or spatial frequency.

Incoherent light of 540 nm was superimposed on the coherent beams (50/50 pellicle), as has been done before,[10,154,185,236] to reduce the prominence of spatial noise or speckle in the coherent beams. The power of the coherent and incoherent beams were measured[237] individually (by occluding the other) using a Newport 1936-C power meter (Newport Corp, Irvine, CA) and neutral density filters were inserted into the beams such that the proportions of coherent and incoherent light were matched; this is termed a 50% *coherence fraction*.[10,185] The incoherent light extended slightly (less than 1 degree) in all directions beyond the edges of the 10 degree coherent patch.

To reduce the detrimental effects of floaters and tear film debris further, subjects were initially positioned with the pupil plane of the eye at the focal length of the Maxwellian-view lens, and were then moved axially to the position where floaters were the least noticeable. In agreement with previous literature,[10,185,236] this typically positioned the Maxwellian-view foci closer to the corneal plane of the eye – this has a negligible effect on spatial frequency at the retina[236,238] and is convenient for eyes with keratoconus because the ectatic cornea is the primary source of higher order aberrations.

The 543 and 540 nm lights are very near to the peak sensitivity of foveal cones (555 nm) and, during collection of pilot data, it was noted that the visibility of the fringes faded rapidly at 500 td levels of retinal illuminance – that is, a grating was perceptible for an instant after blinking and then immediately disappeared. This effect was persistent across observers with and without keratoconus. The stimulus (coherent and incoherent combined) was filtered before the

Maxwellian-view lens to a power level that produced 15 td, which was continuously visible and comfortable for prolonged viewing.

Intensity profiles of the resultant stimulus (sinusoidal interference patterns combined with the incoherent light) were measured using a Lasercam HR camera and BeamView 32-bit software (v 4.8.1; Coherent Inc, Santa Clara CA) that was levelled with the optical table and the bite-bar mount. The stimulus reached the camera via the 50/50 pellicle that was used to introduce the incoherent light and, therefore, was equivalent to that viewed by the observer. Via Fourier analysis, Michelson contrast was calculated and the spatial frequency evaluated with a resolution of 0.27 cycles per degree. The crosshair function in the BeamView software was used to align the gratings to the desired orientation. Although the laser was warmed-up for at least two hours prior to any measurements, calculating contrast at each visit in this way allowed us to compensate for subtle variability in laser intensity across visits.

6.3.4 Psychophysical method

Eyes with keratoconus typically experience directionally-specific (rotationally asymmetric) blur resulting from elevated levels of rotationally-asymmetric higher-order aberrations.[114,150] The degree to which the orientation-specific neural contrast sensitivity function of these eyes might be asymmetric was unknown. Because orientation-specific channels of the visual system have been estimated[221] as spanning 22.5°, neural contrast sensitivity was evaluated at eight orientations (22.5°, 45°, 67.5°, 90°, 112.5°, 135°, 157.5°, and 180°) for each of six spatial frequencies (2, 4, 8, 16, 22.5, and 32 cycles per degree). Randomization tables were

generated in Matlab where spatial frequencies were randomized first and then (within each spatial frequency) orientations were randomized.

Neural contrast sensitivity measurement of each spatial frequency and orientation combination began with a method of adjustment, which started at zero phase offset between the two coherent channels (maximum contrast). Using two buttons on a keypad, subjects modified the phase difference of the two channels in 1 degree steps (holding down a key would change the contrast rapidly) until the grating was just barely perceptible.

The subjective method of adjustment threshold was followed by a two interval forced choice paradigm of seven randomized constant stimulus levels. Pilot data indicated that both control subjects and those with keratoconus underestimated their thresholds subjectively (in agreement with literature[239,205] the method of adjustment threshold was consistently a higher contrast than the forced choice method). Consequently, two levels of constant stimuli were higher contrast (easier to see) and four were lower contrast (more difficult to see) than the method of adjustment threshold, spaced in 0.4 log unit contrast step multiples of that adjustment threshold; the seventh constant stimulus was the method of adjustment threshold. Stimuli were flashed for 0.5 sec each and separated by 1 sec. Each flash was accompanied by an audible tone. Subjects pressed one of two keys to indicate whether they perceived the stimulus in the first or second interval, after which they pressed the same key again to queue the next stimulus. Each constant stimulus was displayed sixteen times. Stimulus generation and subject responses were controlled and recorded in Matlab.

Eyes with more advanced keratoconus struggled to perform the adjustment of some high spatial frequencies. In these cases, the subject was told which orientation was being tested and the constant stimuli started at maximum contrast and decreased in 0.4 log unit multiple steps.

Constant stimulus trials for the 48 unique spatial frequency and orientation combinations were divided into two "runs" in an attempt to offset learning effects (counterbalancing).[240] Method of adjustment and half the constant stimulus trials (*run 1*) were performed on the subject's preferred eye (keratoconus is characteristically asymmetric across the two eyes and the preferred eye was measured first to facilitate more effective training (as described below) and understanding of the task). Thereafter, half of the trials (*run 1*) were then performed on the second eye; each eye followed a unique randomization. The second half of the trials (*run 2*) were then performed in reverse order (opposite to *run 1*) on the second eye, after which the second half of trials (*run 2*) for the first eye were performed in reverse order. Thus the last spatial frequency and orientation measured, was the same as the first combination completed.

Subjects were asked to blink after the two interval presentations and before queuing the next stimulus; they were allowed to rest whenever they felt the need and many breaks were designed into the protocol. Collectively, the adjustment and forced choice components were performed in 2 to 3 minutes, after which the subject rested for 1 to 2 minutes while orientation was changed. After all orientations of a spatial frequency were measured, subjects rested for at least 10 minutes (longer if they desired) while spatial frequency was changed.

6.3.5 Training

At the first visit, subjects underwent training which involved familiarization with correct positioning and alignment, fixation of the stimulus, and use of the keypad. Subjects KC2 and KC3 were unfamiliar with psychophysical concepts and methods. The concept of a method of adjustment threshold was explained and demonstrated such that refining a subjective threshold was understood. Subject KC1 and the two control subjects were experienced with visual psychophysics and had gained some experience with interferometry during the construction and calibration of the system. Training also included measurements for all 8 orientations at 8 cycles per degree (amounting to 8 method of adjustment and 448 forced choice trials) – these data were not included in the analyses.

To acclimate the subject to the stimulus every time spatial frequency was changed, subjects performed a method of adjustment and force choice series (56 trials) for that spatial frequency at a vertical (90°) orientation – these data were also not included in analyses.

6.3.6 Data analyses

After the first half of measurements had been performed on an eye (*run 1*), data were fit with Gumbel psychometric functions[241] in Matlab using the Palamedes[242] toolbox. The function is defined as:

$$PF_{Gumbel}(x;\alpha,\beta) = 1 - \exp(-10^{\beta(x-\alpha)})$$

with $x \in (-\infty, +\infty)$, α (threshold) $\in (-\infty, +\infty)$, β (slope) $\in (0, +\infty)$.

Each spatial frequency and orientation for each eye was inspected and if a subject had set the adjustment threshold such that they saw or missed most forced choice stimuli, stimuli (contrast levels) were added such that they spanned the range from 50% (guess rate) to 100% correct when the second half of data were collected. Contrast levels that were added in *run 2* were repeated within that run such that they were also evaluated 16 times in total. Forced choice data from the two *runs* at the same spatial frequency and orientation were then pooled and fit with psychometric functions. Most eyes performed approximately 500 forced choice trials for each spatial frequency and orientation combination. All psychometric functions were fit using maximum likelihood methods, assuming a lapse rate of 1% (0.01) and guess rate of 50% (0.5).

6.3.7 Visual image quality metric calculation

As described in previous chapters, VSX has historically been calculated as the ratio of the volume of the point spread function (PSF) of an eye (determined from a wavefront error measurement at a specific pupil size) to the volume of the diffraction-limited PSF for the same pupil size, where both PSFs are first weighted by the inverse Fourier transform of a neural contrast sensitivity function from Campbell and Green.[154] More recently, using a constant denominator across all eyes has been advocated.[175,176] This approach is useful in illustrating the effects of different weighting functions in the numerator.

Neural contrast sensitivity values for each individual eye were imported into Matlab and interpolated between the measured spatial frequencies and orientations. The *scatteredInterpolant* function was used to reconstruct and extrapolate the measured data over the range of 0 to 64

cycles per degree in two-dimensions. To examine the effects of these estimation methods (interpolation and extrapolation), the neural contrast sensitivity function of Campbell and Green[154] was sampled at the sampled frequencies tested (2, 4, 8, 16, 22.5, and 32 cycles per degree) and re-generated using the same interpolation and extrapolation. The results are illustrated in Figure 6.1, where differences between the functions can be noted over the extrapolated ranges (below 2 and above 32 cycles per degree).

Unfortunately it is simply not practical to repeat Campbell and Green's experiment,[154] that is, measuring each orientation at many more spatial frequencies between 0 and 64 cycles per degree, and therefore, interpolation and extrapolation were used. To minimize the effects of this difference in the results that follow, when the Campbell and Green function is needed, the reconstructed version (same sampling density as the measured neural contrast sensitivity functions; Figure 6.1B) was used.

Three versions of the VSX metric were calculated; these differed only in terms of the neural weighting function used: (1) the resampled Campbell and Green function (measured at 500 td), (2) the 15 td function from the model defined in Chapter 5, and (3) the function measured on the individual eye.

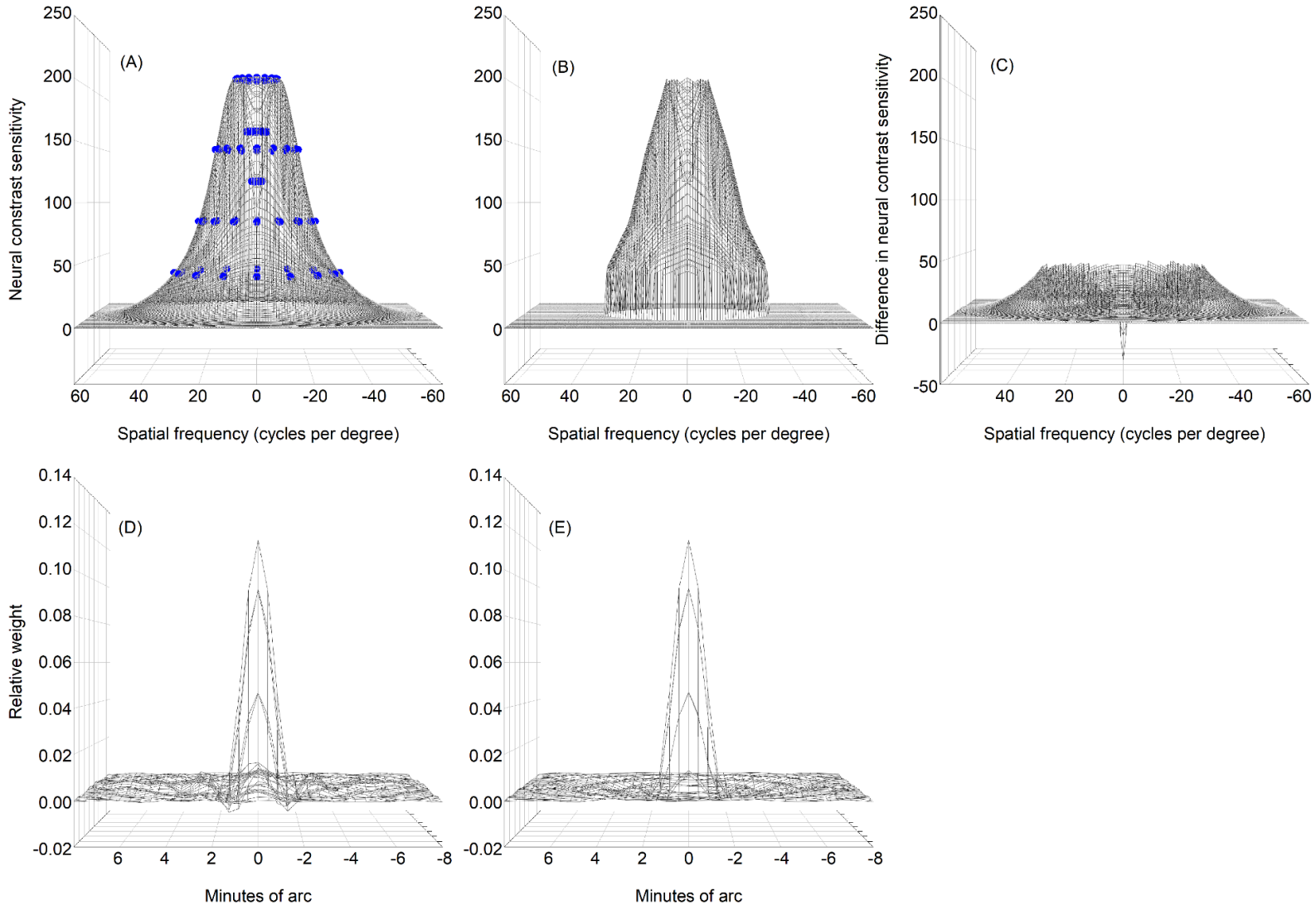
(A)
(B)
(C)
(D)
(E)
Neural constrast sensitivity
Difference in neural contrast sensitivity
Relative weight
Spatial frequency (cycles per degree)
Minutes of arc
250
200
150
100
50
0
-50
0.14
0.12
0.10
0.08
0.06
0.04
0.02
0.00
-0.02
60
40
20
0
-20
-40
-60
6
4
2
0
-2
-4
-6
-8

Figure 6. 1 The effect of interpolating and extrapolating the Campbell and Green neural contrast sensitivity function from data at six spatial frequencies (2, 4, 8, 22.5, and 32 cycles per degree) over the range from 0 to 64 cycles per degree. (A) Cartesian representation of the rotationally symmetric two-dimensional function historically used in VSX. Blue points indicate the sensitivities used in the interpolation and extrapolation of (B). (C) The difference between the functions in (A) and (B). (D) and (E) The neural weighting functions derived from (A) and (B) respectively.

6.4 Results

6.4.1 Neural contrast sensitivity data

6.4.1.1 Fitting of psychometric functions to determine thresholds

Figure 6.2 illustrates an example of data from the left eye of subject KC1 at 2 cycles per degree and 22.5° orientation. Gumbel (log-Weibell) functions are reported because they provided the maximum log-likelihood fit (better than cumulative normal or logistic; automatically evaluated by Palamedes[242]) in all typical eyes and for most spatial frequencies in eyes with keratoconus. Gumbel functions are appropriate in principle because of the logarithmic manner in which the visual system processes contrast (decelerating transducer function). Although the details are challenging to see, Figure 6.3 compiles all data for the left eye of subject KC1.

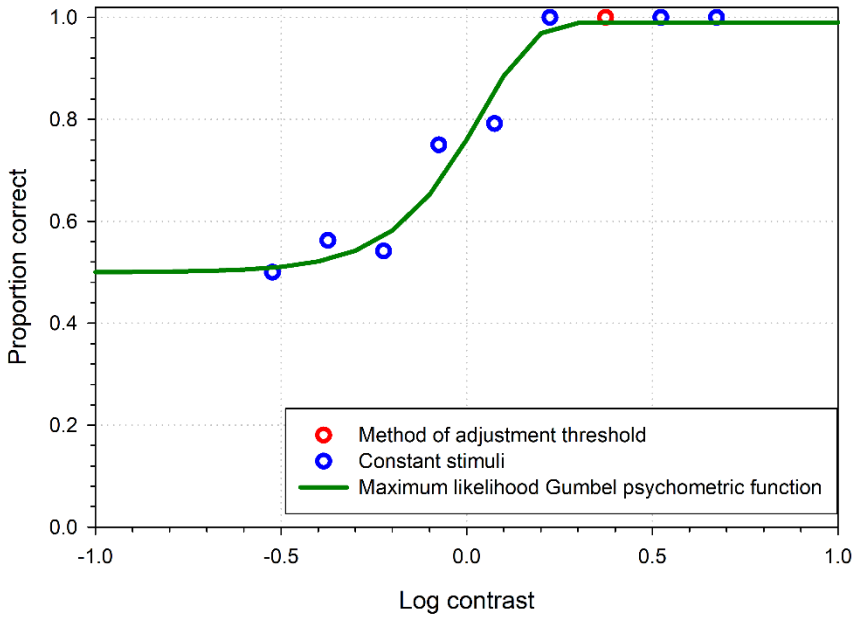

Figure 6. 2 Method of adjustment threshold, constant stimuli, and maximum likelihood Gumbel psychometric function fit for the left eye of subject KC1 at 2 cycled per degree and 22.5° orientation. In this case, two constant stimuli were added during *run 2* that were more difficult to see (lower contrast).

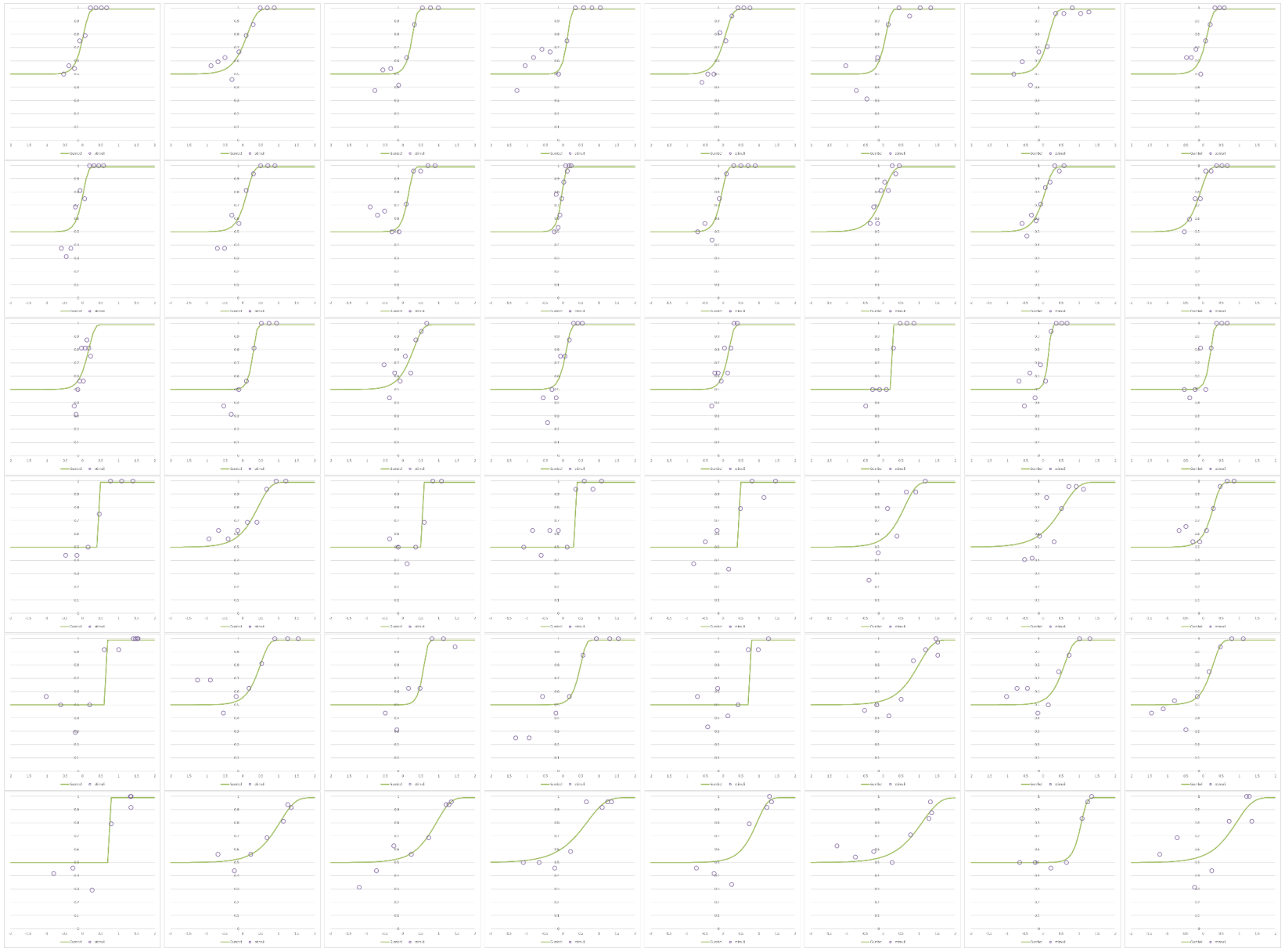

Figure 6. 3 Compilation of all neural contrast sensitivity data for the left eye of subject KC1. Columns are spatial frequencies (top to bottom) 2, 4, 8, 16, 22.5, and 32 cycles per degree. Rows are orientations (left to right) 22.5°, 45°, 67.5°, 90°, 112.5°, 135°, 167.5°, and 180°.

6.4.1.2 Typically-sighted control eyes

Neural contrast sensitivity functions of the seven typically-sighted eyes (five subjects) measured using horizontally-orientated gratings (termed "180°" in subsequent plots) are shown in Figure 6.4 along with the model defined in Chapter 5 for the same (15 td) retinal illuminance. Four typical eyes (two subjects) completed measurements at all eight orientations; logarithmic and linear neural contrast sensitivities are plotted per spatial frequency in polar form for a representative example (the left eye of S01) in Figures 6.5 and 6.6 respectively. This eye was chosen because it has 2.75 D of refractive astigmatism, which is habitually well-corrected. Because of being habitually corrected, note the rotational symmetry of the logarithmic sensitivities as well as the oblique effect (better sensitivity in cardinal than oblique meridians)[219,220] in the linear sensitivities. Logarithmic rotational symmetry is quantitatively examined in Section 6.4.1.4.

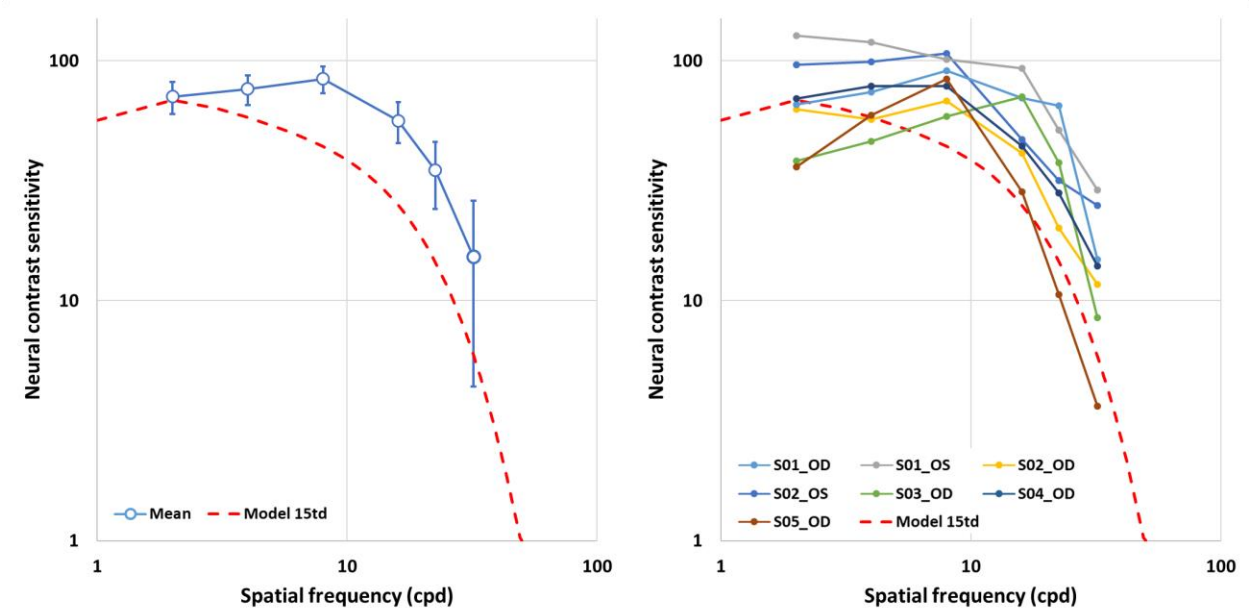

Figure 6. 4 Neural contrast sensitivity functions of seven typically-sighted eyes measured using horizontally-oriented gratings at 15 td. The model (defined in Chapter 5) corresponding to the same retinal illuminance is also plotted.

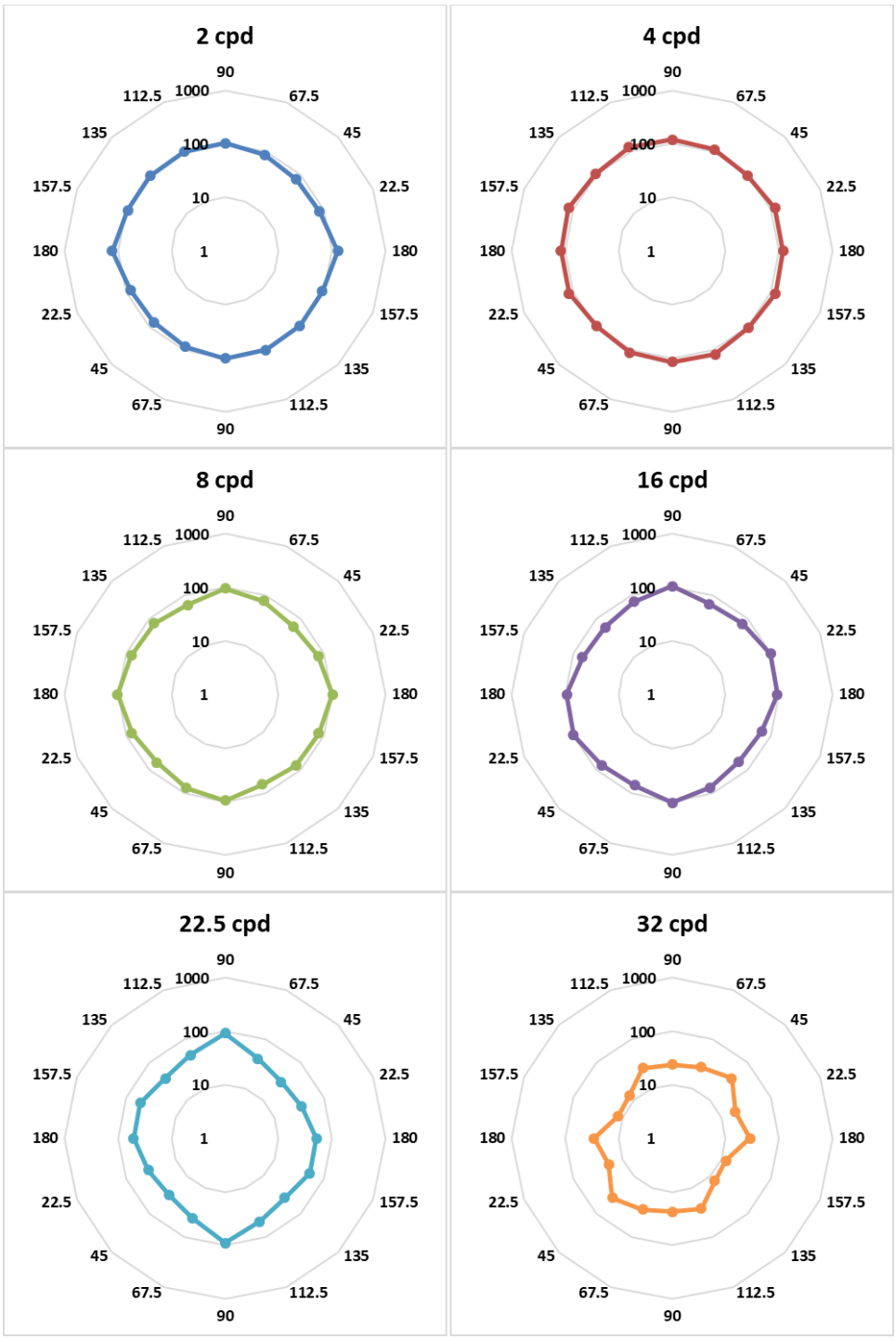

Figure 6. 5 Logarithmic neural contrast sensitivities at eight orientations for each of six spatial frequencies for the left eye of S01. Note that a 2.75 D astigmatic refractive error does not appear to have a substantial effect on sensitivities (because it is habitually well-corrected) and at spatial frequencies below 22.5 cpd, sensitivities are approximately rotationally symmetric.

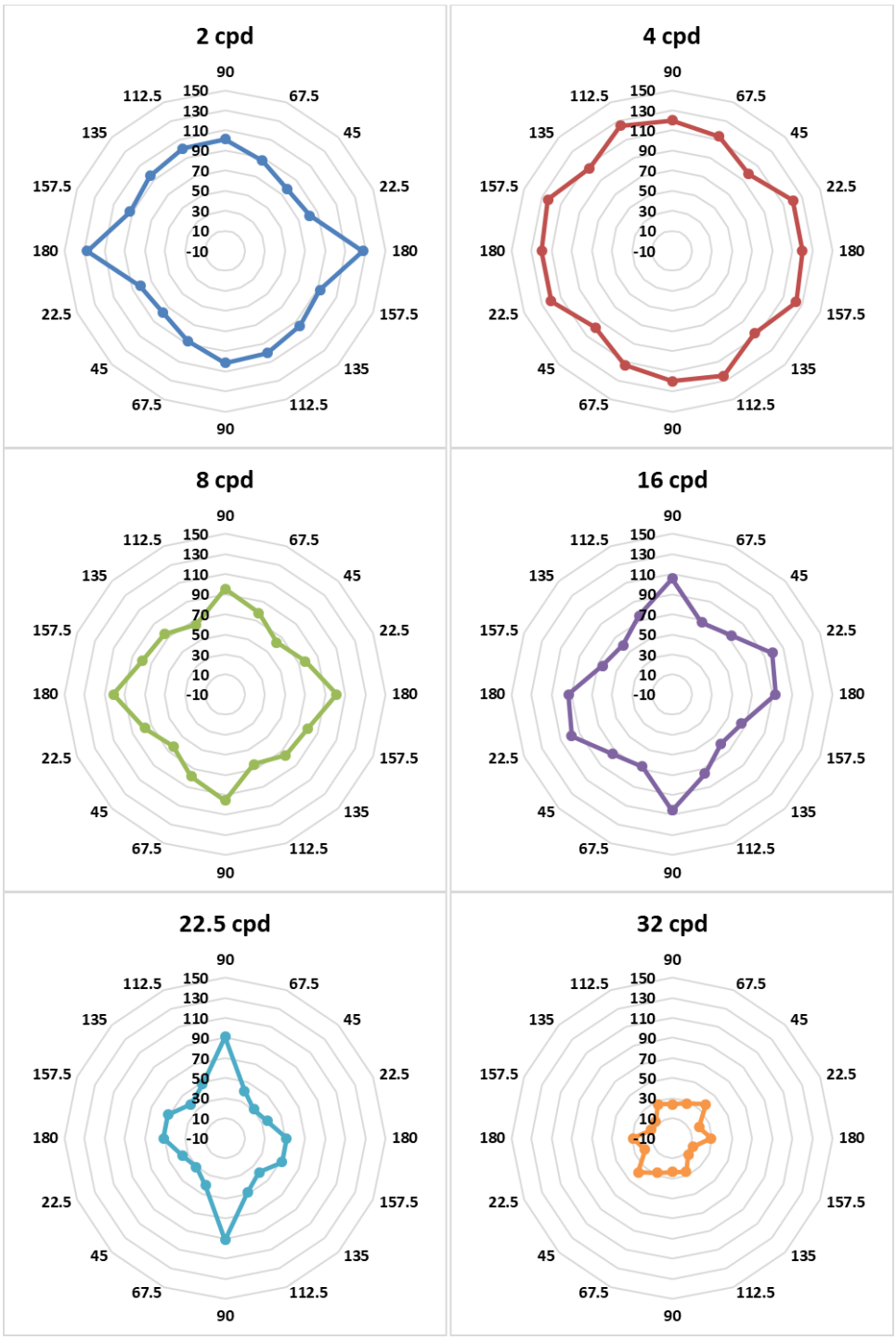

Figure 6. 6 Linear neural contrast sensitivities at eight orientations for each of six spatial frequencies for the left eye of S01. Note that the oblique effect (better sensitivity in cardinal than oblique meridians)[219,220] is visible at most spatial frequencies in the presence of 2.75 D astigmatic refractive error (because it is habitually well-corrected).

6.4.1.3 Eyes with keratoconus

The six eyes (three subjects) with keratoconus displayed substantially different neural contrast sensitivities to the typical eyes. Sensitivities were worse than those of typical eyes and, even when plotted on a logarithmic scale, sensitivities at most spatial frequencies were markedly rotationally asymmetric. Logarithmic neural contrast sensitivities for representative examples of one of the mildest (right eye of subject KC01) and most severe (left eye of subject KC02) disease severities are shown in Figures 6.7 and 6.8 respectively. The left eye of subject KC02 was unable to see 32 cycles per degree (when tested, the subject reported not seeing many of the constant stimuli, and data for all constant stimulus levels were around the 50% guess rate). The responses of this eye to other spatial frequencies were reliable and it was the impression of the investigators that he was motivated and trying his best.

6.4.1.4 Comparison of typical eyes and eyes with keratoconus

The most basic comparison between the neural contrast sensitivity of typical eyes and those with keratoconus is to radially average (across all orientations per spatial frequency) and pool the eyes within each of the two groups; this is shown in Figure 6.9. The eyes with keratoconus were between 20% (lowest spatial frequencies) and 60% (highest spatial frequencies) worse than typical eyes.

When plotted in a polar manner (such as in Figures 6.5 to 6.8) the area (in arbitrary units) enclosed by the neural contrast sensitivities at all orientations of each spatial frequency can be calculated. Here the trapezoid method was used in Matlab, which essentially connects adjacent

points with a straight line and calculates and sums the enclosed areas. The loss in sensitivity with keratoconus is easily appreciable in Figure 6.10; especially at 22.5 and 32 cycles per degree.

To more quantitatively evaluate the rotational symmetry of the neural contrast sensitivity functions, an ellipse was fit using a least-squares method to the polar data (such as in Figures 6.5 to 6.8) of all orientations of each spatial frequency of logarithmic neural contrast sensitivity. Rotational symmetry was then quantified using the ratio of the major and minor diameters of that best-fit ellipse, where the ratio of a circle equals 1 and the lower the number (below 1), the more the asymmetry. These results are shown in Figure 6.11. Asymmetry generally increases with increasing spatial frequency (with the exception of 8 cycles per degree for the eyes with keratoconus) and at all spatial frequencies eyes with keratoconus are less rotationally symmetric than typical eyes.

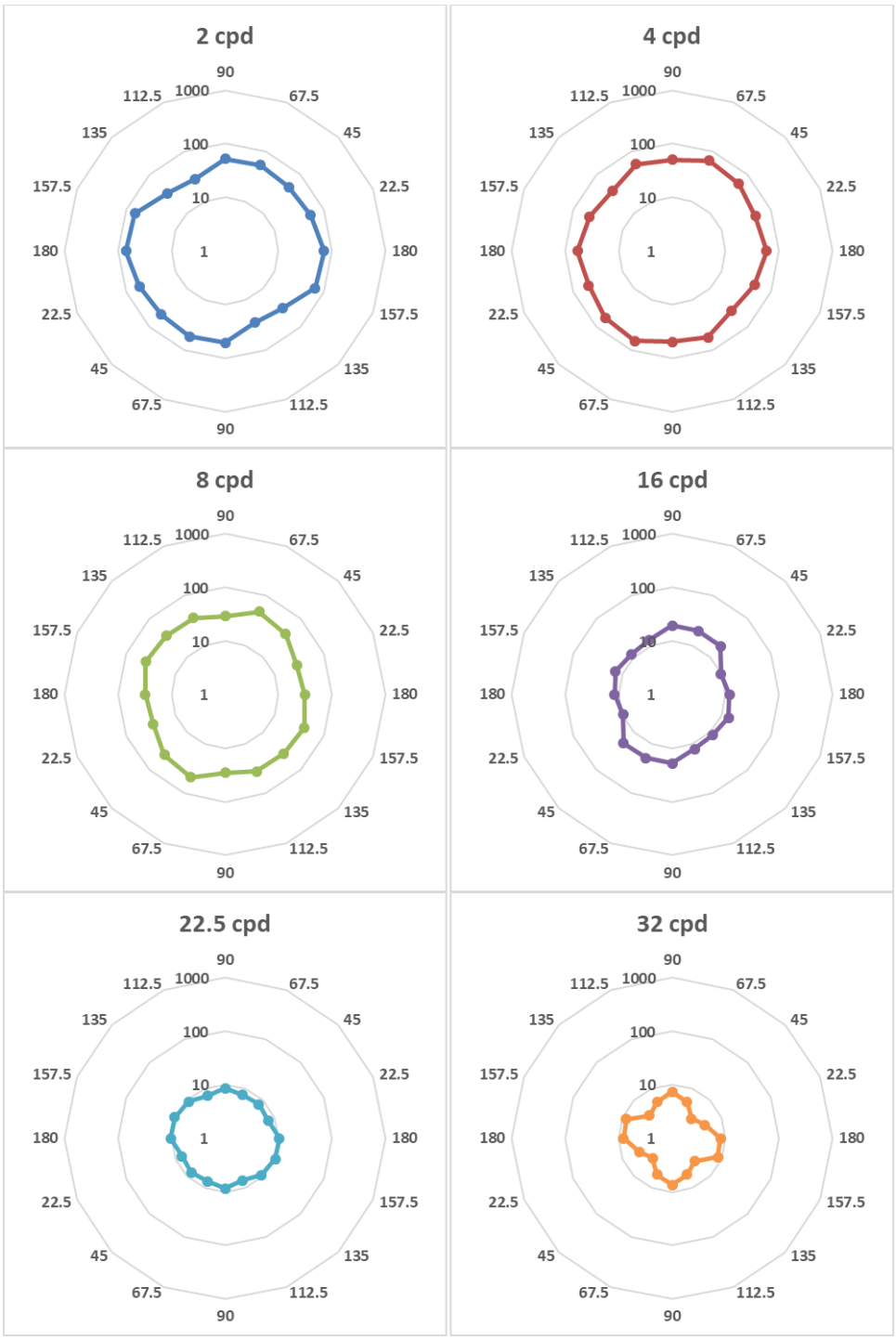

Figure 6. 7 Logarithmic neural contrast sensitivities for the right eye of subject KC01 – one of the mildest disease severities the participated.

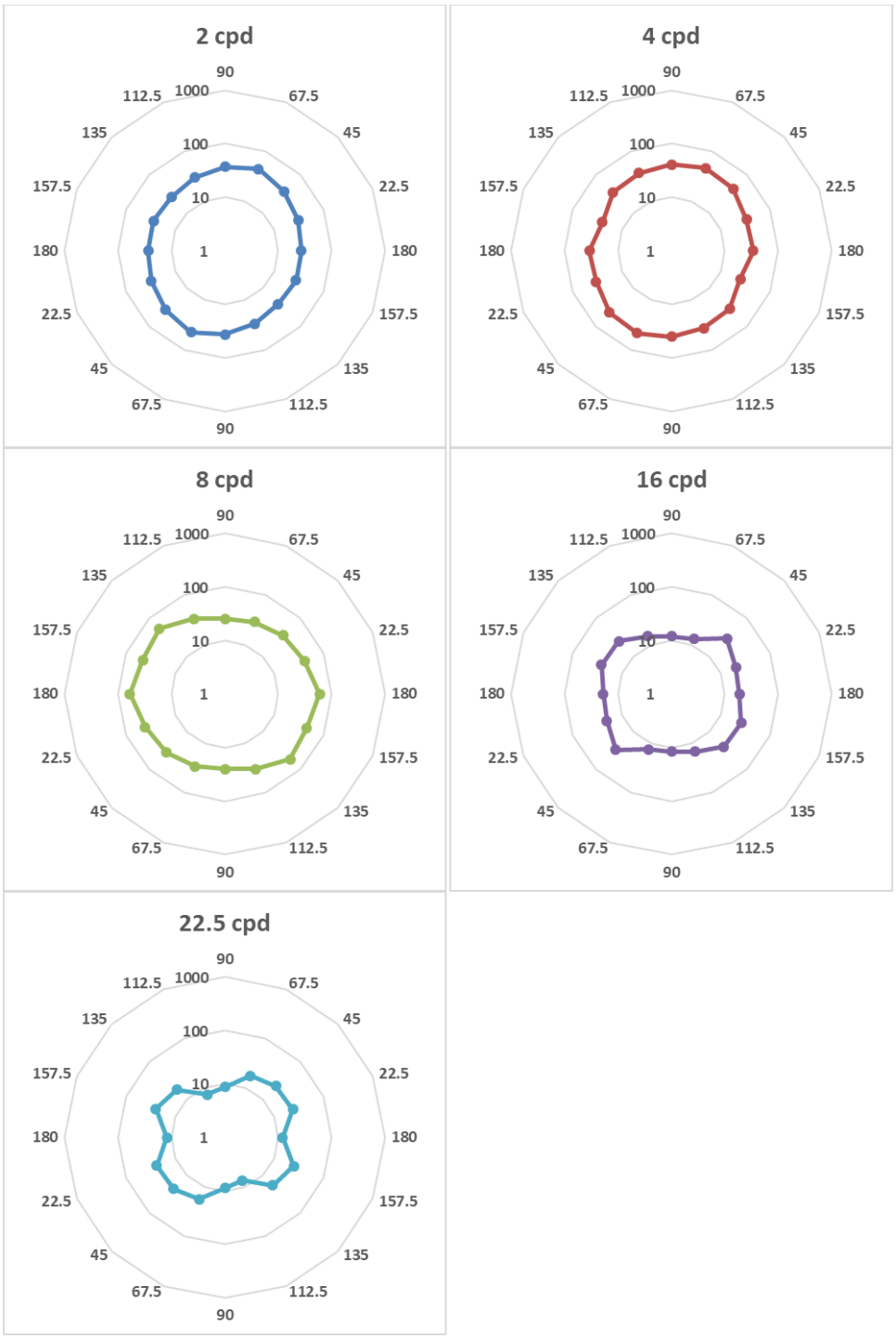

Figure 6. 8 Neural contrast sensitivities for the left eye of subject KC02 – one of the more advanced disease severities that participated. This subject was unable to see 32 cycles per degree (when tested, the subject reported not seeing many of the constant stimuli, and data for all constant stimulus levels were around the 50% guess rate).

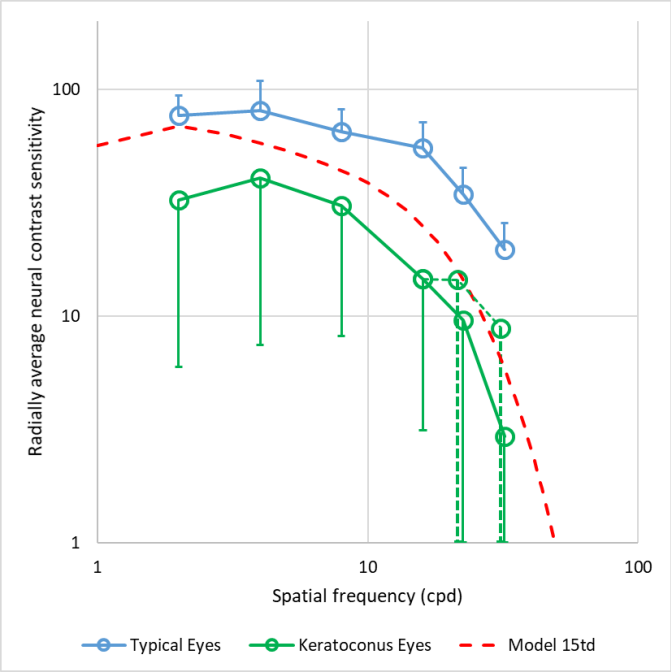

Figure 6. 9 Mean radially averaged neural contrast sensitivities pooled within the groups of typical eyes and those with keratoconus (dashed green lines omit eyes that could not resolve the grating; 2 eyes omitted at 22.5 cpd; 4 eyes at 32 cpd; solid green lines include those eyes at a 100% contrast threshold). Error bars are 1 standard deviation.

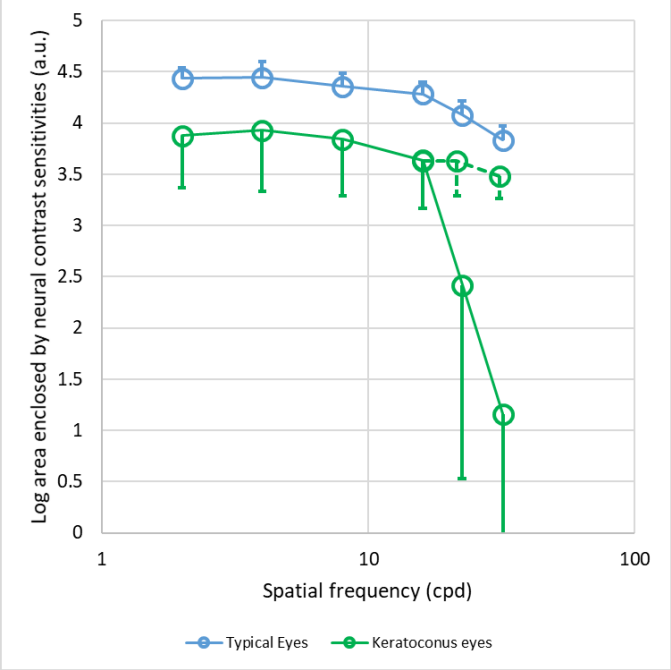

Figure 6. 10 Areas (arbitrary units) enclosed within all orientations of each spatial frequency pooled within the groups of typical eyes and keratoconus (dashed green lines omit eyes that could not resolve the grating; 2 eyes omitted at 22.5 cpd; 4 eyes at 32 cpd; solid green lines include those eyes at a zero area). Error bars are 1 standard deviation.

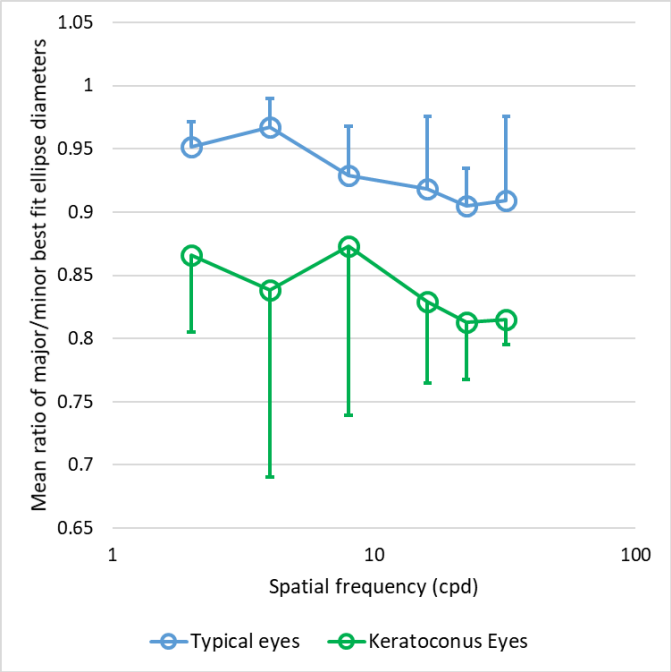

Figure 6. 11 Ellipses were fit using a least-square method to the polar representations of logarithmic neural contrast sensitivity for each spatial frequency (such as in Figures 6.5 to 6.8). The ratio of the major diameter to the minor diameter of those ellipses was used to quantify rotational asymmetry (where a circle = 1, and the lower the value the more the asymmetry). Eyes with keratoconus that could not see gratings at 22.5 and / or 32 cpd were excluded here.

6.4.2 Optimizing objective refractions

Chapter 2 described the objective optimization of refraction using the version VSX that was weighted by the Campbell and Green[154] neural contrast sensitivity function. Work from the University of Houston (Bell ELS, Hastings GD, Nguyen LC, Applegate RA, Marsack JD. (submitted)) has shown that, in keratoconus, it is necessary to consider a large range of corrections when finding the optimal refraction – typically the entire phoropter has been searched and this was done for the eyes with keratoconus here (sphere ranged from –20.00 to +16.00 D and cylinder from 0 to –8.00 D both in respective 0.25 steps; as in Chapters 2, 3, and 5, axis was searched in 2 degree steps).

Table 6.2 contains comparison of the optimized refraction determined using three neural contrast sensitivity functions: (1) the Campbell and Green function measured at 500 td, (2) the model defined in Chapter 5 at 15 td, and (3) the function measured at 15 td. Although there are subtle differences for most of the eyes, the differences are not clinically significant; Euclidean dioptric differences between the corrections determined using functions for 15 td are included.

Figure 6.9 shows the metric values across the three neural functions all arbitrarily normalized to the diffraction-limited PSF for a 3 mm pupil diameter weighted by the Campbell and Green function at 500 td. Across the three versions of the metric, the higher Troland level of the Campbell and Green function resulted in the highest metric value within each eye. In most cases the metric value calculated using the model of Chapter 5 was worse than the metric that used an individual eye's measured function at the same retinal illuminance – note that this is consistent across five of the six eyes with keratoconus despite their measured neural contrast sensitivity functions being of lower sensitivity (radially averaged in Figure 6.9) than the model. The differences between the model at 15 td and the measured functions were statistically significant ($p = 0.046$; Wilcoxon matched pairs) but not for typical eyes ($p = 0.068$). The lowest points on the plot (corresponding to the left eye of subject KC3) are the only data that do not follow this pattern. This was substantially the most severe eye examined and would likely not be a good clinical candidate for spectacles, as evidenced by the poor metric values in Figure 6.12 and the very high correction (–15.75 / –8.00) in Table 6.2.

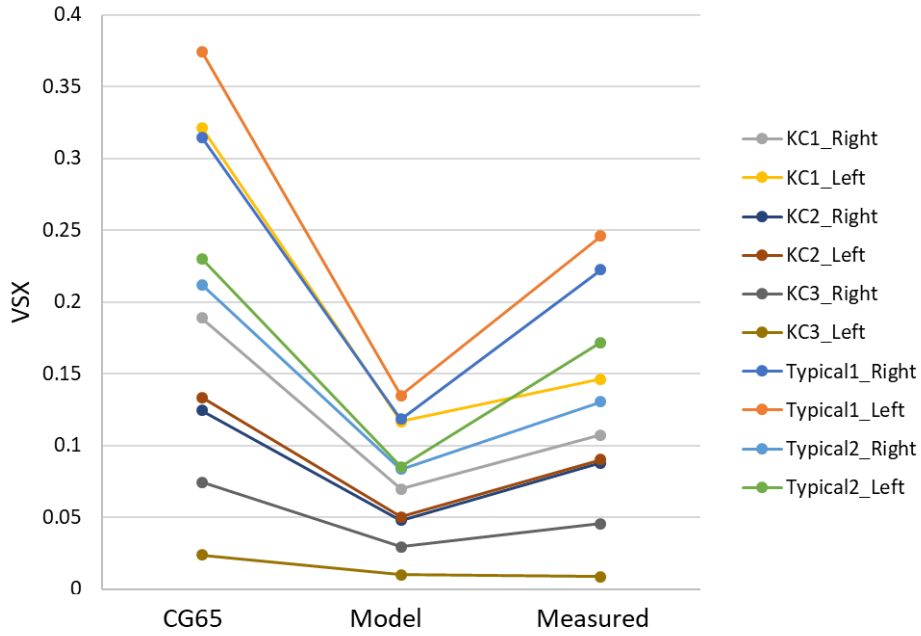

Figure 6. 12 VSX values corresponding to optimal spectacle corrections in Table 6.2, calculated with different weighting functions: Campbell and Green[154] at 500 td ("CG65"), the model from Chapter 5 at 15 td, and the individualized function measured at 15 td.

Table 6. 2 Objectively optimized refractions using the Campbell and Green neural contrast sensitivity function (500 td), the model of neural contrast sensitivity (15 td) and the measured neural contrast sensitivity function for each eye (15 td). Euclidean dioptric difference is calculated (via power vectors[47]) between the corrections determined using the model at 15 td and the function measured at 15 td.

		Campbell & Green 500td			Model 15 td			Measured nCSF 15td			Euclidean Dioptric Distance
		Sphere	Cylinder	Axis	Sphere	Cylinder	Axis	Sphere	Cylinder	Axis	
KC1	Right	–1.50	–2.75	60	–1.50	–2.75	60	–1.50	–2.75	60	0.000
KC1	Left	–1.75	–2.50	122	–1.75	–2.50	122	–1.75	–2.50	122	0.000
KC2	Right	–1.50	–5.75	84	–1.50	–5.75	84	–1.50	–5.50	84	0.177
KC2	Left	–3.00	–1.75	74	–3.00	–1.75	74	–3.00	–2.00	74	0.177
KC3	Right	+3.50	–6.50	50	+3.50	–6.5	50	+3.50	–6.50	50	0.000
KC3	Left	–15.75	–8.00	116	–15.75	–8.00	116	–15.25	–8.00	118	0.573
Typical1	Right	–6.50	–0.50	148	–6.50	–0.50	148	–6.50	–0.50	150	0.017
Typical1	Left	–6.25	–2.75	16	–6.25	–2.75	16	–6.25	–2.75	16	0.000
Typical2	Right	–7.50	–0.25	90	–7.75	0.00	n/a	–7.50	–0.25	82	0.177
Typical2	Left	–7.75	–1.75	86	–7.75	–1.50	88	–7.75	–1.75	86	0.186
										Mean:	0.131
										SD:	0.178

6.4.3 Evaluating conventional and wavefront-guided scleral lens corrections in keratoconus

While most of the eyes with ectasia in Chapter 4 reached typical levels of visual acuity, contrast sensitivity, and higher-order RMS wavefront error while wearing a wavefront-guided scleral lens, the majority did not reach the best-corrected levels of VSX from Chapter 3. Potential optical reasons for this dissonance are explored in Chapter 7, as are concepts such as *floor* and *ceiling* effects in the ability of VSX to track visual perception. Here we consider whether the neural weighting function could have contributed to the finding that performance reached typical levels but VSX did not.

A challenge with this investigation is the difference in retinal illuminance between the neural weighting function used in Chapter 4 (500 td) and that of the measured functions here (15 td). Therefore, comparisons with the measured functions are made using the function defined at 15 td by the model in Chapter 5. Furthermore, for simpler comparison with the Campbell and Green function used in Chapter 4 (to which the 20 to 29 year old data was originally scaled by Xu et al.[9]) comparisons are made with the 20 to 29 year old function at 15 td rather than the 30 to 39 year old group.

Wavefront error measurements were previously recorded while the six eyes with keratoconus were wearing wavefront-guided scleral lenses. These wavefront errors were used to generate PSFs which were independently weighted by the two-dimensional inverse Fourier transform of (1) the two-dimensional measured neural contrast sensitivity function and (2) the rotationally symmetric (model) function defined for the 20 to 29 year old group at 15 td in Chapter 5. For five of the six eyes the PSF weighted by the measured function had greater

volume than that which was weighted by the model function (Figure 6.13) ($p = 0.046$; Wilcoxon matched pairs). Consequently, the metric value calculated using the measured neural contrast sensitivity function was better than that calculated using a rotationally symmetric (model) function at the same retinal illuminance (and a constant denominator). An example for the numerator of the metric for one eye is illustrated in detail in Figure 6.14; the denominator is not shown in Figure 6.14 – as long as a constant denominator is used, it is essentially arbitrary across both conditions.

Unfortunately it is not fair to directly compare these values with the VSX norms reported in Chapter 3 because those norms only used the Campbell and Green[154] neural contrast sensitivity function. For a fair comparison, the norms would need to be re-run using the neural contrast sensitivity function at the level of retinal illuminance that was used (here 15 td). Because the metric for most eyes with keratoconus was better at 15 td when using the measured neural contrast sensitivity function, this might help explain why the performance of these eyes was better than was expected from the metric that used a rotationally symmetric function. Put differently, the rotationally symmetric function appears to over-estimate the detrimental effects of the rotationally-asymmetric aberrations in the eyes with keratoconus.

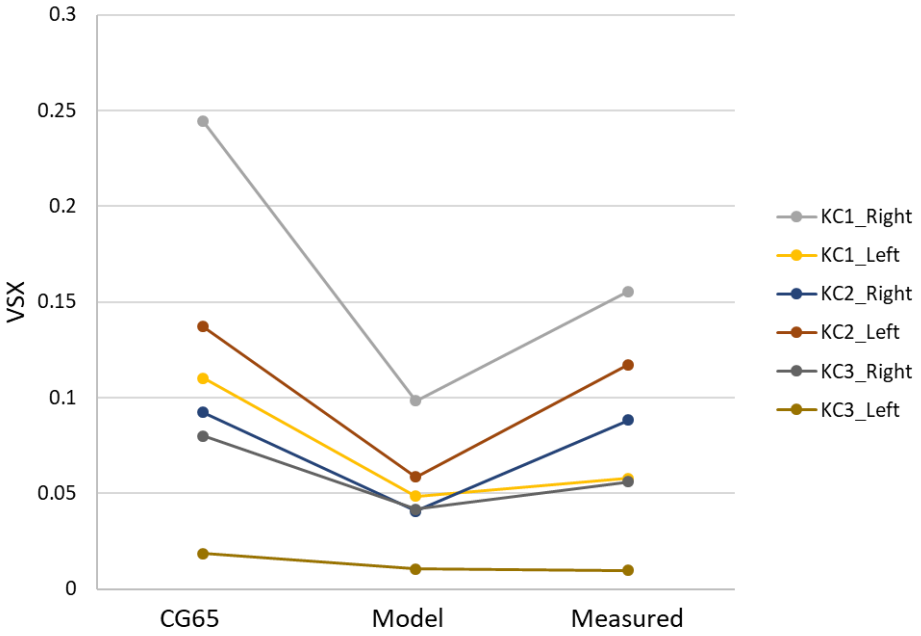

Figure 6. 13 VSX values for the eyes with keratoconus wearing wavefront-guided scleral lenses calculated with different weighting functions: Campbell and Green[154] at 500 td ("CG65"), the model from Chapter 5 at 15 td, and the individualized function measured at 15 td

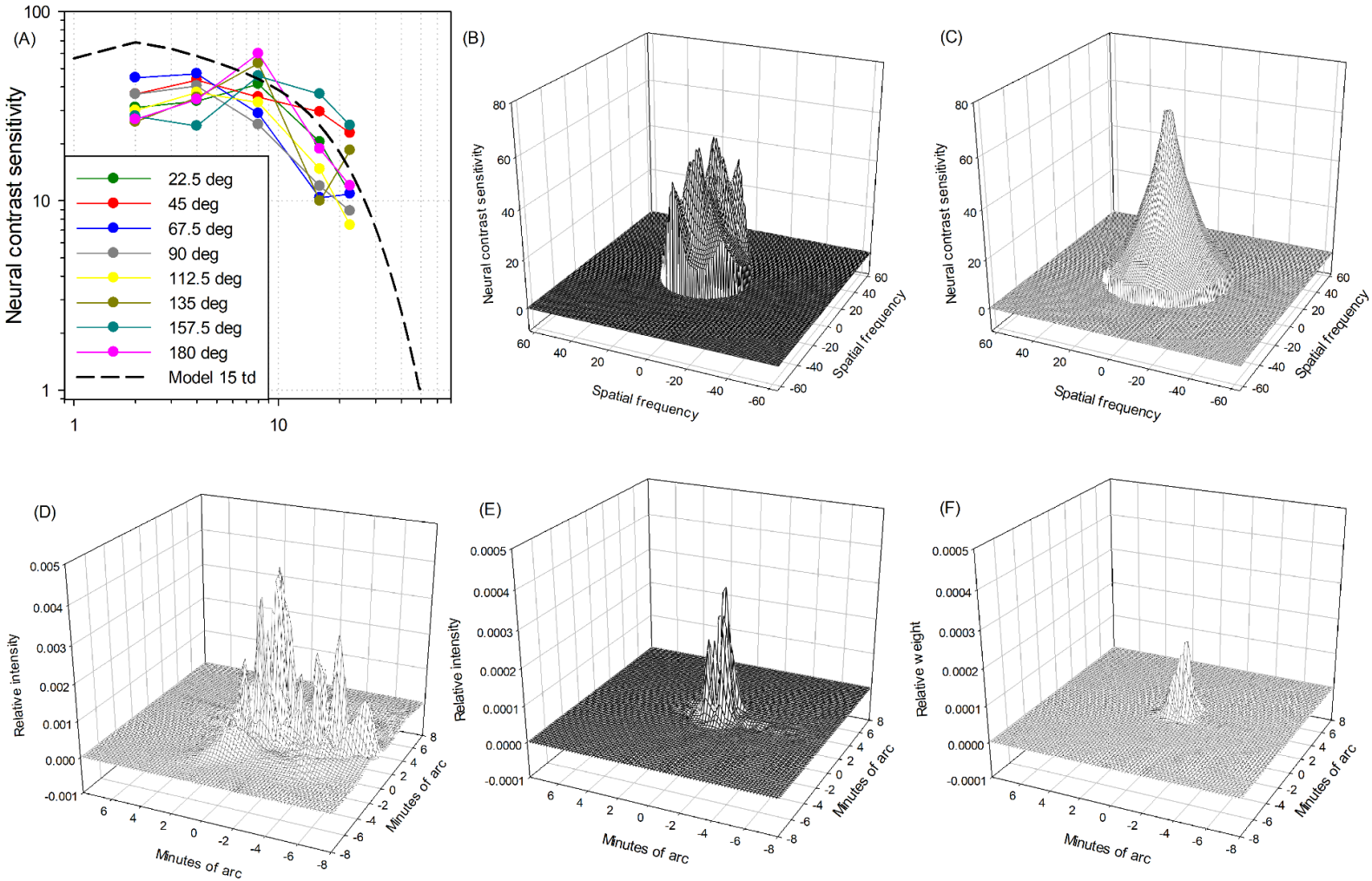
(A)
Neural contrast sensitivity
100
10
1
1
10
22.5 deg
45 deg
67.5 deg
90 deg
112.5 deg
135 deg
157.5 deg
180 deg
Model 15 td
(B)
Neural contrast sensitivity
Spatial frequency
Spatial frequency
(C)
Neural contrast sensitivity
Spatial frequency
Spatial frequency
(D)
Relative intensity
Minutes of arc
Minutes of arc
(E)
Relative intensity
Minutes of arc
Minutes of arc
(F)
Relative weight
Minutes of arc
Minutes of arc

Figure 6. 14 The difference between weighting the PSF of the left eye of subject KC2 with the measured neural contrast sensitivity function (nCSF) and the function defined at 15 td by the model in Chapter 5. (A) One-dimensional nCSFs for all orientations and the model. (B) Two-dimensional measured nCSF. (C) Two-dimensional model nCSF. (D) PSF from wavefront error measurement of the eye while wearing a wavefront-guided scleral lens (this corresponds to an eye and measurements from Chapter 4). (E) The PSF in (D) weighted by the inverse Fourier transform (not shown) of the function in (B). (F) The PSF in (D) weighted by the inverse Fourier transform (not shown) of the function in (C).

6.5 Discussion

6.5.1 General discussion

While there are many interesting analyses that can be performed on neural contrast sensitivity data of eyes with keratoconus, this chapter sought to examine the potential role of these data in the context of visual image quality metrics. Because neural contrast sensitivity was measured at eight orientations, it was a time-consuming measurement that (in its current form) would likely never become clinically commonplace.

A minor shortcoming of the experiment was that the method of adjustment threshold, around which the constant stimuli were defined, was typically set at a much higher contrast than the actual threshold – this happened across typical eyes and those with keratoconus, and even persisted in investigators that were aware of the trend. This ultimately lengthened the experiment further because the second "run" required additional constant stimuli to be added at the low contrast end, such that 50% guess rate could be reached. Future work might benefit from initially estimating the threshold using a staircase paradigm.

We initially elected to avoid staircase and predictive paradigms because we were unsure of whether the assumptions made in those methods (based on the behavior of typical eyes) would be applicable to eyes with elevated levels of higher-order aberrations. We were also conscious of the length and monotony of the experiment and felt that a method of adjustment component would keep the subjects engaged and that a constant stimulus paradigm would ensure that they frequently perceived some stimuli (which may not happen if the stimuli are around the threshold in a staircase procedure). Unfortunately, the addition of low contrast stimuli to the second "run" meant that, despite this goal, the constant stimuli comprised a high proportion of stimuli that were difficult to see. Nonetheless, we were fortunate that subjects appeared motivated and determined, and were mindful of taking regular rests and refreshment.

As mentioned, the wavelength of light (543 nm) was very near to the peak sensitivity of foveal cones and saturated vision rapidly at 500 td levels. While the 15 td retinal illuminance used is still photopic, it meant that comparison with some literature[154,185] (that used longer wavelength stimuli) was challenging. The neural contrast sensitivity performance was comparable to levels reported by Coletta and Sharma[10] at 30 td that also used 543 nm light and a 50% coherence fraction. Coletta and Sharma[10] reported very similar performance (50% coherence fraction) at 300 and 30 td (their Figure 2), which is contrary to performance with longer wavelength light[9,11] and might be due to a similar phenomenon, however, is not discussed in their paper.

Given that the purpose of Chapter 5 (models of neural contrast sensitivity) was to allow the metrics to better respect real-world conditions, another minor limitation of this experiment is

that it was only performed at one retinal illuminance. As mentioned, the models in Chapter 5 could be made relative to (or defined around) the neural contrast sensitivity functions measured here, however, it is unknown whether the visual systems of eyes with keratoconus respond to changes in retinal illuminance and with increasing age in the same manner as those of typical eyes.

6.5.2 Optimizing objective refraction

The clinically small differences in optimal sphere, cylinder, and axis using the Campbell and Green,[154] the model of typical eyes (Chapter 5), and the measured individualized functions agrees with work from the University of Houston (Bell et al.; submitted) that generally found good visual acuity and subjective preference when eyes with mild to moderate keratoconus used a prescription optimized using the VSX and the Campbell and Green[154] neural contrast sensitivity function. As discussed in sections 7.2.1.4 and 7.2.2.1 this is likely due to clinical increments of diopters effecting relatively coarse changes in image quality and VSX, despite the neural weighting functions of eyes with keratoconus being quite different from those of typical eyes.

6.5.3 Evaluating conventional and wavefront-guided scleral lens corrections in keratoconus

As shown in Figure 6.6, the sensitivity of the eye with keratoconus was slightly better in some meridians than that of the model at medium spatial frequencies. This is can be similarly noted in the data of others (Figure 14 of Kawara and Ohzu,[11] and Figure 4 of Kayazama et al.[27]) which illustrate individual eyes measured at one orientation. While this is a small sample of eyes on which to base any conclusion, if the neural processing of visual systems with keratoconus are

able to accentuate processing of medium spatial frequencies in lieu of the high spatial frequencies that are not seen for optical reasons, this might help explain why visual acuity and contrast sensitivity were within normal limits for many eyes with wavefront-guided lenses in Chapter 4, while their VSX values with those lenses were not. The measured neural contrast sensitivity functions apodize (remove the tails / feet of) the PSF more aggressively than the Campbell and Green function – this may indicate the Campbell and Green function is over-estimating the detrimental effects of the aberrated optics, while the visual system of these individuals is less sensitive to those effects.

6.5.4 Towards investigating synergy between optical and neural components

To investigate whether synergy (that is, a beneficial effect of visual image quality) existed between the rotationally asymmetric aberrations and rotationally asymmetry neural contrast sensitivity functions of eyes with keratoconus, three methods of rotating the one component (either the PSF or the neural weighting function) relative to the other component were performed. Although data is included below, the discrete definition (and re-defining after rotation) of the PSFs and neural weighting functions in Matlab ultimately resulted in a level of noise that prevented definitive conclusions being reached regarding this synergy.

Firstly, the PSF (defined over a 512 x 512 grid in Matlab) was rotated. In doing so, the PSF was rotated around the center of the grid and not the peak of the PSF. In the existing metric code, it was challenging to realign the peak of the rotated PSF with the neural weighting function when the PSF was rotated. The misalignment of the PSF and neural weighting function

predominantly influenced the VSX metric value and made it impossible to sensitively detect any effect (or absence of effect) of synergy.

In contrast, the PSF and neural weighting function could be more accurately aligned if the neural function was rotated instead of the PSF. Two methods of doing so were tested: The first method simply modified the input of measured neural contrast sensitivity to the metric such that the measured sensitivities for all spatial frequencies at a given orientation (say, 0°) were assigned to another orientation (say 22.5°; in this example all measured sensitivities were effectively rotated by 22.5°, therefore, those measured at 22.5° were assigned to 45° and so on; similar rotations were performed where the neural contrast sensitivities were effectively rotated by all multiples of 22.5° up to 157.5°. A challenge with this method was noted when Matlab interpolated, over a rectangular (Cartesian) co-ordinate grid, the sensitivities measured in a polar sense, to obtain a two-dimensional neural contrast sensitivity function. The interpolated shape and volume of the neural weighting function (prior to being applied to the PSF) was substantially different at different orientations, which similarly confounded the examination of synergy.

Ultimately, the most successful method only involved inputting neural contrast sensitivities at the measured orientations and then rotating the interpolated two-dimensional neural weighting function immediately before it was used in the metric calculation. Care was taken to align the rotated neural function with the peak of the PSF. Despite being better than the aforementioned methods, there was still variability in the shape and volume of the function caused by rotating it in a polar manner and then redefining it over a rectangular grid. The denominator of the metric (when a diffraction-limited PSF is weighted by the rotated neural

function) was used to gauge the variability caused by rotation. Examples are shown for two eyes where synergy appears to be present (Figure 6.15) and where it does not appear to be present (Figure 6.16). Given that reservations remain regarding the implementation of the rotation of one function with respect to the other, these data should be interpreted with caution until future work can comment on this more definitively.

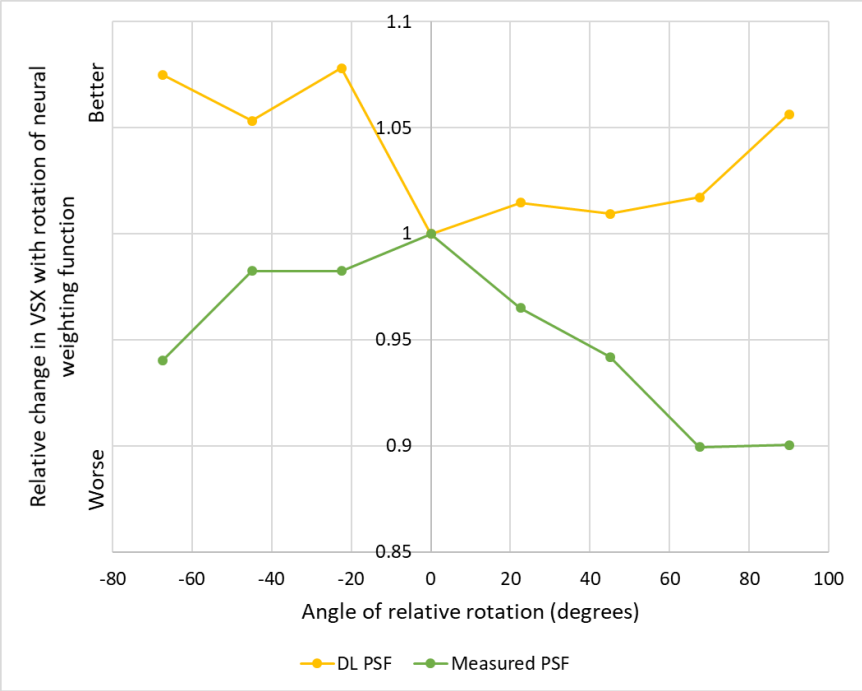

Figure 6. 15 VSX values for the right eye of KC02 where the neural weighting function was rotated (relative to the PSF) by the amount on the abscissa. All metric values have been normalized to the unrotated value (0 on the abscissa). This eye was considered to demonstrate synergy (an interaction between the optical and neural components that was beneficial to image quality) because the metric calculated with the PSF of the eye worsened as the neural function was rotated and the diffraction-limited PSF weighted by the rotated function (which served as control to illustrate noise in the rotation) did the opposite (improved with rotation). Therefore, if one used the diffraction-limited case to adjust (in a corrective sense) the metric values calculated with the PSF of the eye, it would result in a greater decrease in metric value with rotation (emphasize the synergy). This is in contrast to the case in Figure 6.15.

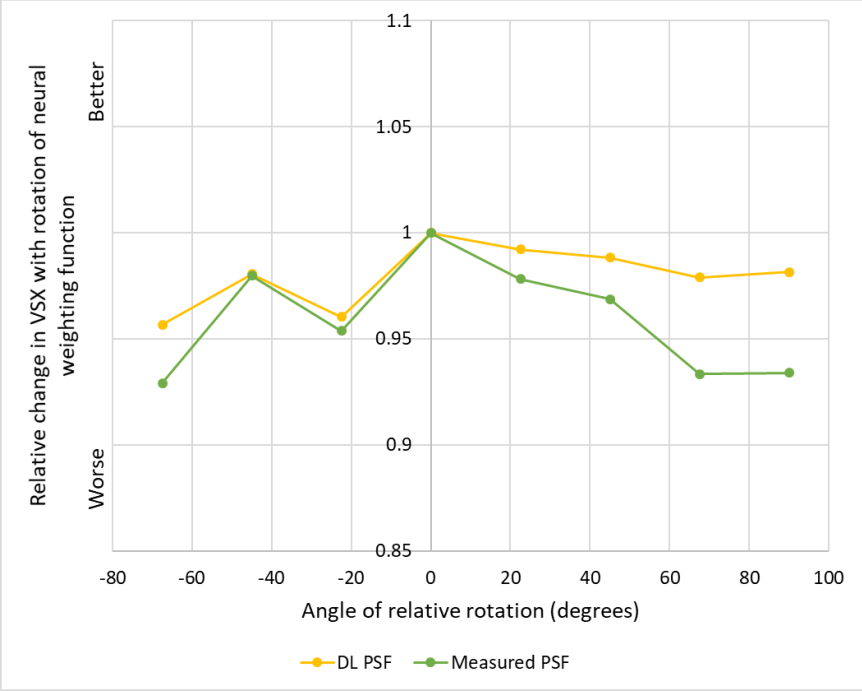

Figure 6. 16 VSX values for the left eye of KC02 where the neural weighting function was rotated (relative to the PSF) by the amount on the abscissa. All metric values have been normalized to the unrotated value (0 on the abscissa). This eye was considered to not demonstrate substantial synergy (beneficial interaction) between the optical and neural components of the metric. Although the metric value calculated with the PSF of the eye generally worsened as the neural weighting function was rotated, the majority of that effect can be explained by noise caused by the rotation, as revealed by the trace for the diffraction-limited PSF.

6.6 Appendix

6.6.1 Calculation of Trolands

The calculation of Trolands followed methods equivalently described by Wyszecki and Stiles[243] (p104) and Burns and Webb[237] (chapter 28).

550 pW (550e-12 W) at 543nm: power measured at the focal point of the Maxwellian-view lens

*0.9472: Vlambda conversion from 543 to 555 nm

= 5.21e-10 W (at 555 nm)

*683 conversion from Watts to lumens

= 3.56e-7 lumens

/6.68e-6: area in m^2 of retina illuminated (the Maxwellian-view lens had a focal length of 60 mm and a limiting aperture on its surface of 10.5 mm diameter; an assumption of 16.67 mm from the focal point to the retina was used[237])

= 5.32e-2 lumens per m2

/0.0035: conversion from lumens per m2 to Trolands[237]

= 15.21 Trolands

Chapter 7: General discussion, conclusions, and future directions

7.1 General summary

The visual image quality metric VSX was applied to the optimization of objective refraction in Chapter 2 and was used to evaluate conventional and wavefront-guided scleral lenses in Chapter 4 using best-corrected benchmark metric values determined in Chapter 3. During these clinical applications, the optical component of the metric was always specific to the individual eye (or eye + ophthalmic correction) being evaluated. Chapters 5 and 6 respectively attempted to make the neural component of the metric more applicable to real-world conditions and more personalized to typical and highly-aberrated eyes.

Throughout this dissertation an attempt has been made to reserve use of the term "normal" to statistical contexts and to use alternative terms when referring to eyes that by clinical evaluations are considered "typical". Exceptions may be found in the experimental chapters that were published because we endeavored to keep those chapters as similar as possible to the manuscripts that were peer-reviewed and exist in the literature.

7.2 Reflections on the experimental chapters

7.2.1 Chapter 2

The sphere power of the VSX-optimized objective refraction was generally more negative than subjective refraction for young myopic eyes and more positive for young

habitually-undercorrected hyperopic eyes. The VSX refraction provided equivalent or better visual acuity than subjective refraction for the myopic eyes (which was also preferred when the myopic eyes viewed a distant outdoor scene) and poorer visual performance for hyperopic eyes.

7.2.1.1 Potential effects of accommodation

As mentioned in Chapter 2, when undilated, accommodation (and instrument myopia) could have contributed to the more negative outcomes of the myopic eyes. However, such a theory conflicts with the behavior of the hyperopic eyes, which appeared to have relaxed their accommodation much more during the wavefront error measurement than when reading letter charts. This apparent difference in the accommodative posture of the young habitually-undercorrected hyperopic eyes could be due a difference in the target and visual task. During wavefront error measurement, subjects gazed inside the wavefront sensor at a scene that attempted to simulate distance vision, however the task was largely passive and involved no resolution or identification by the visual system. In contrast, when focusing and reading a letter chart, it is possible that the visual systems of these hyperopic individuals assumed a habitual tonic accommodative posture. Testable hypotheses of future work are to elaborate on previous work[175,176] and compare wavefront error measurements from open field or through-viewing systems with closed systems, as well as to investigate the effect of different instructions and tasks during the measurement, such as simply being instructed to look towards a distant target versus having to read a letter chart at the same distance.

For the dilated condition, mydriasis was achieved using Tropicamide (1%), which is a moderate cycloplegic with maximal efficacy at approximately 20 to 25 minutes after instillation

(this varies with iris pigmentation).[244] Given the young age of the subjects (and assuming typical age-appropriate accommodative ability), residual accommodation at the time of wavefront error and subjective refraction measurements (20 minutes after instillation) could have contributed to the dioptric differences (despite coinciding with the peak efficacy of Tropicamide).

Additionally, because determination of the objective VSX prescription typically took 15 to 20 minutes, the two corrections were compared approximately 40 minutes after instillation, and the cycloplegic effect of the Tropicamide may have begun wearing off – this could have increased residual accommodative ability as well as caused a change in spherical aberration,[245,246] which will be discussed in the next paragraph. Potential solutions for implementation in future work could involve re-instilling the drops to ensure maximal effect at the time of the performance measures, or the use of a more potent cycloplegic – the reason that Atropine, for instance, was not used, was due to the cycloplegic effect lasting many days and the study being conducted in both eyes of each individual.

7.2.1.2 Spherical aberration

Spherical aberration interacts with defocus such that it has the potential to drive the best spherical equivalent more positive or more negative.[8,179,247] Subjective refraction of a given eye has been shown relatively independent of pupil size,[108] suggesting that the ratio of spherical aberration to defocus remains relatively constant. The spherical equivalent (M) power vector difference between subjective refraction and the VSX-optimized refraction did not correlate with the value of the measured spherical aberration Zernike term for myopic or hyperopic eyes across both natural and dilated pupils (all $R^2 < 0.04$).

After scaling the dilated wavefront errors to 6mm (most undilated eyes did not reach 6mm and were not scaled to a larger size than the measurement), mean (±SD) spherical aberration value were +0.12 ±0.14 and +0.13 ±0.22 μm for myopic and hyperopic eyes respectively. These mean values are less than those reported for 200 well corrected young eyes (approximately +0.38 μm),[102] but were within 1 standard deviation of that mean. While not substantially different, the less positive spherical aberration values of the eyes in Chapter 2 would agree with the observation that positive spherical aberration decreases with accommodation[246] and might support the suspicion of accommodation affecting performance.

7.2.1.3 Comparisons with second-order and Seidel refractions

For further comparison, two additional objective refractions were derived from the measured wavefront errors: one used only second-order Zernike coefficients[151] (also known as least-squares fitting) and the other used the second, fourth, and sixth order Zernike coefficients that contain ρ^2 terms (also known paraxial curve matching or the Seidel formulae for defocus and astigmatism).[15] All refractions (subjective refraction, VSX-optimized, second-order, and Seidel) are compared dioptrically and in terms of VSX below, however, visual performance and preference with the two supplementary corrections was not compared.

Astigmatic components (J0 and J45) of all four corrections were very similar across all eyes (see Table 7.1) as well as across dilated and undilated conditions, which agrees with literature.[15,39,40,44–46] For myopic eyes, the spherical equivalent (M) component of subjective refraction was more positive than all of the objective refractions (undilated and dilated) except

for the dilated Seidel calculation. Subjective refractions of the hyperopic eyes were generally more negative than all objective refractions.

As discussed in Chapter 2, the VSX refraction found the prescription that maximized VSX and therefore the other (subjective and objective) refractions could only perform equivalent or worse in terms of VSX. When undilated, subjective refraction achieved better VSX than the second-order and Seidel refractions in approximately 20% of the myopic eyes and in 1 and 2 hyperopic eyes respectively (Table 7.1). For myopic eyes, this increase to approximately 70% (subjective refraction better VSX) when dilated, but did not change for dilated hyperopic eyes. As discussed in Chapter 2, the sample of 4 hyperopic eyes is too small to make meaningful generalizations.

Table 7. 1 Power vector difference between subjective refraction and three objective refractions (VSX-optimized, calculated from second-order Zernikes, and Seidel formulae for defocus and astigmatism). A positive difference means that subjective refraction was more positive than the particular objective refraction.

		M†	J0†	J45†	Euclid. distance	Subj. refraction more minus (n)	VSX difference †	Subj. refraction better VSX (n)	Predicted logMAR difference (letters)†	Actual logMAR difference †
Undilated										
Myopic	VSX	0.65	-0.07	0.03	0.69	0	-0.54575	0	-11.1	-0.1
n=36	2nd-order	0.45	-0.04	0.02	0.61	6	-0.2801	9	-5.7	
	Seidel	0.38	-0.04	0.01	0.52	4	-0.24249	7	-4.9	
Hyperopic	VSX	-1.09	-0.03	0.02	1.17	3	-1.20772	0	-24.6	7.4
n=4	2nd-order	-1.55	-0.01	0.00	1.55	4	-0.79333	1	-16.2	
	Seidel	-1.54	-0.03	-0.02	1.57	4	-0.96552	2	-19.7	
Dilated										
Myopic	VSX	0.26	0.02	0.02	0.36	9	-0.23291	0	-4.8	0.0
n=36	2nd-order	0.35	0.03	0.00	0.56	10	0.213104	26	4.3	
	Seidel	-0.19	0.03	0.00	0.35	27	0.146234	25	3.0	
Hyperopic	VSX	-0.75	0.00	0.02	0.76	4	-1.18852	0	-24.3	4.4
n=4	2nd-order	-1.04	0.05	0.01	1.05	4	-0.69258	1	-14.1	
	Seidel	-1.60	0.00	-0.02	1.61	4	-0.09409	2	-1.9	

† Calculated as subjective refraction – objective; positive power vectors mean subjective refraction was more positive; negative VSX means subjective refraction worse VSX; predicted negative letters means subjective refraction lost.

7.2.1.4 Ceiling and floor effects in the ability of VSX to track performance

The modelling of Ravikumar et al.[147,235] is frequently cited to predict a change in high contrast logMAR visual acuity from a change or difference in logVSX. It should be obvious that the predictive ability of the model failed for hyperopic eyes because visual acuity was substantially better with the subjective refraction, which corresponded to poorer VSX than the optimized objective refraction.

For myopic eyes, the change in visual acuity predicted by the model[147] was much larger than actual measured acuity difference (Table 7.1). While the neural weighting function in VSX approximately constrains the metric to the retinal sampling and cortical resolution limits of the visual system, it still appears that there is a range of logVSX above which visual image quality improves but there is not accompanying (further) improvement in visual acuity. While this might be partly due to just noticeable differences (JNDs) in blur being detectable before acuity is lost or gained (in this case, blur might reduce slightly as VSX improves), this cannot account for the substantial over-prediction, which is referred to as the *ceiling* of the predictive relationship range between logVSX and visual acuity.

This ceiling effect has not yet been systematically studied, however, it seems to occur when best visual acuity is reached. Prior to reaching maximum acuity, change in logVSX appear to better track changes in visual acuity. The sensitivity of VSX to changes in dioptric power is related to this predictive relationship and is discussed in section 7.2.2. It has also been anecdotally noted that the predictive relationship of logVSX and visual acuity has a *floor*, that is, at very poor levels of visual image quality, logVSX is still sensitive to, say, dioptric changes, but the retinal image is so poor that the visual system is insensitive to changes and visual acuity does not change correspondingly – sometimes the visual system is unable to even discern a difference between two very poor options. Future work could study both of these phenomena using visual acuity and perceptible blur as outcomes to be compared with logVSX.

7.2.1.5 Wavelength differences between wavefront error and objectively applied lens powers

After performing and publishing the work of Chapter 2, a discrepancy was realized between the wavelength at which ophthalmic lens powers are defined, namely that of the sodium D-lines (~589 nm), and the wavelength at which lens powers were mathematically applied to the measured wavefront errors during the objective refraction (555 nm). It should be noted that this is important in the work of Chapter 2 because the prescriptions were physically worn when visual performance was measured.

The effective difference in spherical power between 555 and 589 nm is 0.17296 D. A trial lens of 0 D (plano) is theoretically only 0 D at 589nm and at 555 nm it should be –0.17296 D. Conversely, if an applied lens of –0.17296 D optimized VSX at 555 nm, this should correspond to a plano trial lens. To examine whether this discrepancy in wavelength could explain the excess negative power of the VSX refraction in myopic eyes, the optimization was performed again – unfortunately, performance measures could not be compared, but the dioptric differences were considered.

The method performed was as follows: While a simple numeric adjustment of the previously-determined objective sphere power could have been performed, the question arose of whether subtracting –0.17296 D would have affected rounding to the 0.25 D sphere increment that optimized the metric. Thus, the wavefront errors of the 40 eyes were re-optimized, where the –0.17296 D was first converted[151] into Zernike defocus at the subject's specific pupil size and applied to the wavefront error prior to the mathematical application of the range of sphere and cylinder prescriptions. This was equivalent to modifying each applied prescription by –0.17296

D, because the prescriptions were applied using the same conversion to Zernikes. The ranges of dioptric powers that were searched were identical to those originally searched in Chapter 2.

The results were essentially as expected: While undilated, the dioptric difference between (M power vector) subjective and VSX refractions of myopic eyes decreased from 0.65 D (original 555 nm optimization) to 0.46 D (589 nm), where in both cases the objective refraction was more negative. As expected, this increased the difference for undilated hyperopic eyes from 1.09 to 1.56 D, where in both cases the objective refraction was more positive. The corresponding changes when dilated were from 0.26 (555 nm) to 0.00 D (589 nm) for myopic eyes, where the objective refraction was more negative, and 0.75 (555 nm) to 0.88 D (589 nm) for hyperopic eyes, where the objective refraction was more positive. The changes were not equal to –0.17296 D, due to the aforementioned rounding to the nearest 0.25 D during optimization. This conceptual flaw will be rectified for future work with metric-derived objective refractions.

7.2.1.6 Instructions of subjective refraction versus what is optimized by VSX

As mentioned in Chapter 2, subjective refraction is affected by factors such as adaptation, instructions provided by the clinician, interpretation of those instructions by the patient, internal preferences and expectations of visual quality by the patient, and clinical conventions such as refracting to the hyperfocal distance. While the internal expectations and interpretations of each subject in Chapter 2 were likely – to some degree – unique, the VSX objective refraction consistently differed from subjective refraction for myopic eyes. As discussed in Chapter 2, subjective refraction does not strive for optimal image quality (the center of the depth of focus)

and typically ends with the maximum amount of blur that does not cause a decrease in visual acuity (such is the case at the hyperfocal distance – the dioptrically positive end of the depth of focus).

Subjective refraction in Chapter 2 was performed in this way such that it was representative of typical clinical practice, however, future work could involve instructing the subject to select the lens-option that maximizes contrast and edge definition of letters (which is what the VSX metric appears to optimize). Whether maximizing contrast and edge definition actually maximizes legibility of letters by the visual system is also a possibility of future work. Given that subjective refraction is affected by the adaptation of the visual system to its habitual correction, a future study could dispense the prescription that optimizes a metric of visual quality (such as VSX) and allow the individual to adapt to it.

7.2.1.7 Concluding remarks

Eighteen of the twenty subjects in Chapter 2 were in the 20 to 29 year old age group, so the age-related differences in the neural weighting function discussed in Chapter 5 likely played an insignificant role here. Pupil size varied across these individuals, which would have resulted in different levels of retinal illuminance being experienced, however, these differences also seem unlikely to have impacted the findings of Chapter 2 because the trends of the VSX refraction being more negative in myopic eyes and more positive in hyperopic eyes than subjective refraction occurred across all pupil sizes. Consequently no retrospective analyses using the models described in Chapter 5 were performed on the data of Chapter 2.

The wavelength-modified VSX refraction for myopic eyes remained 0.46 D more negative than subjective refraction while undilated, but agreed well with subjective refraction when dilated. This suggests that factors bearing major responsibility might be residual accommodation (as discussed in section 7.2.1.1) and the convention of ending subjective refraction at the hyperfocal distance (as discussed at length in Chapter 2). Accommodation can be expected to be reduced when Tropicamide was used in the dilated condition, which together with a larger dilated pupil would have decreased depth of focus. The better agreement of the refractions when dilated suggests that reflection of the infrared beam of the wavefront sensor from retinal structures deeper than the photoreceptors (considered in Chapter 2) might play a lesser role.

7.2.2 Chapter 3

Best-corrected values of VSX as a function of age and fixed pupil size were calculated for 146 eyes between 20 and 80 years of age from Applegate et al.[4] and validated using independent wavefront error data from Porter et al.[100] A desirable potential use of such normative metric values is to compare visual image quality of ophthalmic corrections across modalities. Consequently, a substantial portion of the Discussion in Chapter 3 involved whether these objectively optimized normative values were clinically achievable when one considers, for instance, that the 95% confidence limits of sphere during subjective refraction are reported as approximately ±0.50 D.[32,34] The sections that follow add to the discussion of that topic.

7.2.2.1 Sensitivity of VSX to increments in dioptric power

It is worth restating that dioptric power has a logarithmic effect on VSX as can be seen in Figure 7.1 for spherical defocus (most aberrations have a relationship that follows the same shape). Likewise the (base 10) logarithm of VSX has been better correlated with visual performance[24,147] than linear VSX. Strikingly, Figure 7.1 shows that 0.5 D of spherical defocus causes an approximate change in VSX of one log unit in the otherwise aberration-free case.

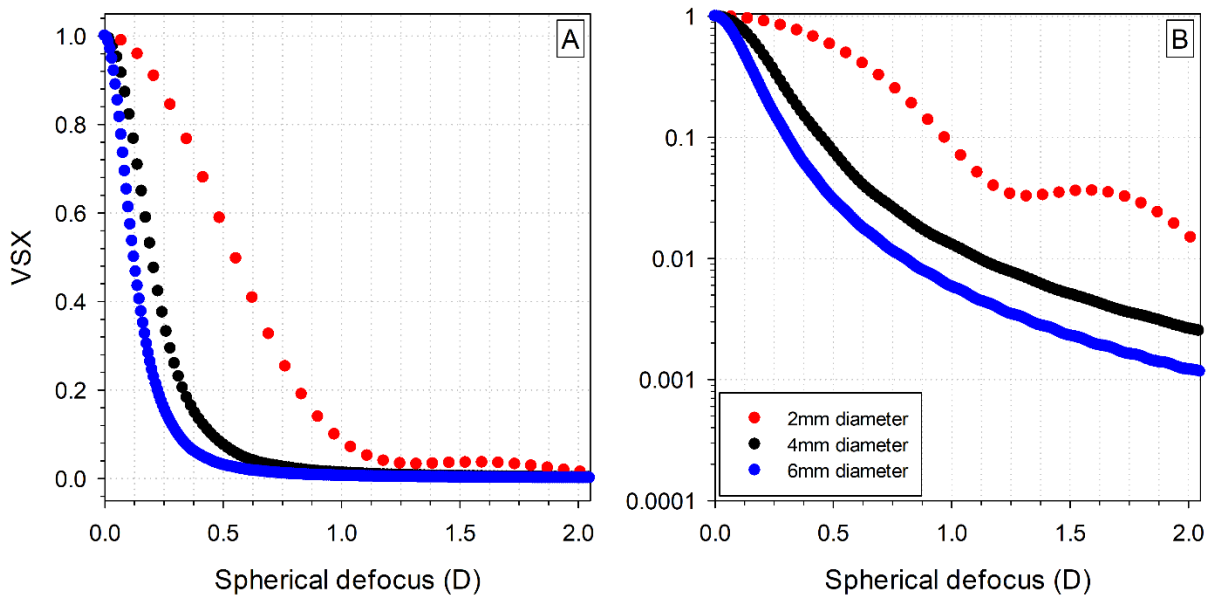

Figure 7. 1 The decrease in VSX caused by the addition of spherical defocus to diffraction limited optics for 2, 4, and 6 mm pupil diameters. VSX is plotted on (A) linear and (B) logarithmic scales.

Across multiple data sets, when the same method of objective optimization is used, the best sphere, cylinder, and axis correction (in 0.25 D and 2° axis steps) (that optimizes VSX) provides a corrected level of VSX within the normative ranges of Chapter 3 for most eyes (95.4% of eyes for Porter et al.,[100] 98.4 and 97.4% for The Indiana Aberration Study[151] at 3 and 6 mm pupil diameters respectively, and 85% of the eyes in Chapter 2 [29]). However, when the

sphere component of that optimal refraction is modified, a similar effect on VSX is observed as in the diffraction limited case above. Figure 7.2 shows how VSX changes for a myopic (MM_OS) and hyperopic (KH_OS) subjects from Chapter 2 when the sphere correction is modified. (These subjects are shown first because their physiological pupil sizes during the experiment were 4mm and they can be directly compared with Figure 7.1; similar relationships are plotted for two other subjects with 5 mm physiological pupil diameters in Figure 7.3.)

Note that the VSX value for the objectively optimized refraction (zero on the abscissa) for MM_OS is within the 95% limits defined in Chapter 3, but decreased to outside those limits when the sphere component of the optimized refraction is modified by between 0.25 and 0.50 D. (Also note that while the other (higher- and lower-order) aberrations present in these eyes renders best-corrected VSX much lower than the diffraction limited case in Figure 7.1, they have a protective effect on visual image quality when defocused.)

Subjects MM_OS (Figure 7.2), RR_OS, and HM_OD (Figure 7.3) are representative of most eyes that have an optimized objective refraction within the normative limits defined in Chapter 3 insofar as a change of between 0.25 and 0.5 D of sphere (from the optimal refraction) decreases the corrected VSX value to outside the normative levels. In the context of the (±0.50 D) reported precision of subjective refraction,[32,34] this sensitivity of best-corrected VSX to dioptric defocus, again, suggests the presence of a ceiling effect in the relationship between VSX and visual performance (already introduced in section 7.2.1.4). It appears that a small range of corrections might allow an eye to surpass a threshold (ceiling) of visual image quality that the observer deems acceptable during subjective refraction. Within this range of corrections, VSX

can quantify differences between them and identify the optimal correction, while the observer might not be able to discern substantial differences and the corrections all appear "good enough". Consequently, at first glance (revisited in section 7.2.2.2 below), subjective refractions performed in both the Indiana Aberration Study[151] and Chapter 2,[30] generally did not provide VSX levels within the norms of Chapter 3 (26.6 and 34.4% of the Indiana eyes at 3 and 6 mm pupil diameter respectively, were within the norms; none of the subjective refractions in Chapter 2 reached the levels of Chapter 3).

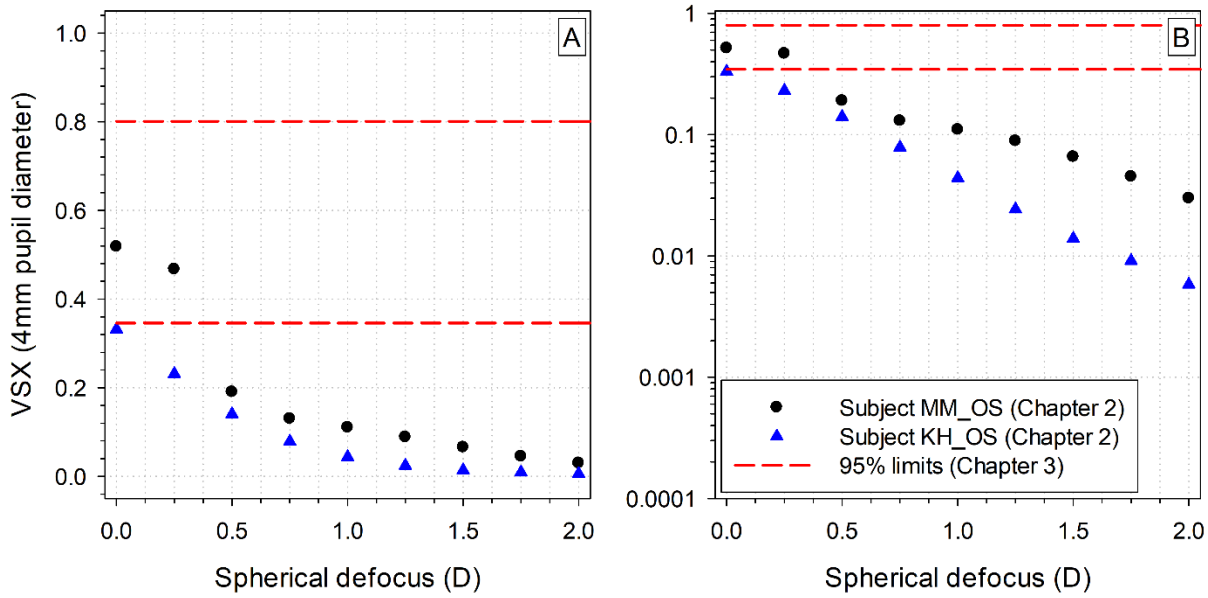

Figure 7. 2 Subjects MM_OS and KH_OS that had 4 mm physiological pupil sizes during the experiment in Chapter 2. Zero on the abscissa is the refraction that optimized VSX. Best VSX decreases rapidly if the sphere of the optimal refraction is modified by 0.25 to 0.50 D. The red dashed lines are the age-matched objectively well-corrected VSX norms from Chapter 3.

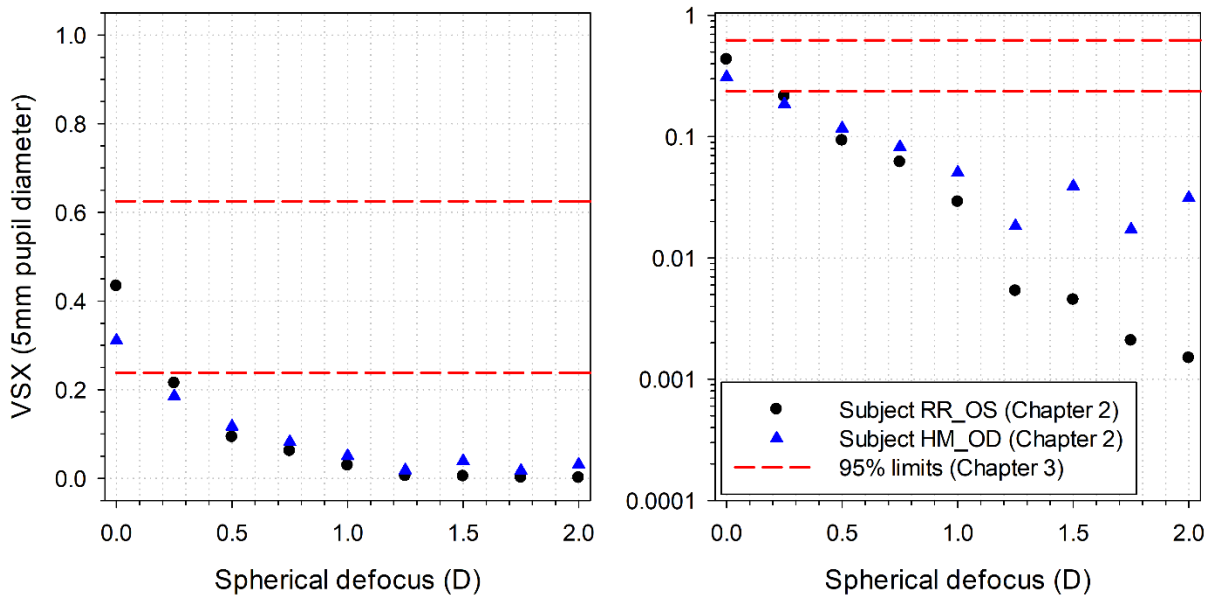

Figure 7. 3 Subjects RR_OS and HM_OD had 5 mm physiological pupil sizes during the experiment in Chapter 2. Zero on the abscissa is the refraction that optimized VSX. Best VSX decreases rapidly if the sphere of the optimal refraction in modified by 0.25 to 0.50 D. The red dashed lines are the age-matched objectively well-corrected VSX norms from Chapter 3.

As discussed in Chapters 2, 3, and earlier in this chapter, subjective refraction is also confounded by clinician instructions, patient interpretations, adaptation, and the convention of refracting to the hyperfocal distance. Subjective refraction is typically performed while viewing a high-contrast letter chart and is evaluated by measuring high contrast visual acuity. High contrast letter charts present a level of contrast that is much higher than typical real-world environments[248–250] and, as such, might compound the insensitivity of an observer to small changes in visual image quality. Future work investigating ceiling and floor effects in the relation of VSX to visual performance would do well to use an assortment of targets that vary in contrast and more closely resemble real-world scenes.

Again, although the neural weighting function in VSX approximately constrains the metric to the retinal sampling and cortical resolution limits of the visual system, it may still

remain more sensitive to higher spatial frequencies than an observer. This would mean that above a satisfactory threshold of visual image quality, small differences between corrections that are significant to VSX, might be clinically insignificant – this remains to be more thoroughly investigated.

7.2.2.2 Wavelength differences between wavefront error and objectively applied lens powers

Section 7.2.1.5 introduced discussion of the difference between the wavelength at which ophthalmic lens powers are defined (~589 nm) and the wavelength at which corrections were mathematically applied to wavefront errors (555 nm). In Chapter 2 this difference was important because corrections were worn during the measurement of visual acuity. The objective norms presented in Chapter 3 are affected differently: The emphasis here is on the resulting metric value rather than the optimal correction.

The objective optimization of wavefront error could essentially be performed at any arbitrary wavelength and similar values of VSX should be obtained. The only differences arise due to rounding to nearest 0.25 D and interaction of all other aberrations with the slightly different second order defocus value (the only term adjusted for chromatic aberration in Chapter 3). These rounding differences balance out when large samples are used and, therefore the normative values in Chapter 3 are largely unaffected. This was also true on average for the eyes in Chapter 2: Mean difference between the optimal VSX values at 555 and 589 nm was 0.018, with approximately halve the eyes (23/40) having a slightly better VSX value for 555nm and the other half (17/40) being better at 589 nm. As mentioned, these differences are due to rounding to the nearest 0.25 D step after effecting the –0.17296 D difference due to wavelength.

This wavelength difference plays a role in individual eyes when VSX is calculated and evaluated for subjective refractions (as discussed in the preceding section 7.2.2.1). Subjective refraction lens powers are defined at 589 nm, thus, if subjective refraction ended at 0 D (plano), the historical calculation of the metric should be attributed to –0.17296 D. When this appropriate change in sphere dioptric power was made, 72.5% of eyes from Chapter 2 reached the Chapter 3 norms with subjective refraction (versus 0% prior to this wavelength change, as mentioned in section 7.2.2.1). As will be discussed in reflection on Chapter 4, this wavelength difference does not play a role when VSX is calculated for a measured wavefront error (say, of an eye wearing a scleral lens); it is only relevant here because subjective refraction spectacle prescriptions were mathematically applied.

7.2.2.3 Variability and concluding remarks

As discussed in Chapters 3 and 5, and evident in Figures 7.2 and 7.3, there is variability in best-corrected VSX across individuals of the same age and at the same pupil size. Because the VSX norms presented in Chapter 3 were calculated for fixed pupil sizes and before the development of the models of neural contrast sensitivity defined in Chapter 5, variability in best-corrected VSX is only due to differences in aberrations. As mentioned in Chapter 5, the norms presented in Chapter 3 should still serve as a useful benchmark to gauge the photopic visual image quality of corrections across modalities as a function of age at fixed pupil sizes.

7.2.3 Chapter 4

Chapter 4 described the translation of wavefront-guided scleral lenses from laboratory settings into the lives of individuals with corneal ectasia. While a tremendous amount of knowledge was gained regarding the various clinical aspects of these lenses, this discussion will try to remain focused on the theme of this dissertation, namely, the application of visual image quality metrics. While wavefront-guided lenses corrected the majority of eyes with ectasia to within normal levels of three outcomes (higher order RMS wavefront error, visual acuity, and letter contrast sensitivity), only 10% of eyes reached the objectively best-corrected levels of VSX presented in Chapter 3.

7.2.3.1 Wavefront error measurement and treatment planes

The question arose as to whether there may be a difference between the plane in which wavefront error was measured versus the plane in which the wavefront-guided correction is placed. This stems from the convention that wavefront error is defined in the pupil plane of the eye,[1] however in principle, it is not of consequence here because the wavefront sensor (COAS HD, Johnson and Johnson, Santa Ana CA) was designed for use in wavefront-guided LASIK and output aberrations in the corneal plane. (Exactly how the instrument defines the corneal plane – whether this is measured or estimated – is not described in the user manual and may still be responsible for some, likely small, errors.) This also explains the larger error encountered when a single subject was fit with a wavefront-guided lens designed using an i-Trace (Tracey Technologies, Houston TX) wavefront sensor, which outputs aberrations defined in the pupil plane. This could be studied in future work theoretically[97] or using an instrument such as the Discovery wavefront sensor (Innovative Visual Systems, Elmhurst, IL) that is able to output

wavefront error in both the corneal and pupil planes (again, the computational assumptions of this conversion would need to be known).

7.2.3.2 Are the VSX norms presented in Chapter 3 clinically achievable for eyes with ectasia?

Again, we must first consider whether the objectively best-corrected VSX values in Chapter 3 are a reasonably attainable benchmark. Recall in section 7.2.2.2 that 72.5% of the eyes from Chapter 2 reached the normative levels of Chapter 3 with spectacle subjective refraction. Recall also that essentially all typical eyes (across three independent samples) in section 7.2.2.1 reached the norms of Chapter 3 with an objectively optimized correction (the same method as used to determine the norms).

As mentioned in Chapter 4, none of the eyes with ectasia reached the VSX norms while wearing conventional scleral lenses and only 10% (2/20) reached the norms with wavefront-guided scleral lenses. When all of these wavefront error measurements were objectively optimized in the same manner as Chapters 2 and 3, only 10% (2/20) of eyes with ectasia reached the VSX norms with a (optimized) conventional scleral lens and 45% (9/20) with a (optimized) wavefront-guided lens. This demonstrates that the objective optimization method of the norms was not primarily responsible for the failure of these eyes to reach those levels, and suggests that the residual higher-order aberration structures could not be adequately balanced by any lower-order correction. Residual aberration structures of these eyes will be examined in the sections that follow.

7.2.3.3 Comparisons with the aberration distributions and structures of typical eyes

It has been illustrated in the earlier chapters (such as Figure 3.1) that RMS can struggle to quantify image quality when more than one aberration is present. The analyses in this section look at individual aberration terms and suffer a similar shortcoming, that is, the visual interaction of aberrations cannot be readily appreciated from a plot of signed aberration magnitudes, nevertheless, examining the individual aberration terms is the best place to start investigating what is affecting VSX.

While the total amount of higher order aberrations (HO RMS) present was within normal levels for 85% of eyes in Chapter 4 wearing wavefront-guided lenses, the distributions of the underlying (residual) aberrations was quite different from that of typical eyes. In the objective optimization described in the preceding section, only second-order terms are optimized and higher-order terms are unchanged. Figures 7.4 and 7.5 plot the higher order aberrations of eyes (from Chapter 4, wearing wavefront-guided lenses) that did (7.4) and did not (7.5) reach the VSX norms respectfully. The difference between Figure 7.4 and 7.5 is readily appreciated. Note in Figure 7.5 (eyes that did not reach VSX norms when objectively optimized), while some aberration terms are within the 95% limits of typical eyes, there are at least a few terms for each eye that are outside typical levels. In particular, Zernike term C13 (vertical secondary astigmatism) will be discussed in greater detail in the section that follows.

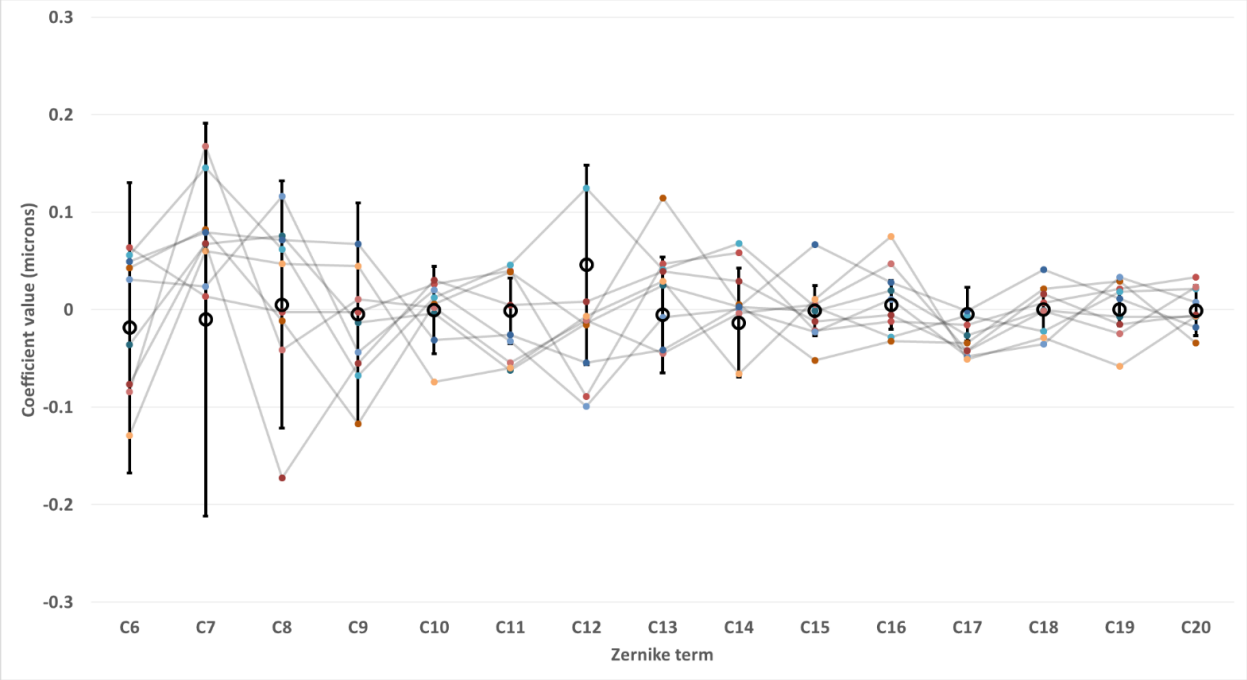

Figure 7. 4 Higher-order (third through fifth order) aberrations of 9 eyes from Chapter 4 wearing wavefront-guided scleral lenses (colored points and grey lines) that reached the best-corrected VSX norms of Chapter 3 when objectively optimized. Black circles and (1.96 SD) error bars are for 200 subjectively best-corrected typical eyes from the Indiana Aberration Study[102,151] scaled[2] to 5mm. Optimization only affects second-order terms (not shown); the aberrations shown are as measured through the wavefront-guided lenses.

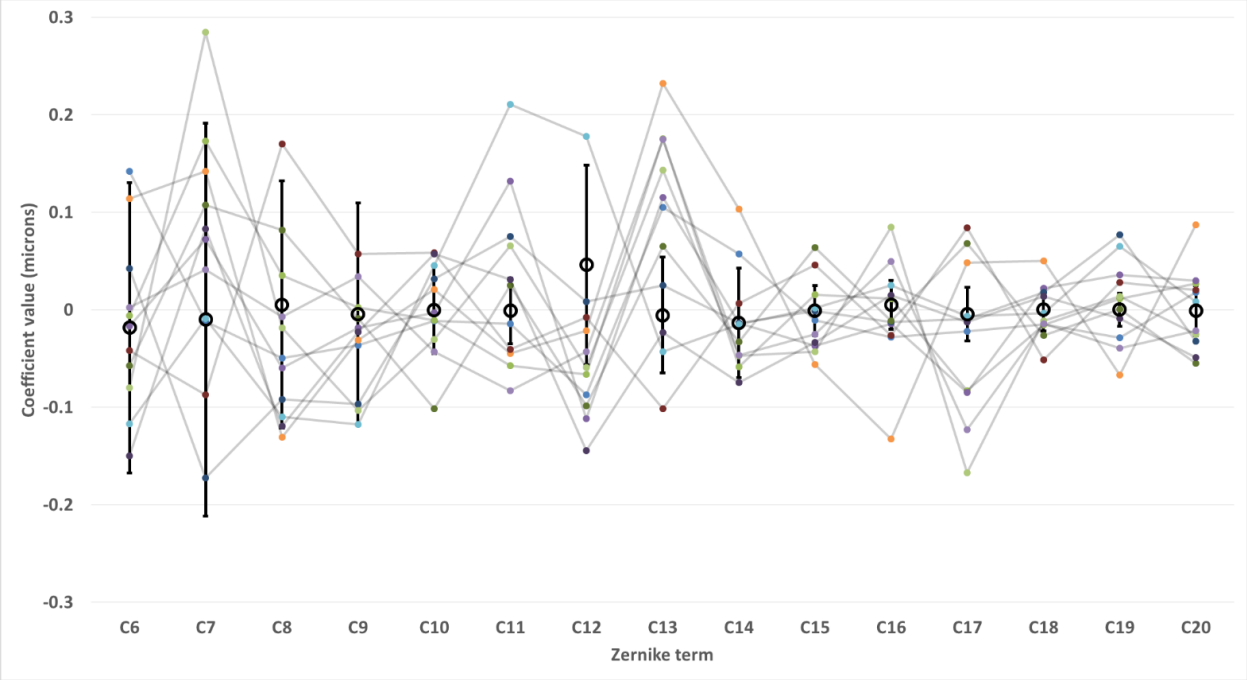

Figure 7. 5 Higher-order (third through fifth order) aberrations of 11 eyes from Chapter 4 wearing wavefront-guided scleral lenses (colored points and grey lines) that did not reach the best-corrected VSX norms of Chapter 3 when objectively optimized. Black circles and (1.96 SD) error bars are for 200 subjectively best-corrected typical eyes from the Indiana Aberration Study[102,151] scaled[2] to 5mm. Optimization only affects second-order terms (not shown); the aberrations shown are as measured through the wavefront-guided lenses.

While lower- and higher-order aberrations in a population of subjectively best-corrected typical eyes each follow a relatively (statistically) normal distribution,[102,151] the residual aberrations of the eyes in Chapter 4 wearing wavefront-guided scleral lenses were not normally distributed. This is understandable for a number of reasons: [1] the sample of eyes in Chapter 4 is much smaller (20), [2] underlying disease severity varied substantially (as described in Table 4.1), which resulted in baseline aberration structures varying substantially, [3] while wavefront-guided lenses were designed based on residual aberrations measured through a best conventional scleral lens, the manufacture of every wavefront-guided lens was not evaluated (and may have differed from design), and the position and orientation of the wavefront-guided lens at the moment of wavefront error measurement was not recorded. Analyzing the accuracy and

precision of wavefront-guided corrections would benefit from future work controlling these factors wherever possible.

7.2.3.3 Differences in aberration structures between conventional and wavefront-guided lenses: Particularly vertical coma and secondary astigmatism

This section attempts to shed to some light on possible explanations for the residual aberrations measured when the eyes of Chapter 4 wore wavefront-guided lenses, and compares those aberrations with measurements of the same eye wearing a conventional scleral lens (which would have been used to design the wavefront-guided lens). Remember that the manufactured aberrations of each wavefront-guided lens were not measured and that the position and orientation of both lenses were not recorded when wavefront error was measured through the lens. Consequently, this section can never amount to a full explanation, but rather merely hopes to inform potential avenues of further investigation.

The figures below plot each Zernike radial order separately; scales are constant within radial orders. Only a few aberration terms show clear trends: Lower-order terms (Figure 7.7) constitute a major source of variability and difference between the two lens types. This agrees with another study[251] and is possibly why only higher-order aberrations have been reported when evaluating the manufacture accuracy of wavefront-guided lenses in some studies.[118,123,252] However, as mentioned in the preceding section, when lower-order terms were objectively optimized (in the presence of higher-orders) the majority of these eyes still did not reach the levels of the VSX norms in Chapter 3.

Third-order vertical coma (C7; Figure 7.8) is one of the few higher-order aberrations with a clear pattern. As discussed in Chapter 3, negative vertical coma is the dominant aberration in keratoconus.[114,150] The sign of coma reverses[112,113] when a rigid lens is worn, hence, the positive vertical coma residual with all conventional lenses in Figure 7.8. Across most eyes (18/20), however, positive vertical coma is still residual through the wavefront-guided lens. Future work might investigate whether this consistently incomplete correction of vertical coma is perhaps due to lens manufacture, position on the eye, or masking by the tear film, and whether a nomogram increase in the designed magnitude of vertical coma (that is, aiming for a greater amount of vertical coma in the wavefront-guided prescription than is measured through the best conventional lens), might benefit these eyes.

As remarked at Figure 7.5 above, secondary astigmatism (C13; Figure 7.9) is prominently residual through both conventional and wavefront-guided lenses. This aberration is particularly detrimental to visual image quality (Figure 7.6) and future work would do well to focus on the correction of this particular aberration.

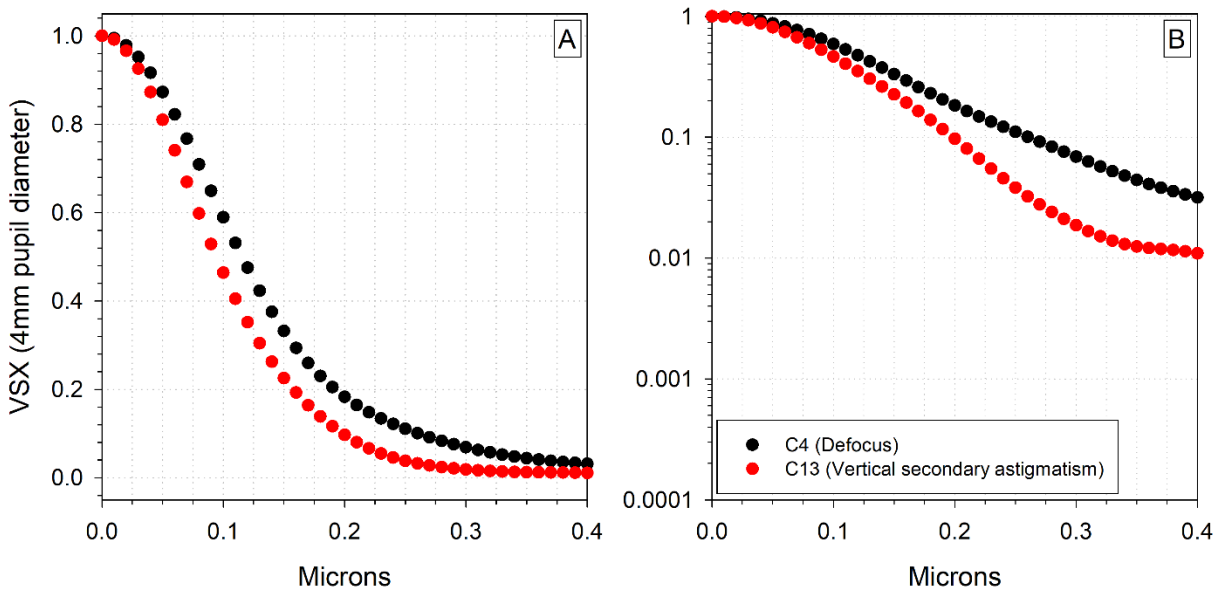

Figure 7. 6 Secondary astigmatism is more detrimental to VSX than defocus.

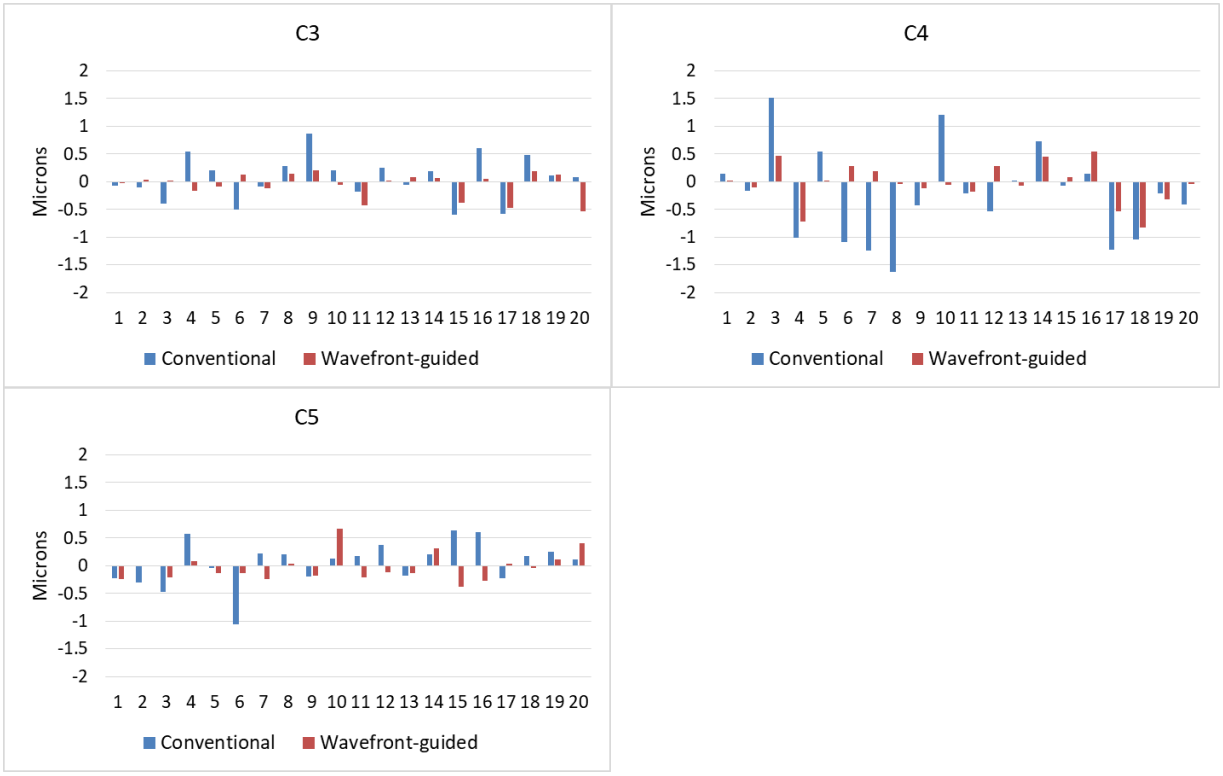

Figure 7. 7 Second-order Zernike aberrations of the eyes from Chapter 4 wearing conventional and wavefront-guided scleral lenses.

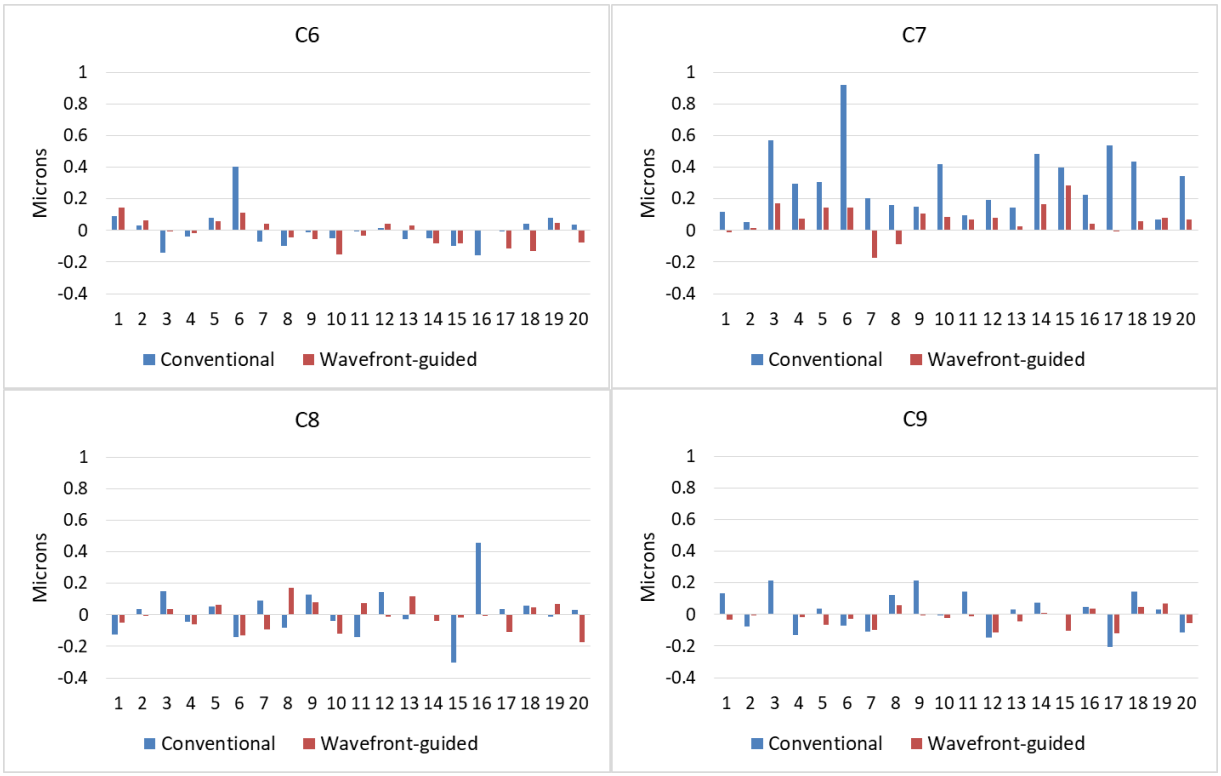

Figure 7. 8 Third-order Zernike aberrations of the eyes from Chapter 4 wearing conventional and wavefront-guided lenses.

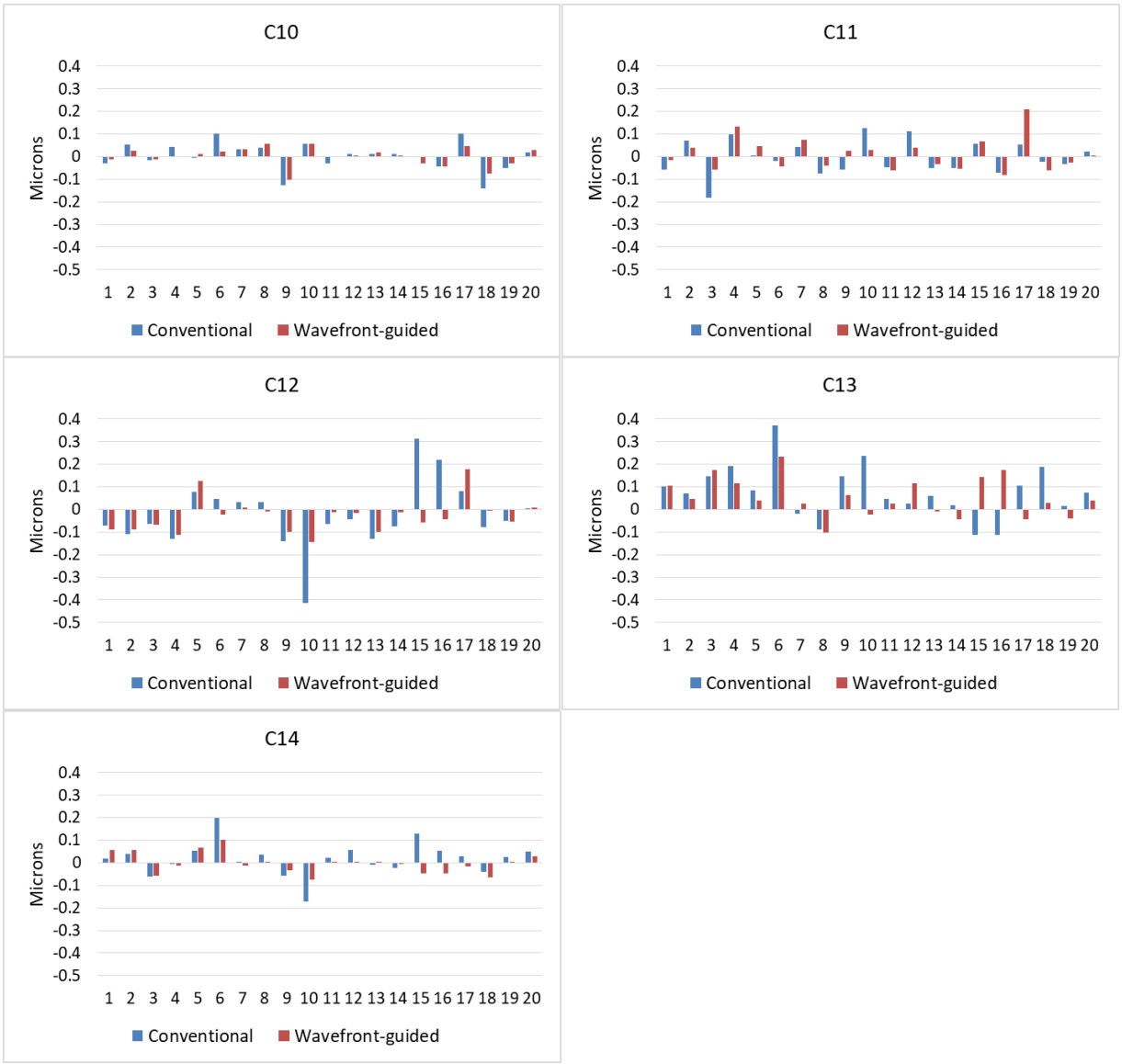

Figure 7. 9 Fourth-order Zernike aberrations of the eyes from Chapter 4 wearing conventional and wavefront-guided lenses.

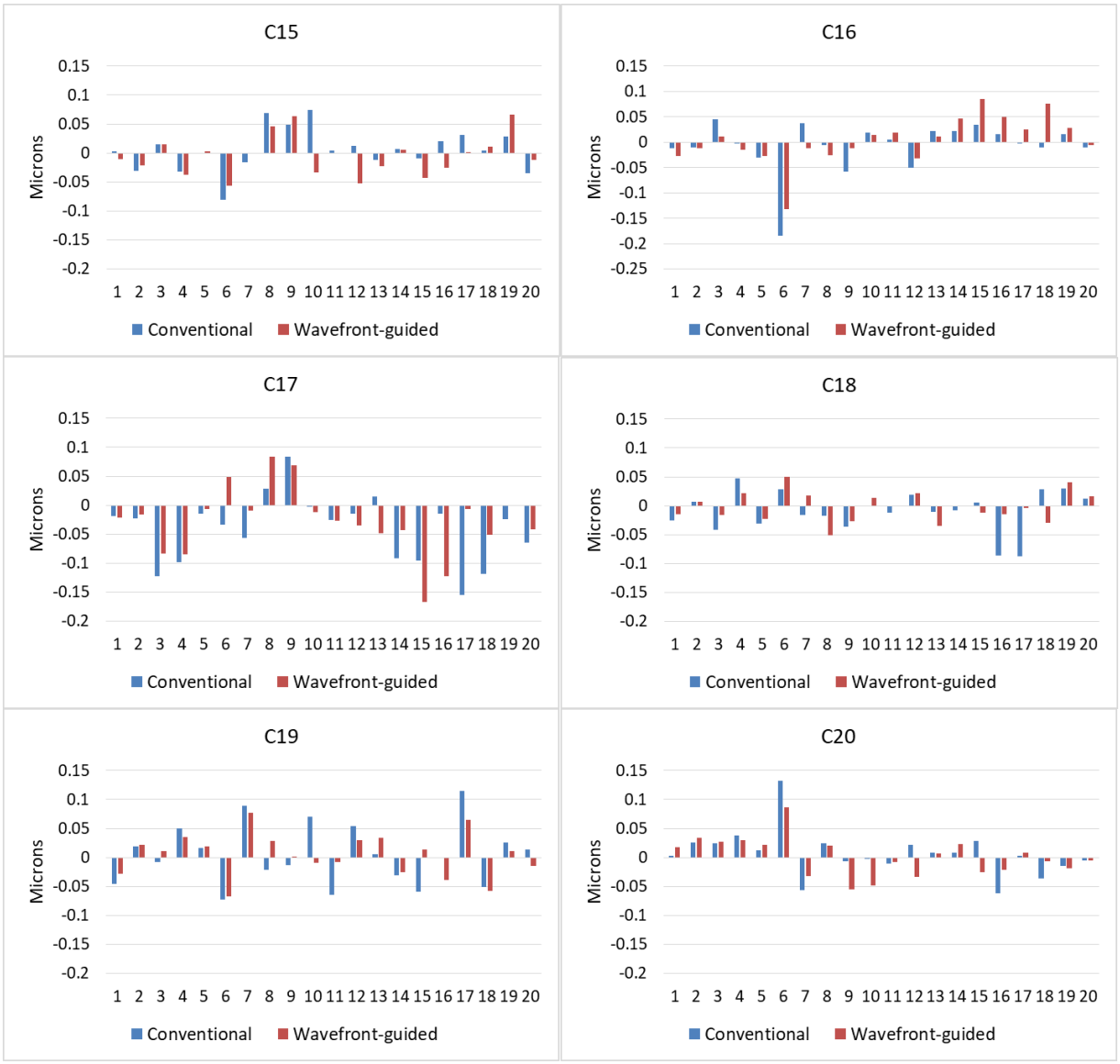

Figure 7. 10 Fifth-order Zernike aberrations of the eyes from Chapter 4 wearing conventional and wavefront-guided lenses.

7.2.3.4 The neural component of VSX and concluding remarks

The above sections have discussed optical explanations for the eyes in Chapter 4 not reaching the VSX norms of Chapter 3 with wavefront-guided lenses, however, the neural component of the metric might also bear some responsibility. Literature has shown that eyes with elevated levels of aberrations adapt their neural processing[28,135,136] to their aberrated images and

it is unknown whether the neural weighting function used in the calculation of VSX is inappropriate for these eyes, particularly in the contexts of optimizing objective refractions and evaluating corrections. This question motivated the work of Chapter 5 and 6 that are discussed next.

7.2.4 Chapter 5

Chapter 5 described the evolution of the neural component of visual image quality metrics to account for how retinal illuminance (VSX(td)) and both retinal illuminance and age (VSX(td,a)) affect the neural contrast sensitivity function. Objectively best-corrected metric values were determined using the same optimization method described in Chapters 2 and 3, and changes in best-corrected metrics as a function of age were compared with change in visual acuity as a function of age from literature.

7.2.4.1 Differences between VSX(td) and VSX(td,a)

The differences between objectively best-corrected VSX(td) and VSX(td,a) as a function of target luminance and age is shown in Figure 7.11. The addition of age-specific weighting resulted in a decrease in VSX(td,a) metric values with age, which was more gradual at high photopic luminances and more pronounced at lower luminances – this could also be gauged from the differences between Figures 5.4A and 5.4B in Chapter 5, but can be more readily appreciated in Figure 7.11. This broadly agrees with the prevailing clinical experience that older individuals report greater visual difficulties in dim light conditions.

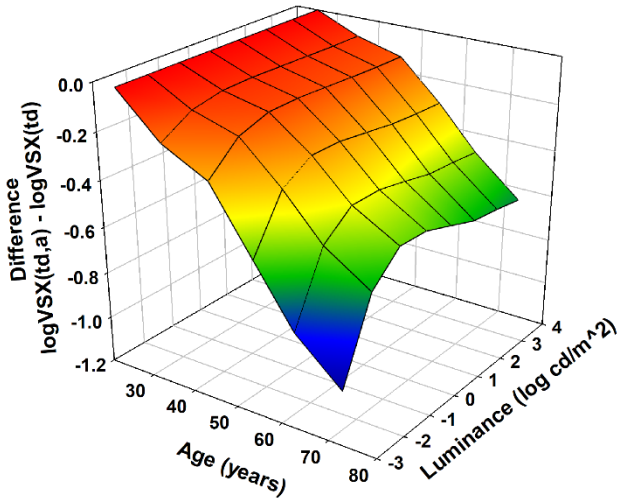

Figure 7. 11 Difference between best-corrected VSX(td) and VSX(td,a) values as a function of target luminance and age.

7.2.4.2 Best-corrected visual image quality as a function of age and retinal illuminance

The question arose as to whether the behavior of best corrected visual image quality as a function of age and retinal luminance (Trolands) would be substantially different from the behavior as a function of age and target luminance presented in Figure 5.4. The two relationships are contrasted in Figure 7.12, where it is easy to appreciate that there is not a substantial difference.

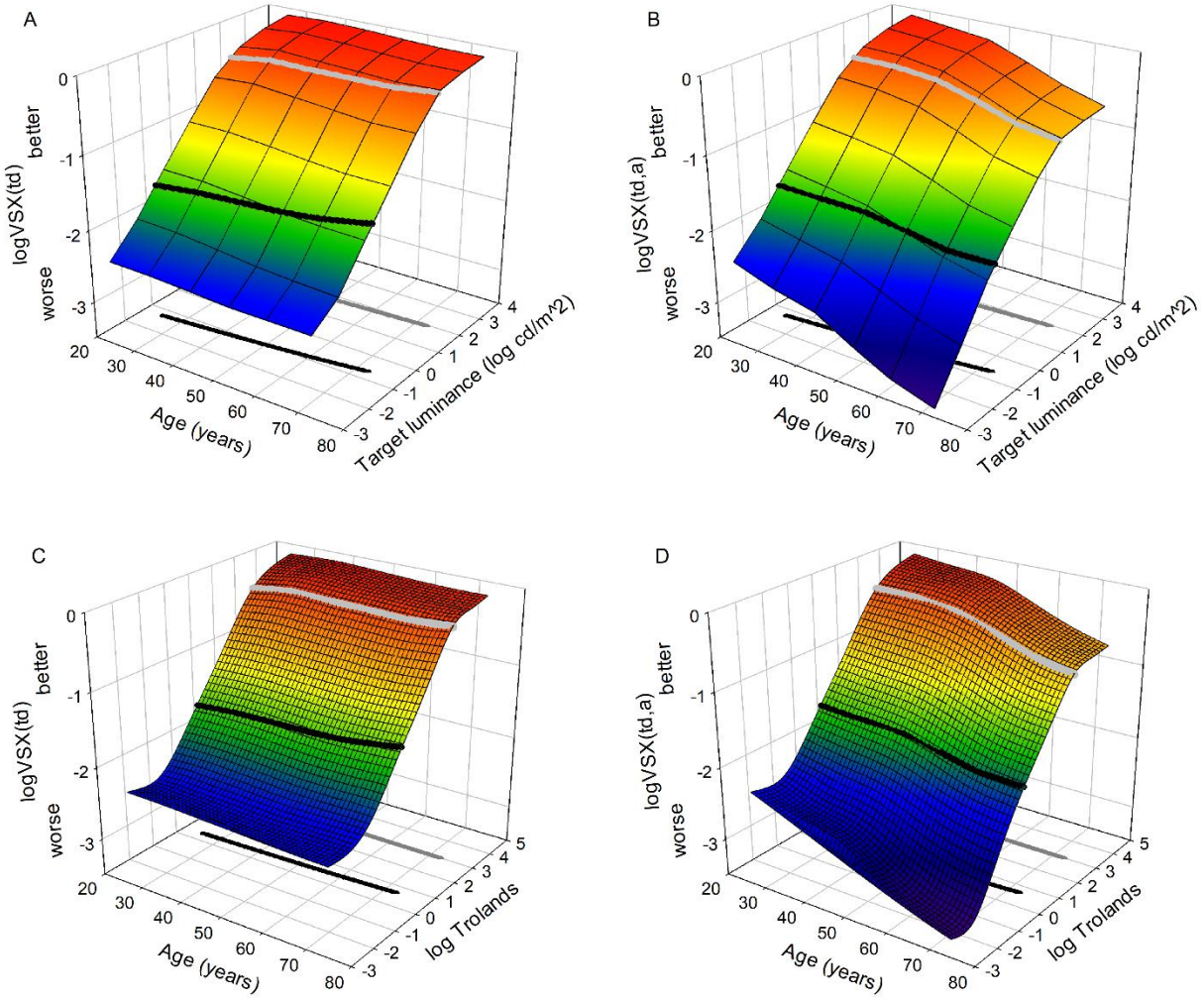

Figure 7. 12 Panels (A) and (B) respectively show best-corrected VSX(td) and VSX(td,a) values as a function of age and target luminance and are repeated from Figure 5.4 to aid comparison with corresponding panels (C) and (D) where the metric values are plotted as a function of age and retinal illuminance (Trolands). The similarity between the target luminance (A and B) and retinal illuminance (C and D) plots is easy to appreciate. The target luminance plots (A and B) were preferred for inclusion in Chapter 5 because, in the modelling, retinal illuminance is not an independent variable – it depends on target illuminance and the calculation of physiological pupil size (also influences by target illuminance).

7.2.4.3 Future directions and concluding remarks

Chapter 5 mentioned potential sources of variability that begin with the physiological pupil size of an individual (which was predicted from a model,[163] and affects both aberrations

and retinal illuminance), and also includes variability in neural contrast sensitivity. Using eyes with keratoconus, Chapter 6 demonstrated the personalization of both the optical and neural parts of visual image quality metrics to an individual eye. As alluded to in Chapter 5, many future projects could involve making predictions around the neural contrast sensitivity functions measured in Chapter 6 by using the models of Chapter 5. At the time of this dissertation, we have begun modelling the effects of the various sources of variability, but the compound interaction of variabilities are so nebulous that it is too early to speak to which ramifications have the least and greatest impact.

Another future direction of this work is to evolve the neural weighting function further by limiting the spatial frequency bandwidth to be specific to a task of interest. This idea formed the basis of early image quality metrics, such as SQF[253] (which passed a band of spatial frequency similar to that used in VSX, but without weighting the spatial frequencies by the sensitivity of the human visual system).

7.2.5 Chapter 6

Many explorations are being performed on the neural contrast sensitivity data of highly aberrated eyes that are outside the application of these data to visual image quality metrics. As mentioned, future work might benefit from estimating the initial threshold using a staircase method rather than a method of adjustment.

The work of Chapter 4 and Chapter 6 could be combined in the future to study the plasticity of high spatial frequency neural contrast sensitivity in eyes that had lost that high

spatial frequency processing ability (due to chronic lack of high spatial frequency information reaching the retina due to highly aberrated optics). This is encouraged by analogous work in amblyopia,[254–256] particularly because individuals with keratoconus had typical visual experience during the sensitive and critical periods of development (which is commonly not the case for individuals with amblyopia). If these eyes were well corrected with wavefront-guided lenses and allowed an appropriate amount of time to adapt to the new percept, they may recover the ability to process high spatial frequencies, given (the assumption) that they experienced typical vision and neural stimulation during the sensitive periods of development (this was the original idea that motivated construction of the interferometry system).

7.3 Summary of future directions

This section serves as a distillation of lessons learned and future directions that have already been identified and discussed in earlier chapters and preceding sections of this chapter.

7.3.1 Spectacle work

During the objective identification of an optimal refraction, dioptric power is defined at 589 nm and, if applied to a 555 nm wavefront error, can result in a slightly overly-myopic (–0.17296 D too much minus) correction (discussed in section 7.2.1.5). This is easy to rectify in future work and is important if that work dispenses optimized corrections (as suggested in section 7.2.1.6), which would allow a perspective on adaptation to the optimized correction.

To investigate differences between subjective and wavefront-based objective refractions the following should be considered (as discussed in Sections 7.2.1.1 and 7.2.1.6):

- Wavefront error measurement:
    - Extend previous work[175,176] by comparing wavefront error measured from closed systems (where distance vision is simulated while gazing into the instrument at a real near distance) with other systems that are open-field or allow through-viewing.
    - Investigate the effects of different instructions and tasks during wavefront error measurement, such as simply instructing the subject to look towards a distant target versus having to read a letter chart at the same distance.
    - As mentioned in Section 7.2.3.1 the COAS HD wavefront sensor output aberrations in the corneal plane. During the simulated through focus experiments, corrections are vertexed back to pupil plane. Whether this difference is significant or not, remains to be investigated.
- Subjective refraction:
    - Experiment with instructions and compare differences in refraction when asking a subject to attend to different qualities of vision such as maximizing letter legibility versus maximizing contrast or edge definition.
    - Compare subjective refractions before and after allowing the subject to adapt to an objectively optimized correction.
    - Comparing the end point of subjective refractions from different starting points (such as autorefraction, an optimized refraction, a habitual correction).

- Eyes with high levels of habitually-undercorrected hyperopia could be re-examined but either a mild cycloplegic (such as tropicamide, that was used) can be re-instilled before measuring visual acuity and preference, or a more potent cycloplegic, such as atropine could be considered to relax accommodation completely.

7.3.2 Wavefront-guided contact lens work

While the randomized cross-over design of Chapter 4 was experimentally rigorous, subjects that wore the wavefront-guided lens first and then crossed-over to the conventional lens expressed considerable unhappiness in relinquishing the wavefront-guided lenses. One subject did not complete the conventional lens part of the cross-over. Alternate designs could be considered in future studies.

Many of the points relating to wavefront-error measurement in the preceding section (7.3.1) are applicable here. Additionally, when measuring highly aberrated eyes, it is important to consider Zernike fit errors (as mentioned in Section 1.5). Poor characterization by Zernikes might explain why some eyes are not corrected to typical levels of aberration with these lenses.

Chapter 4 and Section 7.2.3 identified aberrations (such as primary vertical coma, secondary astigmatism, and secondary coma) that were particularly damaging to vision and often remained higher than typical in eyes with keratoconus even when wearing wavefront-guided lenses. Specific targeting or nomogram-type overcorrection of these aberrations might benefit the eyes being corrected. Two steps necessary in achieving this goal are (1) to measure all lenses

after manufacture – this needs to be seamlessly integrated into the manufacture process and (2) to record the position and orientation of the lens at the time that a wavefront error measurement is made through the lens – this will help exclude manufacture errors and misalignment as contributing factors to noise in the accuracy and precision of these lenses.

7.3.3. Basic metric work

While metrics such as VSX have been shown to track perceived image quality over a range of image quality, both ceiling- and floor-effects have been noted (where the metric fails to track perceived image quality at very high and very low visual image quality values respectively). It was suggested in Section 7.2.1.4 that both the ceiling and floor effects could be studied using visual acuity and perceptible blur as outcomes to be compared with change in logVSX. Furthermore, as discussed in Section 7.2.2.1, these investigations should employ a variety of targets that vary in contrast and more closely resemble real-world scenes.

Although the neural component of visual image quality metrics was evolved during this dissertation, much work remains to be done:

- Section 6.5.1 describes how future measurements of neural contrast sensitivity might benefit from estimating the initial threshold (the starting point for the method of constant stimuli) using a staircase paradigm rather than a method of adjustment.
- As mentioned in Section 7.2.5. the work of Chapter 4 (wavefront-guided lenses) and Chapter 6 (measurement of neural contrast sensitivity) could be combined to study the plasticity of high spatial frequency processing in eyes with keratoconus – these eyes may have lost the ability to process high spatial frequencies due to chronic lack of appropriate

information reaching the retina (due to highly aberrated optics that could not be corrected prior to wavefront-guided lenses). Measuring neural contrast sensitivity of these eyes before and after adaptation to a wavefront-guided correction would give a perspective on that neural plasticity. In designing these experiments, the distinction should be emphasized between passively recovering the ability to process high spatial frequencies (say, by adapting to a wavefront-guided correction in everyday life) and actively training at the task – both are subject to confounding by learning effects, but the latter to a much greater degree.

- The models in Chapter 5 could be used to make predictions about changes in neural contrast sensitivity around the measured functions reported in Chapter 6. That is, the starting point or reference of the model is made relative to the measured function at 15 td and the subject's age. Similarly, the metrics can be made specific to a particular visual task by limiting the spatial frequency bandwidth used in the calculation. This work is already underway.
- Additionally, the modelling of potential variability arising from each step in the methods of Chapter 5 is already underway. This will take into account variability in physiological pupil size, aberrations, and neural processing in the estimation of visual image quality.
- Many analyses are currently being performed on the measured neural contrast sensitivity data in Chapter 6 and remain to be reported in future work. These include the investigation of synergy between the optical and neural components (as described in Section 6.5.4).

7.4 Concluding remarks

Five experiments were described where the visual image quality metric VSX was successfully applied to optimize and evaluate both conventional (spectacle and scleral lens) and individualized (wavefront-guided scleral lens) corrections across modalities. The neural weighting component of VSX was then (1) evolved to a model that respects the effects of retinal illuminance and age and (2) personalized to individual eyes (both typical and those with keratoconus). Because the measurement of orientation-specific neural contrast sensitivity described in Chapter 6 is time-consuming and the gains (when using the measured function of an individual) over the models presented in Chapter 5 were not clinically significant, it is unlikely that recording these measurements will ever become commonplace. The measured functions did, however, provide insights into the behavior of the metric in eyes with ectasia wearing wavefront-guided lenses in Chapter 4 and provided some additional assurance that the corrections in Chapter 2 were suitably determined. Furthermore, the effects of retinal illuminance and, to a lesser degree, age on neural contrast sensitivity are well documented and the models in Chapter 5 should broaden the clinical uses of visual image quality metrics such as VSX to somewhat more individualized (task- and age-specific) real-world applications.

References

1. American National Standards Institute. Methods for reporting optical aberrations of eyes. ANSI Z8028. 2004

2. Schwiegerling J. Scaling Zernike expansion coefficients to different pupil sizes. JOSA A. 2002;19(10):1937–1945.

3. Bará S, Pailos E, Arines J, López-Gil N, Thibos L. Estimating the eye aberration coefficients in resized pupils: is it better to refit or to rescale? J Opt Soc Am A. 2014 Jan 1;31(1):114.

4. Applegate R, Donnelly III W, Marsack J, Koenig D, Pesudovs K. Three-dimensional relationship between high-order root-mean-square wavefront error, pupil diameter, and aging. JOSA A. 2007;24(3):578–587.

5. Brunette I, Bueno JM, Parent M, Hamam H, Simonet P. Monochromatic Aberrations as a Function of Age, from Childhood to Advanced Age. Investig Opthalmology Vis Sci. 2003 Dec 1;44(12):5438.

6. Applegate RA, Sarver EJ, Khemsara V. Are all aberrations equal? J Refract Surg. 2002 Oct;18(5):S556-562.

7. Applegate RA, Ballentine C, Gross H, Sarver EJ, Sarver CA. Visual acuity as a function of Zernike mode and level of root mean square error. Optom Vis Sci. 2003;80(2):97–105.

8. Applegate RA, Marsack JD, Ramos R, Sarver EJ. Interaction between aberrations to improve or reduce visual performance. J Cataract Refract Surg. 2003 Aug;29(8):1487–95.

9. Xu R, Wang H, Thibos L, Bradley A. Interaction of aberrations, diffraction, and quantal fluctuations determine the impact of pupil size on visual quality. J Opt Soc Am A. 2017 Apr 1;34(4):481–92.

10. Coletta N, Sharma V. Effects of luminance and spatial noise on interferometric contrast sensitivity. J Opt Soc Am A. 1995;12(10):2244–2251.

11. Kawara T, Ohzu H. Modulation transfer function of human visual system. Oyobutsuri Jpn. 1977;46:128–38.

12. Nameda N, Kawara T, Ohzu H. Human visual spatio-temporal frequency performance as a function of age. Optom Vis Sci. 1989 Nov;66(11):760–5.

13. Morrison J, McGrath C. Assessment of the optical contributions to the age-related deterioration in vision. Q J Exp Physiol. 1985;70(2):249–269.

14. Elliott D. Contrast sensitivity decline with ageing: a neural or optical phenomenon? Ophthalmic Physiol Opt. 1987;7(4):415–9.

15. Thibos LN, Hong X, Bradley A, Applegate RA. Accuracy and precision of objective refraction from wavefront aberrations. J Vis. 2004 Apr 1;4(4):329–51.

16. Campbell FW, Green DG. Optical and retinal factors affecting visual resolution. J Physiol. 1965;181(3):576.

17. López-Gil N, Martin J, Liu T, Bradley A, Díaz-Muñoz D, Thibos L. Retinal image quality during accommodation. Ophthalmic Physiol Opt. 2013 Jul;33(4):497–507.

18. Sreenivasan V, Aslakson E, Kornaus A, Thibos LN. Retinal image quality during accommodation in adult myopic eyes. Optom Vis Sci Off Publ Am Acad Optom. 2013;90(11):1292.

19. Cheng X, Bradley A, Thibos LN. Predicting subjective judgment of best focus with objective image quality metrics. J Vis. 2004 Apr 23;4(4):310–21.

20. Marsack JD, Thibos LN, Applegate RA. Metrics of optical quality derived from wave aberrations predict visual performance. J Vis. 2004 Apr 1;4(4):8–8.

21. Martin J, Vasudevan B, Himebaugh N, Bradley A, Thibos L. Unbiased estimation of refractive state of aberrated eyes. Vision Res. 2011 Sep;51(17):1932–40.

22. Schoneveld P, Pesudovs K, Coster D. Predicting visual performance from optical quality metrics in keratoconus. Clin Exp Optom. 2009 May;92(3):289–96.

23. Ravikumar A, Applegate RA, Shi Y, Bedell HE. Six just-noticeable differences in retinal image quality in 1 line of visual acuity: Toward quantification of happy versus unhappy patients with 20/20 acuity. J Cataract Refract Surg. 2011 Aug;37(8):1523–9.

24. Ravikumar A, Sarver EJ, Applegate RA. Change in visual acuity is highly correlated with change in six image quality metrics independent of wavefront error and/or pupil diameter. J Vis. 2012 Sep 14;12(10):1–13.

25. Ravikumar A, Benoit J, Marsack J, Anderson H. Image Quality Metric Derived Refractions Predicted to Improve Visual Acuity Beyond Habitual Refraction for Patients With Down Syndrome. Transl Vis Sci Technol. 2019 May 20;8(3):20.

26. Sabesan R. Interaction between optical and neural factors affecting visual performance [Internet]. University of Rochester; 2011 [cited 2017 Jun 5]. Available from: http://search.proquest.com/openview/a5dd1dd07066fe195ccd92eff5cb7b13/1?pq-origsite=gscholar&cbl=18750&diss=y

27. Kayazawa F, Yamamoto T, Itoi M. Clinical measurement of contrast sensitivity function using laser generated sinusoidal grating. Jpn J Ophthalmol. 1981;25:229–36.

28. Michael R, Guevara O, de la Paz M, Alvarez de Toledo J, Barraquer R. Neural contrast sensitivity calculated from measured total contrast sensitivity and modulation transfer function. Acta Ophthalmol (Copenh). 2011 May;89(3):278–83.

29. Hastings G, Marsack J, Nguyen L, Cheng H, Applegate R. Is an objective refraction optimised using the visual Strehl ratio better than a subjective refraction? Ophthalmic Physiol Opt. 2017 May;37(3):317–25.

30. Hastings G, Marsack J, Thibos L, Applegate R. Normative best-corrected values of the visual image quality metric VSX as a function of age and pupil size. J Opt Soc Am A. 2018 May 1;35(5):732–9.

31. Perrigin J, Perrigin D, Grosvenor T. A comparison of clinical refractive data obtained by three examiners. Am J Optom Physiol Opt. 1982 Jun;59(6):515–9.

32. Goss DA, Grosvenor T. Reliability of refraction--a literature review. J Am Optom Assoc. 1996 Oct;67(10):619–30.

33. Bullimore MA, Fusaro RE, Adams CW. The repeatability of automated and clinician refraction. Optom Vis Sci. 1998 Aug;75(8):617–22.

34. Pesudovs K, Parker KE, Cheng H, Applegate RA. The precision of wavefront refraction compared to subjective refraction and autorefraction. Optom Vis Sci. 2007;84(5):387–392.

35. Anderson L, Marsack JD, Ravikumar A, Applegate RA. Accounting for both lower and higher order aberration in objective refraction to improve image and visual quality. J Vis. 2013 Dec 27;13(15):P25–P25.

36. Cheng X, Himebaugh NL, Kollbaum PS, Thibos LN, Bradley A, others. Validation of a clinical Shack-Hartmann aberrometer. Optom Vis Sci. 2003;80(8):587–595.

37. Artal P, Chen L, Fernández EJ, Singer B, Manzanera S, Williams DR. Neural compensation for the eye's optical aberrations. J Vis. 2004 Apr 16;4(4):4.

38. Guirao A, Williams D. A method to predict refractive errors from wave aberration data. Optom Vis Sci. 2003;80(1):36–42.

39. Kilintari M, Pallikaris A, Tsiklis N, Ginis H. Evaluation of image quality metrics for the prediction of subjective best focus. Optom Vis Sci. 2010;87(3):183–189.

40. Iskander DR. A subjective refraction-based assessment of image quality metric. Photonics Lett Pol. 2011 Dec 31;3(4).

41. Teel D, Jacobs R, Copland J, Neal D, Thibos L. Differences between wavefront and subjective refraction for infrared light. Optom Vis Sci. 2014;91(10):1158–1166.

42. Lin H, Chen C, Lee Y. Comparisons of wavefront refraction, autorefraction, and subjective manifest refraction. Tzu Chi Med J. 2013 Mar;25(1):43–6.

43. Bennett J, Stalboerger G, Hodge D, Schornack M. Comparison of refractive assessment by wavefront aberrometry, autorefraction, and subjective refraction. J Optom. 2015 Apr;8(2):109–15.

44. Reinstein D, Archer T, Couch D. Accuracy of the WASCA aberrometer refraction compared to manifest refraction in myopia. J Refract Surg. 2006;22(3):268–274.

45. Zhu X, Dai J, Chu R, Lu Y, Zhou X, Wang L. Accuracy of WASCA Aberrometer Refraction Compared to Manifest Refraction in Chinese Adult Myopes. J Refract Surg. 2009 Nov 1;25(11):1026–33.

46. Jinabhai A, O'Donnell C, Radhakrishnan H. A Comparison between Subjective Refraction and Aberrometry-Derived Refraction in Keratoconus Patients and Control Subjects. Curr Eye Res. 2010 Aug;35(8):703–14.

47. Thibos LN, Wheeler W, Horner D. Power vectors: an application of Fourier analysis to the description and statistical analysis of refractive error. Optom Vis Sci. 1997 Jun;74(6):367–75.

48. Bailey IL, Bullimore MA, Raasch TW, Taylor HR. Clinical grading and the effects of scaling. Invest Ophthalmol Vis Sci. 1991;32(2):422–432.

49. Carkeet A. Modeling logMAR visual acuity scores: effects of termination rules and alternative forced-choice options. Optom Vis Sci. 2001;78(7):529–538.

50. Hastings GD, Marsack JD, Applegate RA. Can superior image quality and better visual acuity than that provided by subjective refraction be objectively determined? Optom Vis Sci. 2015;92:E-abstract 155111.

51. Rabbetts RB. Bennett & Rabbetts' clinical visual optics. 4th ed. Edinburgh ; New York: Elsevier/Butterworth Heinemann; 2007. 470 p.

52. Schwartz SH. Geometrical and visual optics: a clinical introduction. Second edition. New York: McGraw/Medical; 2013.

53. Thibos LN, Hong X, Bradley A, Cheng X. Statistical variation of aberration structure and image quality in a normal population of healthy eyes. JOSA A. 2002;19(12):2329–2348.

54. Armstrong RA. Statistical guidelines for the analysis of data obtained from one or both eyes. Ophthalmic Physiol Opt. 2013 Jan;33(1):7–14.

55. Armstrong RA, Eperjesi F, Gilmartin B. The application of analysis of variance (ANOVA) to different experimental designs in optometry. Ophthalmic Physiol Opt. 2002;22(3):248–256.

56. Raasch TW, Bailey IL, Bullimore MA. Repeatability of visual acuity measurement. Optom Vis Sci. 1998 May;75(5):342–8.

57. Manny R, Hussein M, Gwiazda J, Marsh-Tootle W. Repeatability of ETDRS Visual Acuity in Children. Investig Opthalmology Vis Sci. 2003 Aug 1;44(8):3294.

58. Elliott DB, Yang KC, Whitaker D. Visual acuity changes throughout adulthood in normal, healthy eyes: seeing beyond 6/6. Optom Vis Sci Off Publ Am Acad Optom. 1995 Mar;72(3):186–91.

59. Chui TYP, Yap MKH, Chan HHL, Thibos LN. Retinal stretching limits peripheral visual acuity in myopia. Vision Res. 2005 Mar;45(5):593–605.

60. Coletta NJ, Watson T. Effect of myopia on visual acuity measured with laser interference fringes. Vision Res. 2006 Mar;46(5):636–51.

61. Strang NC, Winn B, Bradley A. The role of neural and optical factors in limiting visual resolution in myopia. Vision Res. 1998;38(11):1713–1721.

62. Atchison DA, Smith G, Efron N. The effect of pupil size on visual acuity in uncorrected and corrected myopia. Am J Optom Physiol Opt. 1979 May;56(5):315–23.

63. Smith G. Relation between spherical refractive error and visual acuity. Optom Vis Sci. 1991 Aug;68(8):591–8.

64. Elsner AE, Burns SA, Weiter JJ, Delori FC. Infrared imaging of sub-retinal structures in the human ocular fundus. Vision Res. 1996 Jan;36(1):191–205.

65. Almeida M, Carvalho L. Different schematic eyes and their accuracy to the in vivo eye: a quantitative comparison study. Braz J Phys. 2007;37(2A):378–387.

66. Smith G. Angular diameter of defocus blur discs. Am J Optom Physiol Opt. 1982 Nov;59(11):885–9.

67. Raasch T. Spherocylindrical refractive errors and visual acuity. Optom Vis Sci. 1995 Apr;72(4):272–5.

68. Westheimer G, Campbell F. Light distribution in the image formed by the living human eye. JOSA. 1962;52(9):1040–1045.

69. Krauskopf J. Light distribution in human retinal images. JOSA. 1962;52(9):1046–1050.

70. Campbell F, Gubisch R. Optical quality of the human eye. J Physiol. 1966;186(3):558–578.

71. Santamaría J, Artal P, Bescós J. Determination of the point-spread function of human eyes using a hybrid optical–digital method. JOSA A. 1987;4(6):1109–1114.

72. Artal P. Calculations of two-dimensional foveal retinal images in real eyes. JOSA A. 1990;7(8):1374–1381.

73. Artal P, Ferro M, Navarro R, Miranda I. Effects of aging in retinal image quality. JOSA A. 1993;10(7):1656–1662.

74. Navarro R, Artal P, Williams D. Modulation transfer of the human eye as a function of retinal eccentricity. JOSA A. 1993 Feb;10(2):201–12.

75. Guirao A, Gonzalez C, Redondo M, Geraghty E, Norrby S, Artal P. Average optical performance of the human eye as a function of age in a normal population. Invest Ophthalmol Vis Sci. 1999;40(1):203–213.

76. Calver R, Cox M, Elliott D. Effect of aging on the monochromatic aberrations of the human eye. J Opt Soc Am A Opt Image Sci Vis. 1999 Sep;16(9):2069–78.

77. Salmon T, van de Pol C. Normal-eye Zernike coefficients and root-mean-square wavefront errors. J Cataract Refract Surg. 2006 Dec;32(12):2064–74.

78. Plainis S, Atchison D, Charman W. Power profiles of multifocal contact lenses and their interpretation. Optom Vis Sci. 2013 Oct;90(10):1066–77.

79. Marsack J, Parker K, Applegate R. Performance of wavefront-guided soft lenses in three keratoconus subjects. Optom Vis Sci. 2008;85(12):E1172.

80. Marsack J, Ravikumar A, Nguyen C, Ticak A, Koenig D, Elswick J, et al. Wavefront-guided scleral lens correction in keratoconus. Optom Vis Sci. 2014 Oct;91(10):1221–30.

81. Chung S, Jarvis S, Cheung S. The effect of dioptric blur on reading performance. Vision Res. 2007 Jun;47(12):1584–94.

82. Fujikado T, Saika M. Evaluation of actual retinal images produced by misaligned aspheric intraocular lenses in a model eye. Clin Ophthalmol. 2014 Nov;2415.

83. Navarro R, Rozema J, Tassignon M. Optical changes of the human cornea as a function of age. Optom Vis Sci. 2013;90(6):587–598.

84. IJspeert J, van den Berg T, Spekreijse H. An improved mathematical description of the foveal visual point spread function with parameters for age, pupil size and pigmentation. Vision Res. 1993 Jan;33(1):15–20.

85. Watson A. A formula for the mean human optical modulation transfer function as a function of pupil size. J Vis. 2013 Jan 1;13(6):18–18.

86. Piotrowski L, Campbell F. A demonstration of the visual importance and flexibility of spatial-frequency amplitude and phase. Perception. 1982;11(3):337–346.

87. Sarver E, Applegate R. The importance of the phase transfer function to visual function and visual quality metrics. J Refract Surg Thorofare NJ 1995. 2004 Oct;20(5):S504-507.

88. Watson A, Ahumada A. A standard model for foveal detection of spatial contrast. J Vis. 2005;5(9):6–6.

89. Iskander D. Computational aspects of the visual Strehl ratio. Optom Vis Sci. 2006 Jan;83(1):57–9.

90. Pesudovs K, Marsack J, Donnelly W, Thibos L, Applegate R. Measuring visual acuity - mesopic or photopic conditions, and high or low contrast letters? J Refract Surg Thorofare NJ 1995. 2004 Oct;20(5):S508-514.

91. Chylack L, Wolfe J, Singer D, Leske M, Bullimore M, Bailey I, et al. The Lens Opacities Classification System III. Arch Ophthalmol. 1993 Jun 1;111(6):831.

92. Campbell C. Matrix method to find a new set of Zernike coefficients from an original set when the aperture radius is changed. JOSA A. 2003;20(2):209–217.

93. Bará S, Pailos E, Arines J, López-Gil N, Thibos L. Estimating the eye aberration coefficients in resized pupils: is it better to refit or to rescale? J Opt Soc Am A. 2014 Jan 1;31(1):114.

94. Thibos L, Ye M, Zhang X, Bradley A. The chromatic eye: a new reduced-eye model of ocular chromatic aberration in humans. Appl Opt. 1992;31(19):3594–3600.

95. Llorente L, Diaz-Santana L, Lara-Saucedo D, Marcos S. Aberrations of the human eye in visible and near infrared illumination. Optom Vis Sci. 2003 Jan;80(1):26–35.

96. Fernández E, Unterhuber A, Prieto P, Hermann B, Drexler W, Artal P. Ocular aberrations as a function of wavelength in the near infrared measured with a femtosecond laser. Opt Express. 2005;13(2):400–409.

97. Nam J, Rubinstein J, Thibos L. Wavelength adjustment using an eye model from aberrometry data. J Opt Soc Am A Opt Image Sci Vis. 2010 Jul 1;27(7):1561–74.

98. Fernández E, Artal P. Ocular aberrations up to the infrared range: from 632.8 to 1070 nm. Opt Express. 2008;16(26):21199–21208.

99. American National Standards Institute. Ophthalmics - Prescription Ophthalmic Lenses - Recommendation. ANSI Z801. 2015;

100. Porter J, Guirao A, Cox I, Williams D. Monochromatic aberrations of the human eye in a large population. JOSA A. 2001;18(8):1793–803.

101. Thibos L. Retinal image quality for virtual eyes generated by a statistical model of ocular wavefront aberrations. Ophthalmic Physiol Opt. 2009 May;29(3):288–91.

102. Thibos L, Bradley A, Hong X. A statistical model of the aberration structure of normal, well-corrected eyes. Ophthalmic Physiol Opt. 2002;22(5):427–433.

103. Owsley C. Aging and vision. Vision Res. 2011 Jul;51(13):1610–22.

104. Dressler M, Rassow B. Neural contrast sensitivity measurements with a laser interference system for clinical and screening application. Invest Ophthalmol Vis Sci. 1981;21(5):737–744.

105. Burton K, Owsley C, Sloane M. Aging and neural spatial contrast sensitivity: photopic vision. Vision Res. 1993 May;33(7):939–46.

106. van den Berg TJTP, Franssen L, Coppens JE. Straylight in the human eye: testing objectivity and optical character of the psychophysical measurement. Ophthalmic Physiol Opt. 2009 May;29(3):345–50.

107. van den Berg T. The (lack of) relation between straylight and visual acuity. Two domains of the point-spread-function. Ophthalmic Physiol Opt. 2017 May;37(3):333–41.

108. Charman W, Jennings J, Whitefoot H. The refraction of the eye in the relation to spherical aberration and pupil size. Br J Physiol Opt. 1978;32:78–93.

109. Ravikumar S, Thibos L, Bradley A. Calculation of retinal image quality for polychromatic light. JOSA A. 2008;25(10):2395–407.

110. Hastings G, Applegate R, Nguyen L, Kauffman M, Hemmati R, Marsack J. Comparison of Wavefront-Guided and Best Conventional Scleral Lenses after Habituation in Eyes with Corneal Ectasia. Optom Vis Sci. 2019;96(4):238–47.

111. Tomidokoro A, Oshika T, Amano S, Higaki S, Maeda N, Miyata K. Changes in anterior and posterior corneal curvatures in keratoconus. Ophthalmology. 2000 Jul;107(7):1328–32.

112. Choi J, Wee W, Lee J, Kim M. Changes of ocular higher order aberration in on-and off-eye of rigid gas permeable contact lenses. Optom Vis Sci. 2007;84(1):42–51.

113. Chen M, Yoon G. Posterior corneal aberrations and their compensation effects on anterior corneal aberrations in keratoconic eyes. Invest Ophthalmol Vis Sci. 2008;49(12):5645–5652.

114. Kosaki R, Maeda N, Bessho K, Hori Y, Nishida K, Suzaki A, et al. Magnitude and orientation of Zernike terms in patients with keratoconus. Invest Ophthalmol Vis Sci. 2007;48(7):3062–3068.

115. Negishi K, Kumanomido T, Utsumi Y, Tsubota K. Effect of Higher-Order Aberrations on Visual Function in Keratoconic Eyes with a Rigid Gas Permeable Contact Lens. Am J Ophthalmol. 2007 Dec;144(6):924-929.e1.

116. Gumus K, Gire A, Pflugfelder S. The Impact of the Boston Ocular Surface Prosthesis on Wavefront Higher-Order Aberrations. Am J Ophthalmol. 2011 Apr;151(4):682-690.e2.

117. López-Gil N, Chateau N, Castejón-Monchón J, Artal P, Benito A. Correcting ocular aberrations by soft contact lenses. Afr Optom. 2003;62(4):173–177.

118. Jeong T, Yoon G. Customized correction of wavefront aberrations in abnormal human eyes by using a phase plate and a customized contact lens. J-KOREAN Phys Soc. 2006;49(1):121.

119. Chen M, Sabesan R, Ahmad K, Yoon G. Correcting anterior corneal aberration and variability of lens movements in keratoconic eyes with back-surface customized soft contact lenses. Opt Lett. 2007;32(21):3203–3205.

120. Marsack J, Parker K, Niu Y, Pesudovs K, Applegate R. On-eye performance of custom wavefront-guided soft contact lenses in a habitual soft lens-wearing keratoconic patient. J Refract Surg. 2007;23(9):960–964.

121. Sabesan R, Jeong T, Carvalho L, Cox I, Williams D, Yoon G. Vision improvement by correcting higher-order aberrations with customized soft contact lenses in keratoconic eyes. Opt Lett. 2007;32(8):1000–1002.

122. Katsoulos C, Karageorgiadis L, Vasileiou N, Mousafeiropoulos T, Asimellis G. Customized hydrogel contact lenses for keratoconus incorporating correction for vertical coma aberration. Ophthalmic Physiol Opt. 2009 May;29(3):321–9.

123. Sabesan R, Johns L, Tomashevskaya O, Jacobs D, Rosenthal P, Yoon G. Wavefront-guided scleral lens prosthetic device for keratoconus. Optom Vis Sci. 2013 Apr;90(4):314–23.

124. Jinabhai A, O'Donnell C, Tromans C, Radhakrishnan H. Optical quality and visual performance with customised soft contact lenses for keratoconus. Ophthalmic Physiol Opt. 2014 Sep;34(5):528–39.

125. Guirao A, Williams D, Cox I. Effect of rotation and translation on the expected benefit of an ideal method to correct the eye's higher-order aberrations. J Opt Soc Am A Opt Image Sci Vis. 2001 May;18(5):1003–15.

126. Guirao A, Cox I, Williams D. Method for optimizing the correction of the eye's higher-order aberrations in the presence of decentrations. JOSA A. 2002;19(1):126–128.

127. De Brabander J, Chateau N, Marin G, Lopez-Gil N, Van Der Worp E, Benito A. Simulated optical performance of custom wavefront soft contact lenses for keratoconus. Optom Vis Sci. 2003;80(9):637–643.

128. Ho A. Aberration correction with soft contact lens: is the postlens tear film important? Eye Contact Lens. 2003;29(1):S182–S185.

129. Thibos L, Cheng X, Bradley A. Design principles and limitations of wave-front guided contact lenses. Eye Contact Lens. 2003;29(1):S167–S170.

130. López-Gil N, Castejón-Mochón J, Fernández-Sánchez V. Limitations of the ocular wavefront correction with contact lenses. Vision Res. 2009 Jul;49(14):1729–37.

131. Jinabhai A, Charman W, O'Donnell C, Radhakrishnan H. Optical quality for keratoconic eyes with conventional RGP lens and simulated, customised contact lens corrections: a comparison: Simulating customised corrections for keratoconus patients. Ophthalmic Physiol Opt. 2012 May;32(3):200–12.

132. Shi Y, Queener HM, Marsack JD, Ravikumar A, Bedell HE, Applegate RA. Optimizing wavefront-guided corrections for highly aberrated eyes in the presence of registration uncertainty. J Vis. 2013 Jun 11;13(7):8–8.

133. Shi Y, Applegate RA, Wei X, Ravikumar A, Bedell HE. Registration tolerance of a custom correction to maintain visual acuity. Optom Vis Sci. 2013;90(12):1370–1384.

134. Sabesan R, Yoon G. Visual performance after correcting higher order aberrations in keratoconic eyes. J Vis. 2009 May 1;9(5):6–6.

135. Sabesan R, Barbot A, Yoon G. Enhanced neural function in highly aberrated eyes following perceptual learning with adaptive optics. Vision Res. 2017 Mar;132:78–84.

136. Sabesan R, Yoon G. Neural compensation for long-term asymmetric optical blur to improve visual performance in keratoconic eyes. Invest Ophthalmol Vis Sci. 2010;51(7):3835–3839.

137. Zadnik K, Steger-May K, Fink B, Joslin C, Nichols J, Rosenstiel C, et al. Between-eye asymmetry in keratoconus. Cornea. 2002;21(7):671–679.

138. Belin M, Duncan J, Ambrosio Jr R, Gomes J. Keratoconus: The ABCD Grading System. Int J Keratoconus Ectatic Corneal Dis. 2015;4(3):85–93.

139. Applegate R, Hilmantel G, Howland H. Area under log contrast sensitivity function: A concise method of following changes in visual performance. Vis Sci Its Appl. 1997;1:98–101.

140. Visser E, Visser R, Van Lier H. Advantages of toric scleral lenses. Optom Vis Sci. 2006;83(4):233–236.

141. Ticak A, Marsack J, Koenig D, Ravikumar A, Shi Y, Nguyen L, et al. A Comparison of Three Methods to Increase Scleral Contact Lens On-Eye Stability: Eye Contact Lens Sci Clin Pract. 2015 Nov;41(6):386–90.

142. Marsack J, Pesudovs K, Sarver E, Applegate R. Impact of Zernike-fit error on simulated high- and low-contrast acuity in keratoconus: implications for using Zernike-based corrections. J Opt Soc Am A Opt Image Sci Vis. 2006 Apr;23(4):769–76.

143. Lo H, Yeh S, Cheng H. Scleral contact lenses for visual rehabilitation in keratoconus and irregular astigmatism after refractive surgery. Taiwan J Ophthalmol. 2014 Jun;4(2):73–6.

144. Lo H, Yeh S, Cheng H. Scleral contact lenses for visual rehabilitation in keratoconus and irregular astigmatism after refractive surgery. Taiwan J Ophthalmol. 2014 Jun;4(2):73–6.

145. Schornack M, Patel S. Scleral Lenses in the Management of Keratoconus: Eye Contact Lens Sci Clin Pract. 2010 Jan;36(1):39–44.

146. Yang B, Liang B, Liu L, Liao M, Li Q, Dai Y, et al. Contrast sensitivity function after correcting residual wavefront aberrations during RGP lens wear. Optom Vis Sci. 2014;91(10):1271–1277.

147. Ravikumar A, Applegate R, Shi Y, Bedell H. Six just-noticeable differences in retinal image quality in 1 line of visual acuity: Toward quantification of happy versus unhappy patients with 20/20 acuity. J Cataract Refract Surg. 2011 Aug;37(8):1523–9.

148. Pelli D, Robson J, Wilkins A. The design of a new letter chart for measuring contrast sensitivity. Clin Vis Sci. 1988;2(3):187–99.

149. Charman W, Walsh G. The optical phase transfer function of the eye and the perception of spatial phase. Vision Res. 1985;25(4):619–23.

150. Pantanelli S, MacRae S, Jeong T, Yoon G. Characterizing the Wave Aberration in Eyes with Keratoconus or Penetrating Keratoplasty Using a High–Dynamic Range Wavefront Sensor. Ophthalmology. 2007 Nov;114(11):2013–21.

151. Thibos L, Hong X, Bradley A, Cheng X. Statistical variation of aberration structure and image quality in a normal population of healthy eyes. J Opt Soc Am A. 2002;19(12):2329–2348.

152. Chen L, Singer B, Guirao A, Porter J, Williams D. Image metrics for predicting subjective image quality. Optom Vis Sci. 2005;82(5):358–369.

153. Thibos L, Hong X, Bradley A, Applegate R. Accuracy and precision of objective refraction from wavefront aberrations. J Vis. 2004 Apr 1;4(4):329–51.

154. Campbell F, Green D. Optical and retinal factors affecting visual resolution. J Physiol. 1965;181(3):576–93.

155. Elliott S, Choi S, Doble N, Hardy J, Evans J, Werner J. Role of high-order aberrations in senescent changes in spatial vision. J Vis. 2009 Feb 1;9(2):24–24.

156. Sabesan R, Barbot A, Yoon G. Enhanced neural function in highly aberrated eyes following perceptual learning with adaptive optics. Vision Res. 2017 Mar;132:78–84.

157. Elliott D, Yang K, Whitaker D. Visual acuity changes throughout adulthood in normal, healthy eyes: seeing beyond 6/6. Optom Vis Sci. 1995 Mar;72(3):186–91.

158. Owsley C, Sekuler R, Siemsen D. Contrast sensitivity throughout adulthood. Vision Res. 1983;23(7):689–99.

159. Elliott D. Contrast sensitivity decline with ageing: a neural or optical phenomenon? Ophthalmic Physiol Opt. 1987;7(4):415–9.

160. Sloane M, Owsley C, Jackson C. Aging and luminance-adaptation effects on spatial contrast sensitivity. J Opt Soc Am A. 1988 Dec 1;5(12):2181.

161. Sloane M, Owsley C, Alvarez S. Aging, senile miosis and spatial contrast sensitivity at low luminance. Vision Res. 1988 Jan;28(11):1235–46.

162. Schwiegerling J. Scaling Zernike expansion coefficients to different pupil sizes. J Opt Soc Am A. 2002;19(10):1937–1945.

163. Watson A, Yellott J. A unified formula for light-adapted pupil size. J Vis. 2012 Sep 25;12(10):12–12.

164. Applegate R, Donnelly III W, Marsack J, Koenig D, Pesudovs K. Three-dimensional relationship between high-order root-mean-square wavefront error, pupil diameter, and aging. J Opt Soc Am A. 2007;24(3):578–587.

165. Chylack L, Wolfe J, Singer D, Leske M, Bullimore M, Bailey I, et al. The Lens Opacities Classification System III. Arch Ophthalmol. 1993 Jun 1;111(6):831.

166. CIE. Light as a true visual quantity: Principles of measurement. Comm Int Eclairage. 1978;41.

167. D'Errico J. polyfitn [Internet]. 2018. Available from: https://www.mathworks.com/matlabcentral/fileexchange/34765-polyfitn

168. Rovamo J, Mustonen J, Näsänen R. Modelling contrast sensitivity as a function of retinal illuminance and grating area. Vision Res. 1994;34(10):1301–1314.

169. Nameda N, Kawara T, Ohzu H. Human visual spatio-temporal frequency performance as a function of age. Optom Vis Sci. 1989 Nov;66(11):760–5.

170. Devaney K, Johnson H. Neuron loss in the aging visual cortex of man. J Gerontol. 1980 Nov;35(6):836–41.

171. Balazsi A, Rootman J, Drance S, Schulzer M, Douglas G. The effect of age on the nerve fiber population of the human optic nerve. Am J Ophthalmol. 1984 Jun;97(6):760–6.

172. Gao H, Hollyfield J. Differential Loss of Neurons and Retinal Pigment Epithelial Cells. Invest Ophthalmol Vis Sci. 1992;33(1):1–17.

173. Curcio C, Millican C, Allen K, Kalina R. Aging of the Human Photoreceptor Mosaic: Evidence for Selective Vulnerability of Rods in Central Retina. Invest Ophthalmol Vis Sci. 1993;34(12):19.

174. Porciatti V, Burr D, Morrone M, Fiorentini A. The effects of ageing on the pattern electroretinogram and visual evoked potential in humans. Vision Res. 1992 Jul;32(7):1199–209.

175. López-Gil N, Martin J, Liu T, Bradley A, Díaz-Muñoz D, Thibos L. Retinal image quality during accommodation. Ophthalmic Physiol Opt. 2013 Jul;33(4):497–507.

176. Sreenivasan V, Aslakson E, Kornaus A, Thibos LN. Retinal image quality during accommodation in adult myopic eyes. Optom Vis Sci. 2013;90(11):1292–303.

177. Cheng X, Bradley A, Thibos L. Predicting subjective judgment of best focus with objective image quality metrics. J Vis. 2004 Apr 23;4(4):310–21.

178. Marsack J, Thibos L, Applegate R. Metrics of optical quality derived from wave aberrations predict visual performance. J Vis. 2004 Apr 1;4(4):322–8.

179. Martin J, Vasudevan B, Himebaugh N, Bradley A, Thibos L. Unbiased estimation of refractive state of aberrated eyes. Vision Res. 2011 Sep;51(17):1932–40.

180. Hastings G, Marsack J, Nguyen L, Cheng H, Applegate R. Is an objective refraction optimised using the visual Strehl ratio better than a subjective refraction? Ophthalmic Physiol Opt. 2017 May;37(3):317–25.

181. Schoneveld P, Pesudovs K, Coster D. Predicting visual performance from optical quality metrics in keratoconus. Clin Exp Optom. 2009 May;92(3):289–96.

182. Ravikumar A, Sarver E, Applegate R. Change in visual acuity is highly correlated with change in six image quality metrics independent of wavefront error and/or pupil diameter. J Vis. 2012 Sep 14;12(10):1–13.

183. Van Nes F, Bouman M. Spatial Modulation Transfer in the Human Eye. J Opt Soc Am. 1967 Mar 1;57(3):401.

184. Yoss R, Moyer N, Hollenhorst R. Pupil size and spontaneous pupillary waves associated with alertness, drowsiness, and sleep. Neurology. 1970 Jun;20(6):545–54.

185. Williams DR. Visibility of interference fringes near the resolution limit. J Opt Soc Am A. 1985 Jul;2(7):1087–93.

186. Still D. Optical limits to contrast sensitivity in human peripheral vision. UMI #9020696. Indiana University; 1989.

187. Dressler M, Rassow B. Neural contrast sensitivity measurements with a laser interference system for clinical and screening application. Invest Ophthalmol Vis Sci. 1981;21(5):737–744.

188. Artal P, Ferro M, Navarro R, Miranda I. Effects of aging in retinal image quality. J Opt Soc Am A. 1993;10(7):1656–1662.

189. Calver R, Cox M, Elliott D. Effect of aging on the monochromatic aberrations of the human eye. J Opt Soc Am A. 1999 Sep;16(9):2069–78.

190. Guirao A, Gonzalez C, Redondo M, Geraghty E, Norrby S, Artal P. Average optical performance of the human eye as a function of age in a normal population. Invest Ophthalmol Vis Sci. 1999;40(1):203–213.

191. McLellan JS, Marcos S, Burns SA. Age-related changes in monochromatic wave aberrations of the human eye. Invest Ophthalmol Vis Sci. 2001;42(6):1390–1395.

192. Artal P, Berrio E, Guirao A, Piers P. Contribution of the cornea and internal surfaces to the change of ocular aberrations with age. J Opt Soc Am A. 2002 Jan 1;19(1):137.

193. Hennelly M, Barbur J, Edgar D, Woodward E. The effect of age on the light scattering characteristics of the eye. Ophthalmic Physiol Opt. 1998;18(2):197–203.

194. van den Berg T. Analysis of intraocular straylight, especially in relation to age. Optom Vis Sci. 1995 Feb;72(2):52–9.

195. Pokorny J, Smith V, Lutze M. Aging of the human lens. Appl Opt. 1987 Apr 15;26(8):1437.

196. Werner J. Development of scotopic sensitivity and the absorption spectrum of the human ocular media. J Opt Soc Am. 1982 Feb 1;72(2):247.

197. Elliott D, Yang K, Dumbleton K, Cullen A. Ultraviolet-induced lenticular fluorescence: Intraocular straylight affecting visual function. Vision Res. 1993 Sep;33(13):1827–33.

198. van den Berg T. The (lack of) relation between straylight and visual acuity. Two domains of the point-spread-function. Ophthalmic Physiol Opt. 2017 May;37(3):333–41.

199. Sagawa K, Takahashi Y. Spectral luminous efficiency as a function of age. J Opt Soc Am A. 2001 Nov 1;18(11):2659.

200. Weale R. Age and the transmittance of the human crystalline lens. J Physiol. 1988 Jan 1;395(1):577–87.

201. Delori F, Burns S. Fundus reflectance and the measurement of crystalline lens density. J Opt Soc Am A. 1996 Feb 1;13(2):215.

202. Kulikowski J. Some stimulus parameters affecting spatial and temporal resolution of human vision. Vision Res. 1971 Jan;11(1):83–93.

203. Sturr J, Church K, Taub H. Temporal summation functions for detection of sine-wave gratings in young and older adults. Vision Res. 1988 Jan;28(11):1247–53.

204. Wright C, Drasdo N. The influence of age on the spatial and temporal contrast sensitivity function. Doc Ophthalmol. 1985 Jun;59(4):385–95.

205. Higgins K, Jaffe M, Caruso R, deMonasterio F. Spatial contrast sensitivity: effects of age, test–retest, and psychophysical method. J Opt Soc Am A. 1988 Dec 1;5(12):2173.

206. Elliott D, Whitaker D, MacVeigh D. Neural contribution to spatiotemporal contrast sensitivity decline in healthy ageing eyes. Vision Res. 1990 Jan;30(4):541–7.

207. Schefrin BE, Tregear SJ, Harvey LO, Werner JS. Senescent changes in scotopic contrast sensitivity. Vision Res. 1999 Nov;39(22):3728–36.

208. Bennett P, Sekuler A, Ozin L. Effects of aging on calculation efficiency and equivalent noise. J Opt Soc Am A. 1999 Mar 1;16(3):654.

209. Pardhan S. Contrast sensitivity loss with aging: sampling efficiency and equivalent noise at different spatial frequencies. J Opt Soc Am A. 2004 Feb 1;21(2):169.

210. Burton K, Owsley C, Sloane M. Aging and neural spatial contrast sensitivity: photopic vision. Vision Res. 1993 May;33(7):939–46.

211. Elliott D, Whitaker D, Thompson P. Use of displacement threshold hyperacuity to isolate the neural component of senile vision loss. Appl Opt. 1989 May 15;28(10):1914.

212. Curcio C, Drucker D. Retinal ganglion cells in Alzheimer's disease and aging. Ann Neurol. 1993;33:248–57.

213. Marshall J. The ageing retina: Physiology or pathology. Eye. 1987 Mar;1(2):282–95.

214. Watson A, Ahumada A. A standard model for foveal detection of spatial contrast. J Vis. 2005;5(9):714–40.

215. Watson A, Ahumada A. Predicting visual acuity from wavefront aberrations. J Vis. 2008 Apr 22;8(4):17.

216. Howarth P, Zhang X, Bradley A, Still D, Thibos L. Does the chromatic aberration of the eye vary with age? J Opt Soc Am A. 1988 Dec 1;5(12):2087.

217. Morrell A, Whitefoot H, Charman W. Ocular chromatic aberration and age. Ophthalmic Physiol Opt J Br Coll Ophthalmic Opt Optom. 1991 Oct;11(4):385–90.

218. Ravikumar S, Thibos L, Bradley A. Calculation of retinal image quality for polychromatic light. JOSA A. 2008;25(10):2395–407.

219. Campbell F, Kulikowski J, Levinson J. The effect of orientation on the visual resolution of gratings. J Physiol. 1966;187(2):427.

220. Mitchell D, Freeman R, Westheimer G. Effect of orientation on the modulation sensitivity for interference fringes on the retina. J Opt Soc Am A. 1967 Feb;57(2):246–9.

221. McMahon MJ, Macleod DI. The origin of the oblique effect examined with pattern adaptation and masking. J Vis. 2003;3(3):4–4.

222. Kilintari M, Pallikaris A, Tsiklis N, Ginis H. Evaluation of image quality metrics for the prediction of subjective best focus. Optom Vis Sci. 2010;87(3):183–189.

223. Robson J, Graham N. Probability summation and regional variation in contrast sensitivity across the visual field. Vis Res. 1981 Jan;21(3):409–18.

224. Howell E, Hess R. The functional area for summation to threshold for sinusoidal gratings. Vis Res. 1978 Jan;18(4):369–74.

225. Hoekstra J, van der Goot D, van den Brink G, Bilsen F. The influence of the number of cycles upon the visual contrast threshold for spatial sine wave patterns. Vis Rec. 1974 Jun;14(6):365–8.

226. Goss D, Grosvenor T. Reliability of refraction--a literature review. J Am Optom Assoc. 1996 Oct;67(10):619–30.

227. Bullimore M, Fusaro R, Adams C. The repeatability of automated and clinician refraction. Optom Vis Sci. 1998 Aug;75(8):617–22.

228. Raasch T, Bailey I, Bullimore M. Repeatability of visual acuity measurement. Optom Vis Sci. 1998 May;75(5):342–8.

229. Manny R, Hussein M, Gwiazda J, Marsh-Tootle W. Repeatability of ETDRS Visual Acuity in Children. Investig Opthalmology Vis Sci. 2003 Aug 1;44(8):3294.

230. Applegate R, Marsack J, Thibos L. Metrics of retinal image quality predict visual performance in eyes with 20/17 or better visual acuity. Optom Vis Sci Off Publ Am Acad Optom. 2006;83(9):635.

231. Villegas E, Alcon E, Artal P. Optical Quality of the Eye in Subjects with Normal and Excellent Visual Acuity. Investig Opthalmology Vis Sci. 2008 Oct 1;49(10):4688.

232. Sabesan R, Yoon G. Neural compensation for long-term asymmetric optical blur to improve visual performance in keratoconic eyes. Invest Ophthalmol Vis Sci. 2010;51(7):3835–3839.

233. Shi Y, Applegate RA, Wei X, Ravikumar A, Bedell HE. Registration tolerance of a custom correction to maintain visual acuity. Optom Vis Sci. 2013;90(12):1370–84.

234. Shi Y, Queener HM, Marsack JD, Ravikumar A, Bedell HE, Applegate RA. Optimizing wavefront-guided corrections for highly aberrated eyes in the presence of registration uncertainty. J Vis. 2013 Jun 11;13(7):1–15.

235. Ravikumar A, Marsack J, Bedell H, Shi Y, Applegate R. Change in visual acuity is well correlated with change in image-quality metrics for both normal and keratoconic wavefront errors. J Vis. 2013 Nov 26;13(13):1–16.

236. Williams DR. Aliasing in human foveal vision. Vision Res. 1985;25(2):195–205.

237. Bass M, editor. Handbook of optics. 2nd ed. New York: McGraw-Hill; 1995. 4 p.

238. Thibos L. Optical limitations of the Maxwellian view interferometer. Appl Opt. 1990;29(10):1411–1419.

239. Vaegan, Halliday B. A forced-choice test improves clinical contrast sensitivity testing. Br J Ophthalmol. 1982 Aug 1;66(8):477–91.

240. Gaito J. Repeated measurements designs and counterbalancing. Psychol Bull. 1961;58(1):46–54.

241. Kingdom F, Prins N. Psychophysics: a practical introduction. 1. ed. Amsterdam: Elsevier [u.a.]; 2010. 279 p.

242. Prins N, Kingdom F. Applying the Model-Comparison Approach to Test Specific Research Hypotheses in Psychophysical Research Using the Palamedes Toolbox. Front Psychol [Internet]. 2018 Jul 23 [cited 2019 Apr 3];9. Available from: https://www.frontiersin.org/article/10.3389/fpsyg.2018.01250/full

243. Wyszecki G, Stiles WS. Color science: concepts and methods, quantitative data, and formulae. Wiley classics library ed. New York: John Wiley & Sons; 2000. 950 p. (Wiley classics library).

244. Lovasik J, Kergoat H. Time course of cycloplegia induced by a new phenylephrine-tropicamide combination drug. Optom Vis Sci. 1990 May;67(5):352–8.

245. Carkeet A, Velaedan S, Tan Y, Lee D, Tan D. Higher Order Ocular Aberrations After Cycloplegic and Non-cycloplegic Pupil Dilation. 2003;19:8.

246. López-Gil N, Fernandez-Sanchez V. The change of spherical aberration during accommodation and its effect on the accommodation response. J Vis. 2010 Nov 12;10(13):1–15.

247. Thibos L, Bradley A, Liu T, López-Gil N. Spherical aberration and the sign of defocus. Optom Vis Sci. 2013;90(11):1284–1291.

248. Bex P, Makous W. Spatial frequency, phase, and the contrast of natural images. J Opt Soc Am A. 2002 Jun 1;19(6):1096.

249. Frazor R, Geisler W. Local luminance and contrast in natural images. Vision Res. 2006 May;46(10):1585–98.

250. Ruderman D. The statistics of natural images. Netw Comput Neural Syst. 1994 Jan;5(4):517–48.

251. Hastings G, Zanayed J, Nguyen L, Applegate R, Marsack J. Do polymer coatings change the aberrations of wavefront-guided and conventional scleral lenses? :in press.

252. Jeong T, Menon M, Yoon G. Measurement of wave-front aberration in soft contact lenses by use of a Shack–Hartmann wave-front sensor. Appl Opt. 2005 Jul 20;44(21):4523–7.

253. Granger E, Cupery K. An optical meric function (SQF), which correlates with subjective image judgments. Photogr Sci Eng. 1972;16(3):221–30.

254. Levi D, Polat U. Neural plasticity in adults with amblyopia. Proc Natl Acad Sci. 1996;93(13):6830–6834.

255. Levi D. Visual Processing in Amblyopia: Human Studies. Strabismus. 2006 Jan;14(1):11–9.

256. Rahi J, Logan S, Borja M, Timms C, Russell-Eggitt I, Taylor D. Prediction of improved vision in the amblyopic eye after visual loss in the non-amblyopic eye. The Lancet. 2002 Aug;360(9333):621–2.

Appendices

Appendix A: Other publications.

The author has contributed to the following papers, which are related to the dissertation, but have not been included in it.

A1. **Hastings GD**, Zanayed JZ, Nguyen LC, Applegate RA, Marsack JD. Do Polymer Coatings Change the Aberrations of Wavefront-guided and Conventional Scleral Lenses? Optom Vis Sci 2020;97 doi:10.1097/OPX.0000000000001462.

A2. Nguyen LC, **Hastings GD**, Kauffman MJ, Applegate RA, Marsack JD. Alignment of a Wavefront-Guided Scleral Lens Correction in the Presence of a Lens Capsulotomy. (submitted)

A3. Bell ELS, **Hastings GD**, Nguyen LC, Applegate RA, Marsack JD. Utilizing a visual image quality metric to optimize spectacle prescriptions for individuals with keratoconus. (submitted)

A4. Wilting SM, **Hastings GD**, Kauffman MJ, Nguyen LC, Bell ELS, Hu C, Rijal S, Marsack JD. Quantifying the Optical and Physical Consequences of Daily Cleaning on Conventional and Wavefront-Guided Scleral Lenses. (submitted)

A5 Rijal S, **Hastings GD**, Nguyen LC, Kauffman MJ, Applegate RA, Marsack JD. Can higher-order aberration compensating optics be placed at a common location for individuals wearing wavefront-guided scleral lenses? (submitted)